The synthesis and characterisation of novel precursors for the CVD of tin sulfides and related materials

Kana, Aliki Theodora

Award date:
2002

Awarding institution:
University of Bath

THE SYNTHESIS AND CHARACTERISATION OF NOVEL PRECURSORS FOR THE CVD OF TIN SULFIDES AND RELATED MATERIALS

Submitted by Aliki Theodora Kana
for the degree of PhD
of the University of Bath
2002

COPYRIGHT

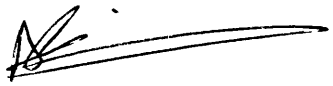

ProQuest LLC
789 East Eisenhower Parkway
P.O. Box 1346
Ann Arbor, MI 48106-1346

ABSTRACT

The research described in this thesis has been concerned with the synthesis and characterisation of a range of novel precursors for the CVD of tin sulfides and transition metal-doped tin sulfide materials.

The preparation, characterisation and properties of dithiocarbamate derivatives of tin were examined. The decomposition of $(Et_2NCS_2)_4Sn$ to SnS_2 as well as the synthesis and decomposition of mixed ligand species such as $(Et_2NCS_2)(RS)_2Sn$ have been studied.

The successful synthesis and characterisation of pentacarbonyl transition metal (Cr, Mo) tin sulfides has been reported. Their decomposition to tin containing transition metal sulfide films by the CVD method has been examined.

The successful synthesis and characterisation of transition metal tetracarbonyl complexes of chelating organotin (IV) aminothiols has been reported, as well as the synthesis and characterisation of sulfur-bridged transition metal carbonyl complexes. The suitability of the former as single-source precursors for the deposition of ternary materials has been assessed.

Finally, the syntheses and characterisation of two triphenylphosphine gold alkyltinsulfides have been examined and some preliminary results on their decomposition properties have been reported.

ACKNOWLEDGEMENTS

I feel I owe a big 'THANKS' to my supervisor, Dr Kieran C. Molloy for all his guidance and support during the past few years. Especially for the hours he spent trying to make sense of this thesis.

I would also like to thank Dr Mary Mahon for her help with the crystal structures and data presented here.

I also feel I need to thank all the people I worked with during the past few years, for their advise and guidance and for making our curry outings so special.

Finally, I would like to thank wholeheartedly my husband Dr Lee Edwards as well as my family for their support during the highs and lows of the last three years.

ABBREVIATIONS

AACVD	Aerosol-Assisted Chemical Vapour Deposition
APCVD	Atmospheric Pressure Chemical Vapour Deposition
ap	Antiperiplanar, trans (t)
bp	Boiling Point
bp	Bond Pair
^{n}Bu	n-Butyl
^{t}Bu	Tertiary Butyl
CVD	Chemical Vapour Deposition
Cy	Cyclohexyl
d	Doublet
dtc	Diethyl Dithiocarbamate
EDAX	Energy Dispersive X-Ray Analysis
Et	Ethyl
IR	Infra-Red Spectroscopy
L	Ligand
LED	Light Emitting Diode
lp	Lone Pair
LPE	Liquid Phase Epitaxy
LPCVD	Low Pressure Chemical Vapour Deposition
LP-MOCVD	Low Pressure Metalorganic Chemical Vapour Deposition
m	Multiplet
MBE	Molecular Beam Epitaxy
Me	Methyl
MOCVD	Metalorganic Molecular Beam Epitaxy
mp	Melting Point Temperature
NMR	Nuclear Magnetic Resonance
PECVD	Plasma Enhanced Chemical Vapour Deposition
Ph	Phenyl
RT	Room Temperature
s	Singlet
sc	Synclinal, gauche (g)

SEM	Scanning Electron Microscopy
t	Triplet
TGA	Thermal Gravimetric Analysis
THF	Tetrahydrofuran
tmhd	2,2,6,6-tetramethyl-3,5-heptadionate
Tol	Toluene
UV	Ultraviolet
XRD	X-Ray Diffraction

CONTENTS

CHAPTER ONE

Introduction

1. Introduction

The work described in this thesis involves the synthesis and characterisation of several novel compounds containing tin, sulfur and/or other metals. Further study of these complexes as suitable precursors for CVD reveals their use in growing tin sulfide or metal-containing tin sulfide films. The aims of this first chapter are: to provide some background information on the basic principles of semiconductivity, to summarise the CVD process, to discuss tin sulfides and related materials, to provide some background information on the current progress in this field and to discuss the specific aims during this research study.

1.1 Compound Semiconductors

1.1.1 Introduction

Since the discovery of the transistor in the late 1940s society has been following a path of ever-increasing electronic-device diversification and sophistication, resulting to a truly remarkable cultural revolution. Communications, computational ability, photonics, diagnostic capabilities, power and process manipulation, have all progressed to levels only fictionalised about a few decades ago. [2]

Silicon semiconductor electronics has, and still is, leading this change, although probably not forever, as alternative materials continue to advance and product needs diversify. At present however, a vast sub-technology of compound semiconductors has developed; principally those made of III-V group elements, but also those of II-VI, IV-IV and even oxides and organics. [2] **Fig.1.1** shows the portion of the periodic table of primary interest for the compound semiconductors.

	13/III	14/IV	15/V	16/VI	17/VII
	B	C	N	O	F
12	Al	Si	P	S	Cl
Zn	Ga	Ge	As	Se	Br
Cd	In	Sn	Sb	Te	I
Hg	Tl	Pb	Bi	Po	At

Fig.1.1 The part of the periodic table showing the elements around silicon that comprise important compound semiconductors. [2]

The majority of important semiconducting materials are iso-electronic with elemental silicon. In silicon each atom provides 4 valence electrons one to each of 4 neighbours, which leads to a filled valence band. Other important materials are III-V materials, e.g. GaAs, InP or II-VI materials such as CdS or ZnSe.

1.1.2 Basic Concepts of Semiconductivity

Semiconductors are materials that contain a relatively small number of current carriers as compared to conductors such as metals. The electronic structure of solids is usually explained in terms of the band theory (**Fig.1.2**), which may be viewed as the formation of bands rather than discrete orbitals when a large number of atoms are brought together to form a solid. [5]

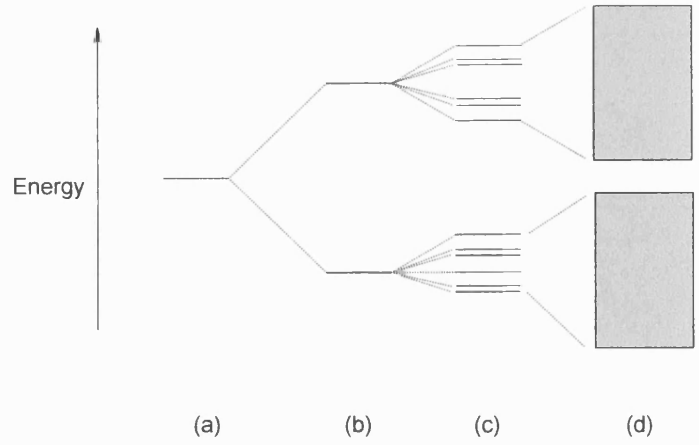

Fig.1.2 Orbital energies of: (a) a single atom, (b) a diatomic system, (c) a molecular system and (d) a solid. [4]

The crucial difference between a semiconductor and an insulator is the magnitude of the energy separation between the bands, the band gap (E_g). In typical semiconducting materials the band gap is of the order of 1 eV (e.g. 1.12 eV for silicon and 0.67 eV for germanium), compared to a value of 9 eV or greater for insulators. At absolute zero semiconductors behave as insulators as there is insufficient thermal energy to promote electrons to the conduction band (**Fig.1.3**).

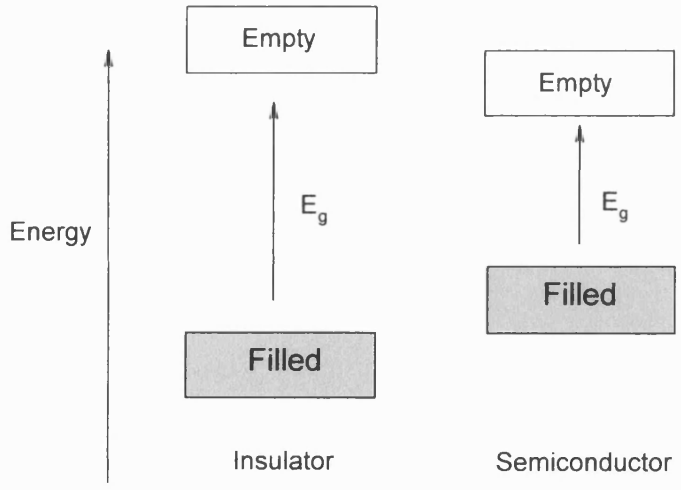

Fig.1.3 Band diagrams for an insulator and an intrinsic semiconductor. [4]

In metals the bands overlap, which leads to high mobility for electrons and the high conductivity of metals. The biggest difference between the properties of metals and semiconductors is that for metals conductivity decreases with temperature. This is essentially because the scattering of carrier electrons within the material increases with temperature. However, in semiconductors, although scattering will still increase with temperature, the most important effect is the promotion of electrons to the conduction band and conductivity in general increases with temperature. [4]

Semiconducting compounds can be divided into two classes, those having a direct and those having an indirect band gap. **Fig. 1.4** illustrates the differences. In an indirect semiconductor (**Fig. 1.4a**) an excited electron, in order to conserve momentum, must decay through a two-particle process in order to emit a photon. This is an inefficient process. Alternatively, in a direct band gap material (**Fig. 1.4b**) photon decay is sufficient to conserve momentum and energy. This is a more efficient process and the difference between the two may be several orders of magnitude. This is important as the direct or indirect nature of a semiconductor determines its usefulness for opto-electronic devices. [2] For example, direct band gap materials are more suitable for devices where fast generation of photons (or other energy carriers) is required, most notably for laser operation.

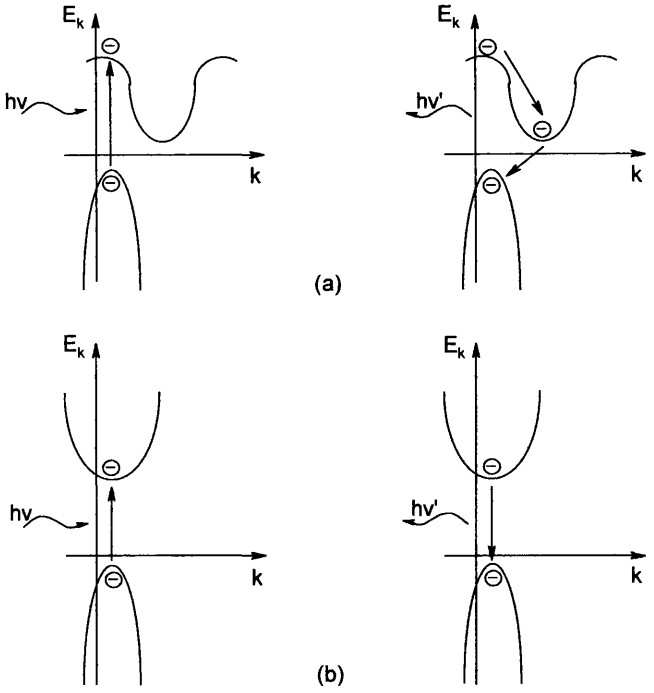

Fig.1.4 (a) Indirect and (b) direct semiconductor band gap diagrams showing photon transition. [2]

Intrinsic semiconductors (were conductivity is brought about by thermal excitation) are materials in which electrons can be excited across a forbidden zone so that there are current carriers in both the valence (holes, p-type semiconductor) and conduction bands (electrons, n-type semiconductor). [4]

The most common mechanism for conductivity in a semiconductor is extrinsic conduction (i.e. conductivity due to the insertion of dopant energy levels). Four main types of atomic defects are associated with extrinsic conduction:

(i) Lattice sites, which would be occupied in a perfect crystal, are vacant.

(ii) Interstitial atoms, which occupy a site, are not permitted in the perfect crystal.

(iii) Atoms located on an incorrect lattice site, e.g. an anion on a cation site.

(iv) Atoms with a higher or lower valency residing on a lattice site. [4]

The most important semiconducting materials are probably those obtained by intentional doping, i.e. substituting into the correct lattice site an element containing one electron less, which then acts as an acceptor, a p-type dopant (e.g. N in ZnSe or Zn or Cd in GaAs), or one extra electron, which then acts as a donor, an n-type dopant (e.g. Si or S in GaAs), **Fig.1.5** . [4]

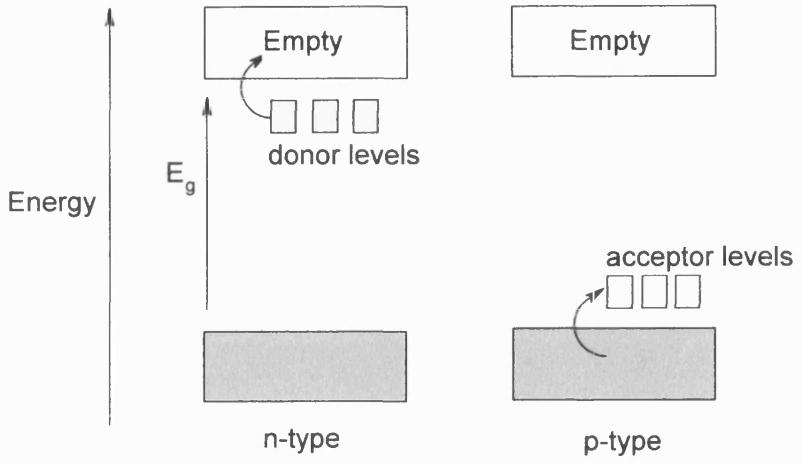

Fig.1.5 Band gap diagrams for p- and n-type semiconductors. [4]

A key feature of the compound semiconductors is that in almost all applications they rely on single crystal structures, and for thin films this generally means epitaxial deposition processes. [2] The principal compound semiconductors have structures related to those of diamond and are based on close packed anion layers with the metal ions occupying interstitial positions. [4]

The situation is relatively straightforward for the majority of III-V materials and their ternary alloys, (compound materials such as: GaAs, InP and $Al_xGa_{1-x}As$), since the parent materials exist exclusively in the cubic phase. These materials can be obtained as relatively high quality substrates (as wafers) by conventional methods. The ability to grow films of alloys from III-V materials in which the band gap can be controlled is very important. The growth of such materials forms the basis of the fabrication of solid state lasers and is used in a wide range of opto-electronics applications. In contrast, the situation is more complicated for the II-VI materials, (e.g. zinc sulfide), since there are two simple crystalline forms of ZnS, the low temperature cubic polymorph (β-ZnS, zincblende or

sphalerite) and the high temperature hexagonal phase (α-ZnS, wurtzite or zincsite). [4]

The structure of materials is important because defects in materials can lead to loss of efficiency of opto-electronic devices or to their early failure. Many devices are based on epitaxial growth, which means that there is a precise crystallographic, 3-dimensional relationship between the two phases, e.g. the various layers composing a device. [4]

One important feature of compound semiconductors is that many of these materials have band gaps that correspond to useful regions of the electromagnetic spectrum (**Fig.1.6**). In particular, we can identify the visible region for use in energy conversion (solar cells) and display technologies and the infrared region for thermal imaging technologies. [4]

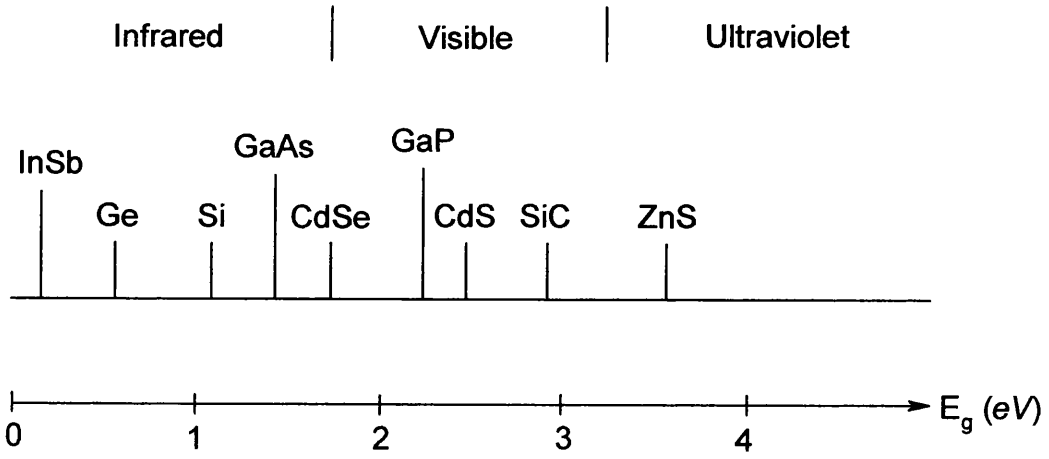

Fig.1.6 The band gaps of some common compound semiconductors and the optical spectrum. [2]

The compound semiconductors are important for several reasons:

(i) Many of them have direct band gaps, allowing them to be efficient photon emitters.

(ii) Their band gaps span an extraordinarily wide range, thus allowing them to be used in addressing a wide variety of applications (from high speeds, to high temperature, to high power, as well as to cover the photonic ranges from the near UV to the visible and to the far IR).

(iii) They often exhibit higher mobilities than Si, allowing greater speeds.

The compound semiconductors, indeed, dominate in photonic emitter applications and offer significant advantages at high speeds, high power and high temperature. Primary application areas of compound semiconductors are solar cells, infrared detectors, and LEDs, followed by microwave (cellular phones being a prime example) and high speed computing. Presently, much development effort is in the opto-electronics area, primary lasers and light emitting diodes (LEDs), for communications, displays, data storage and spectroscopy. High efficiency solar cells (primarily for space based power sources), account for a large amount of the net production area.

The rapidly increasing consumption of opto-electronic, solar cell devices and the development of high yield automated production tools, may increase the production level of compound semiconductors to a comparable level to that of silicon production. Already, the increased demand and competition has forced equipment vendors and merchant houses of epitaxial films to incorporate many of the features associated with silicon production (e.g. automated clean room production) to this market place. As the economies of production, automation, scale and improved yield grow, so too will the reliance on these materials for higher performance applications. We can expect to see significant increases in the utilisation of compound semiconductors in a wide variety of commonplace applications. [2]

1.2 Chemical Vapour Deposition (CVD)

1.2.1 Introduction

The formation of metal-containing thin film materials is currently an area of immense research activity and interest. These materials have found increasing applications to a wide variety of technological problems including electronic materials, opto-electronics devices, complex heterostructures, superconducting materials and device interconnects. In addition, metal and metal alloy films are typically very hard and inert materials that are often resistant to attack even in harsh chemical environments. Thus, metal-containing thin films have found increased use in not only traditional applications, such as hard coatings for cutting tools, but also in thermally and chemically-taxed aerospace components, high energy optical systems, high temperature devices and new magnetic materials.

Metal-containing thin films have been prepared traditionally by a number of techniques including sputtering methods, molecular beam epitaxy (MBE), liquid phase epitaxy (LPE) and lithographic techniques. The older epi- growth techniques, such as LPE and vapour phase epitaxy (VPE), operate close to thermodynamic equilibrium. Consequently, growth rates and compositions of the epitaxial materials are highly temperature sensitive. In addition, heterostructures with sharp interfaces are very difficult to prepare using these older technologies, primarily due to contamination and rapid reactant clearing problems. [1, 2] However, each of these technologies still remains active and satisfies many niche markets.

LPE is one of the earliest techniques employed to produce epitaxial films. It is also one of the simplest and most reliable. In this technique, elemental or compound reservoirs are held at their melting temperatures, which are maintained very accurately. The deposition substrate is then passed over the melt and a film is allowed to solidify from solution. Since elements can be obtained in extremely pure forms, this technique produces some of the purest materials. Problems ensue with the fact that all subsequent layers must be

deposited at constantly lower temperatures so as not to melt the previous layers. Furthermore, dopants tend to diffuse over time and lastly highly abrupt interfaces or well-controlled graded layers are difficult to achieve. [5]

MBE is still the method of choice for the highest purity materials and precise layer deposition control in most cases, although MOCVD has surpassed it in some instances (e.g. InP). It is however expensive, slow and temperamental to operate. Similarly to LPE, MBE produces extremely high purity materials, layer by layer, through the use of high purity elemental sources. The molecular beam impinges the substrate simultaneously with one or more other beams to grow a film. To maintain this high purity extremely tight tolerances must be maintained on the vacuum system. Typically UHV systems are used with base pressures in the range of 10^{-11} to 10^{-12} Torr. Some of the difficulties with MBE include: cross contamination of sources especially when highly volatile elements are used (e.g. Zn, P), particulate generation by the shutters, other coated components or gas phase condensation, long cycle times between depositions, precision grading of layers, scalability and growth rate. [5]

The term VPE generally is ascribed to processes using only gas reactants. In general element halides are used (e.g. $AsCl_3$, PCl_3, GaCl, etc). However, other hybrids may be mixed in with the process. Often chlorine or a halide such as $HCl_{(g)}$ is passed over a melt (e.g. As, Ga, In, etc) to transport an element in a chemical form and thereby deposit it downstream onto a substrate. High purity materials such as InP, GaInP, GaInAsP, GaAsP, GaP and GaAs can be grown this way. However, there are no Al hybrids available that work well with this technique and in addition AlCl reacts with quartz, the reactor material choice for VPE. Furthermore, stainless steel reactors suffer from chlorine reactivity if water is present at any time. Therefore VPE has limited flexibility and that is the reason it has not been developed further. [5]

Metal organic chemical vapour deposition (MOCVD), also commonly known as organometallic vapour phase epitaxy (OMVPE) and the related metal organic molecular beam epitaxial (MOMBE) techniques show great promise as the best technologies for the formation of metal-containing thin films. Since these are

kinetically controlled they circumvent many of the problems associated with the other deposition technologies.

The growth of thin films by Chemical Vapour Deposition (CVD) has become one of the most important methods of film formation and constitutes a corner stone for modern technologies such as solid-state electronics. The reasons for the rapidly growing importance of CVD in the past decade lie primarily in its versatility for depositing a very large variety of elements at relatively low temperatures and with high purity. In addition, CVD processes do not suffer from the limitations of LPE techniques related to complex solution dynamics and phase equilibria requirements. Moreover, CVD technology provides advantages over traditional deposition methods including: [3]

(a) Kinetic deposition control.
(b) Selective area and pattern deposition with sharp boundary features.
(c) Lower deposition temperatures with clean and controllable stoichiometric deposition processes (resultant films are often only dependent on the choice of precursor material and on easily controlled deposition conditions).
(d) Superior thin film uniformity.
(e) Superior step coverage.
(f) Monolayer interfacial control.
(g) Formation of high purity materials.
(h) Significant migration reduction at film-substrate interfaces.
(i) Experimental ease of deposition from starting precursor materials.
(j) Facility for larger scale production processes.

An additional important advantage of CVD is that deposition is often accomplished at significantly reduced temperature relative to many of the non-CVD processes. The older non-CVD depositions that are typically carried out at elevated temperatures frequently show severe interlayer diffusion and result in vague interlayer junctures. In recognition of these advantages, considerable effort has been directed towards employing CVD techniques for manufacturing semiconductor and refractory thin film materials.

1.2.2 Basic Principles

The technique of CVD is a relatively old chemical process, dating from the 1880s. It was first used in the production of carbon filaments for the incandescent lamp industry. Shortly after the initial use of CVD for making carbon films, Mond and others began to use organometallic compounds, primarily nickel tetracarbonyl, in the formation of metal-containing films in vapour phase processes. Since then, numerous metal-containing solid-state materials have been deposited from gas phase organometallic precursor complexes. [3]

Chemical Vapour Deposition is a process where one or more volatile inorganic, metal-organic or organometallic precursors are transported in the vapour phase, often in a carrier gas, to the reactor chamber where they decompose on a heated substrate and subsequently deposit a solid film. The decomposition results in elimination of volatile by-products. Inert carrier gases such as Ar and N_2 are often used to enhance the rate of transport of solid or liquid phase precursors to the reactor chamber. However, other reactive carrier gases such as H_2, NH_3, H_2S and O_2 are also used which participate in the chemistry of film deposition by acting as reducing or oxidising agents. Epitaxial, polycrystalline and amorphous films can be deposited, dependent upon the deposition conditions and the material to be deposited. [2]

Chemical vapour deposition involves a variety of steps. As the gas flows over the substrate a boundary layer can be formed across which temperature, velocity and concentration vary rapidly. This boundary layer occurs primarily near atmospheric pressure conditions. The gaseous species have to diffuse through the boundary layer from the bulk gas in order to reach the substrate surface. On reaching the substrate, they chemisorb and undergo surface reactions to deposit a solid film with the formation of volatile by-products. The by-products desorb from the surface, diffuse across the boundary layer and are eliminated from the reaction chamber (**Fig.1.7**). The relative rates of these various processes are important because the slowest rate limits the overall deposition rate. [2]

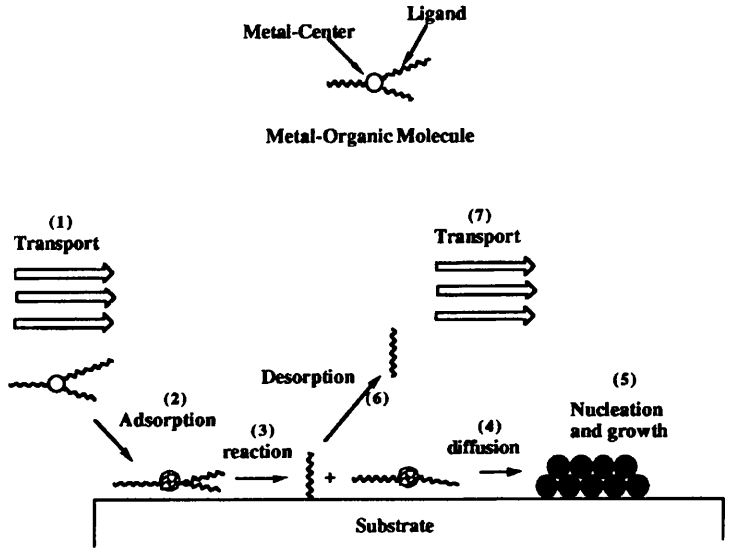

Fig.1.7 The fundamental steps involved in Chemical Vapour Deposition. [2]

Chemical reactions may also occur in the gas phase depending on the reactivity of the gas species and the pressure. These gas phase reactions are however, undesirable and can lead to nucleation of solid particles, which can result in films containing impurities, defects, particulates and exhibiting poor adhesion. Reduction of precursor concentration before it reaches the substrate, resulting in lower deposition rates may also occur. For such systems the distribution of source gases into the CVD reactor becomes critical, and the gases are mixed only above the substrate surface in order to minimise gas-phase reactions. Lower operating pressures also tend to reduce gas-phase reactions due to reduction in the number of intermolecular collisions.

Gas-phase transport rates and surface reaction rates are important for CVD and any one of them can be rate limiting. [1, 2]

(i) If the surface is at a sufficiently high temperature the reaction can proceed much more rapidly than the rate at which reactant gases are supplied to the substrate. This results in a mass-transport-limited process.

(ii) If the mass-transport is sufficiently fast, the deposition rate may then be limited by the feed-rate of the reactants to the chamber. In such case, the deposition is feed-rate limited.

In both mass-transport and feed-rate limited conditions the deposition rate is relatively insensitive to temperature. On the other hand, in a surface reaction-controlled process, the rate increases exponentially with temperature according to the Arrhenius relationship. The temperature at which the deposition characteristics become surface reaction or mass transport limited is dependent on: [2]

(i) The apparent activation energy of the reaction.
(ii) The gas flow conditions in the reactor.
(iii) The precursor delivery system.

1.2.3 Film Growth Mechanisms

Film growth takes place when the precursor adsorbs on the surface and diffuses to a growth site. The growth mechanism is dependent on the kind of interactions between the forming film and the substrate. It also depends on the thermodynamics of adsorption, the kinetics of crystal growth and the substrate temperature. Film growth on a surface follows these classical mechanisms (**Fig.1.8**) [3]:

(a) The layer or Franck-van der Merwe growth. The formation of a complete monolayer on the substrate is observed, with the deposited atoms bonded more strongly to the substrate than to each other. This monolayer is further covered with more layers. This growth approach is referred to as simultaneous multilayer growth and its presence depends on the relative rates of nucleation and growth during deposition.

(b) The layer plus island or Stranski-Krastanov growth. Initially layers are deposited until the point where further deposition becomes unfavourable and therefore islands are formed on the previously deposited layers.

(c) The island or Volmer-Webber growth. Islands are initially formed on the substrate by nucleation of small droplets. Growth occurs on these island sites, which subsequently coalesce to form a film. This growth mechanism prevails when the depositing atoms bind to each other more strongly than to the substrate.

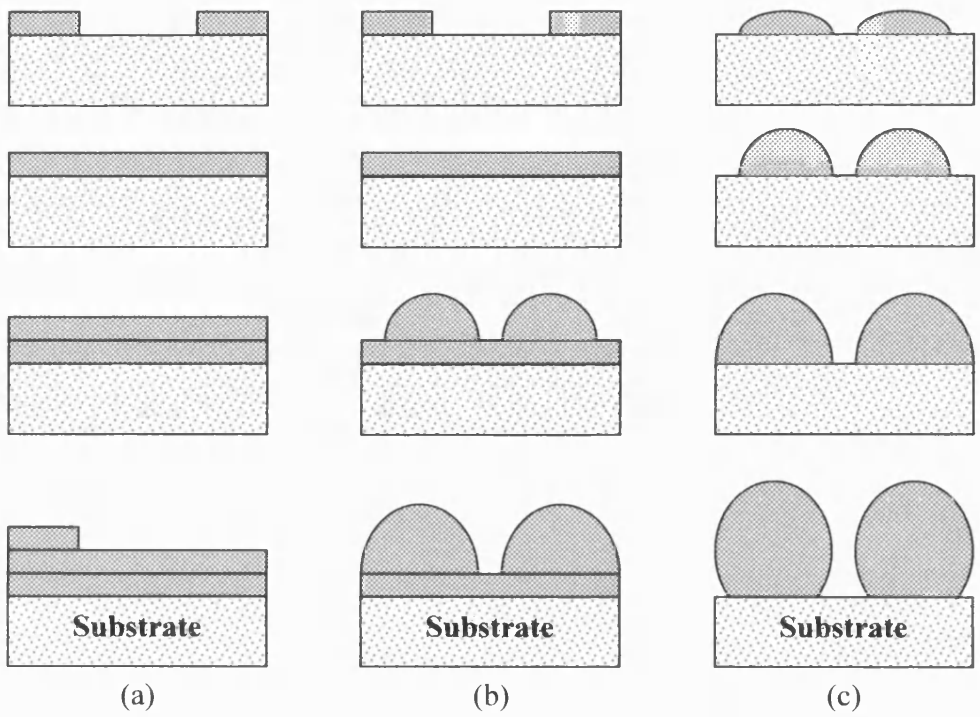

Fig.1.8 Film growth mechanisms. [3]

1.2.4 Reactor Types and Reactor Behaviour

Chemical vapour deposition reactors are often distinguished by the method for heating the substrate and by the operating pressures. In a hot-wall reactor, the substrate, as well as the reactor walls are heated via radiant heating. Deposition occurs on the walls, because they are also hot, as well as on the substrate(s). As a result, the reactor is maintenance intensive. In cold-wall reactors, the substrate is heated to the process temperature and the walls of the reactor are kept at room temperature or just warm enough to prevent condensation of the reactant species. Cold-wall reactors are advantageous because they suppress precursor

depletion due to the lack of deposition on the reactor walls. However, the throughput of cold-wall reactors is typically lower than for hot-wall reactors. [2]

Another consideration in the design of CVD reactors is the operating pressure. For deposition at atmospheric pressure (APCVD) the diffusion of gas species through the boundary layer is often rate limiting. Therefore, a uniform concentration across the substrate surface is difficult to achieve. However, for reactors operating at low pressures (LPCVD) the diffusion coefficients of gaseous species increase and a boundary layer ceases to exist due to the long mean free paths of the gas species. Under these conditions, mass transport to the substrate no longer limits the deposition process and results in a uniform reactant concentration across the surface. However, it is often difficult to control the temperature and therefore the thickness of the film across the substrate for low pressure CVD (LPCVD) processes. This is due to the fact that the deposition rate is surface-reaction limited, which is strongly dependent on temperature.

For certain applications a high substrate temperature is not desirable. An alternative is to transfer energy to the reactant gases in an rf glow discharge to make the species more reactive by the time they reach the wafer surface rather than by relying solely on thermal energy to initiate the chemical reaction. Additionally, bombardment of the surface by radicals and ions can modify the surface reaction pathways. Since the reactants can be in an excited state, the surface reaction can be initiated at a lower substrate temperature. This can be accomplished by plasma-enhanced CVD (PECVD). Both thermal and plasma assisted CVD have been used for depositing metals, metal silicides and metal nitrides, as well as for insulating films such as silicon oxide and silicon nitride used in IC fabrication. [1-3]

A CVD process consists of several factors:

(i) The reactant

(ii) The reactant delivery system

(iii) The reactor

(iv) The substrate

Fig.1.9 shows the processes involved when a precursor is introduced into a CVD reactor as a vapour, droplets of a liquid precursor or solution. If the precursor is delivered in an aerosol form, as particles or droplets then, it must first evaporate into the gas phase before CVD can occur. This forms the basis for aerosol precursor delivery systems. The characteristics of CVD reactors influence all of the processes shown in **Fig.1.9**.

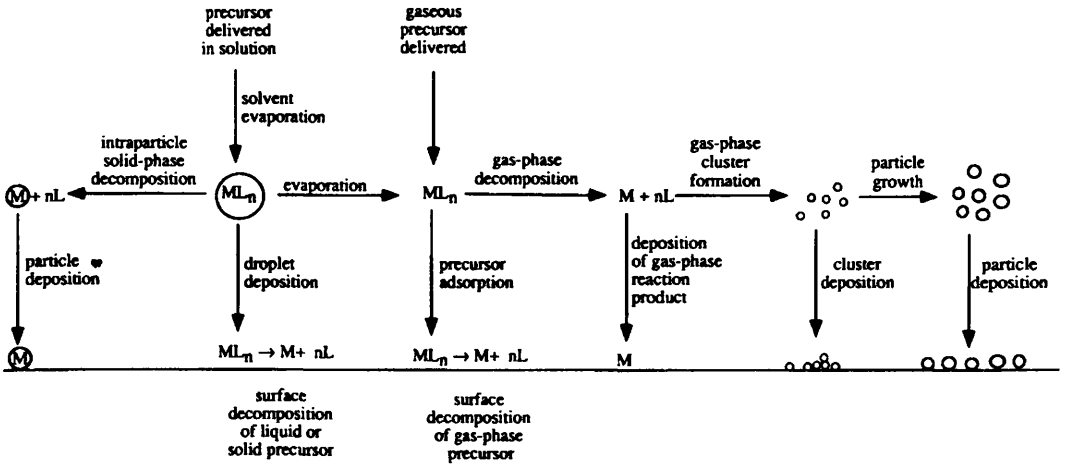

Fig.1.9 Schematic of overall reactor behaviour. [2]

Once the reactant has evaporated or if the reactant is delivered as a vapour into a given type of reactor, the standard reaction pathways are available to the precursor as in **Fig 1.7**. The precursor can be transported to the surface and react to deposit a film. However, the deposition rate can be rate limited by various other steps (e.g. boundary layers, temperature and concentration dependencies). The precursor can also react in the gas phase to form low vapour pressure species, which can nucleate to form particles in the gas phase. Particle deposition in most cases leads to poor film properties and is undesirable.

Depending on the physical properties of the precursor, delivery methods may vary. The method of delivery plays a critical role in CVD, because the overall deposition rate can be limited by the rate of precursor delivery into the reactor. In the best scenario, the precursor is a gas at room temperature, as with IrF_6 and WF_6. In this case, the precursor can be delivered with conventional mass-flow controllers and so, feed rate limitations do not occur. However, metal film precursors are more often liquids or solids, with relatively low vapour pressures

and are generally introduced through bubblers or by direct vaporisation. In some cases the precursors are also thermally unstable which hinders the possibility of high vapour pressures. For these precursors, conventional delivery methods are either unsuitable or provide delivery rates that are slow and result in feed-rate limited deposition. Therefore, two categories of delivery systems have been developed: liquid transport with flash vaporisation and aerosol delivery with evaporation. [2]

Bubblers and Direct Evaporation

This approach relies on direct evaporation or sublimation of precursors with or without carrier gas. For precursors with low vapour pressure, a carrier gas is passed over the heated solid, through a bed of the heated solid or through the heated liquid in a bubbler and then transports the vapour through heated lines to the reactor. This approach is most reliable for liquids, were the carrier gas can be bubbled through the precursor so that constant and reproducible delivery rates can be obtained. A successful application of this approach involves organometallic vapour-phase epitaxy (OMVPE) of semiconductors from liquid metal alkyls, which often have vapour pressures of less than 10 Torr at 25 °C.

Several problems are encountered with this delivery system. Passing the carrier gas over or through a heated solid powder precursor is undesirable because the decrease in surface area of the precursor produces changes in the overall vaporisation rate. This can lead to lower precursor partial pressures and a reduced deposition rate, i.e. changes in the stoichiometry of the film. A further problem is that bubblers must be heated to high temperatures to obtain useful vapour pressures. Under these conditions, the precursor often slowly decomposes. Furthermore, the formation of metal may catalyse the decomposition of the remaining precursor. Condensation in the heated lines can also occur and lead to problems in obtaining constant delivery rates. For these reasons there is a drive to use alternative delivery systems in which the precursors are not held at raised temperatures. [1, 2]

Liquid Delivery

Instead of passing a carrier gas over a hot liquid or solid, the precursor can be fed into a vaporiser as a pure liquid or as a solution where the precursor is continuously vaporised. To provide a constant overall gas flow rate a carrier gas is usually mixed with the precursor in or near the vaporisation region. The precursor vapour is then passed through heated lines to the reactor. A liquid delivery system is suitable for liquids and solutions where the precursor is thermally sensitive and would slowly decompose if heated for extended periods of time. It is also useful for multicomponent systems where several precursors can be dissolved in the same solution. One disadvantage is that the precursor is in contact with a warm surface where chemical reactions can occur over time to give a metal film, which in turn can catalyse the decomposition of the precursor. In addition, the precursor delivery rate is still limited by the vapour pressure of the precursor at the vaporisation temperature.

A variation of liquid delivery is aerosol evaporation. For this approach, the liquid precursor or solution is atomised into droplets, which form a vapour when they come in contact with the hot carrier gas and evaporate. The vapour is then delivered through heated lines to the reactor. [2]

Aerosol Delivery

Aerosol delivery is similar to liquid delivery with aerosol evaporation except that it relies on introducing aerosol droplets directly into the reactor where they evaporate. This technique has been referred to by several names such as: aerosol-assisted CVD (AACVD), spray pyrolysis and pyrosol process spray MOCVD. Droplets evaporate in the reactor because the gas above the substrate is heated. Alternatively, the reactor walls may be warm which also results in gas heating. In both cases, the droplets entering the heated region evaporate (at least partially) before reaching the substrate, after which conventional CVD occurs. [2] Aerosol delivery has several advantages over bubblers and liquid delivery systems. Because the precursors are held outside the reactor at room temperature, thermal degradation of the precursors does not occur. The

precursor delivery rates are constant with time because the concentration of precursors in the solution, the droplet size and delivery rate do not change with time. This allows reproducible deposition of multicomponent films with consistent composition. Precursor vaporisation occurs without contact with hot surfaces and can therefore be performed at higher temperatures, leading to higher partial pressures and higher deposition rates. As a result, feed rate-limited deposition can be avoided. Finally, heat-traced transport lines are not necessary.

One of the disadvantages of this method is that it requires total pressures near atmospheric or high enough so that the droplets do not settle in the reactor before evaporating. Also, heating of the gas at high temperatures and using high pressures favour gas phase reactions, which can result in reduced deposition rates and degraded film properties.

A significant process in aerosol delivery is evaporation of the solvent and precursor, which must occur at least partially before the droplets reach the surface. As solvent vapour pressures are typically much higher than precursor vapour pressures, precursor evaporation is the rate-limiting step for droplet evaporation. Typical droplet generators, such as the ultrasonic systems, produce droplet diameters of less than 10 μm. In addition, it must be noted that droplet evaporation ceases when the partial pressure of the precursor in the gas phase reaches its vapour pressure. This can result in precursor particles being in equilibrium with precursor vapour at the vaporisation temperature, resulting in incomplete vaporisation of the particles. [2]

1.2.5 Precursors

The factors that affect the choice of a particular source molecule for CVD are complex and depend on the application being considered. For example, high-purity dense metal films with smooth surfaces deposited at relatively low temperatures (<500 ^{o}C) and high deposition rates are required for

microelectronic applications. These constraints may be more flexible for other coating applications where, for example, high substrate temperatures can be tolerated or impurities are not detrimental. However, some of the most important general features of CVD precursors are listed below: [1, 3]

(i) Highly volatile, with high vapour pressure for high transport rates.
(ii) Clean decomposition pathways, for high purity films.
(iii) Stability for ease of handling.
(iv) Cheap to manufacture, for use in industry.

Organometallic CVD precursor materials must be prepared in reasonable quantities such that they are available for deposition processes. Therefore, materials that require elaborate synthetic manipulations and handling, have low yields and involve expensive reagents typically preclude their use in the CVD processes. Furthermore, any CVD source complex must be available in very high purity as a solvent free compound. Minimal purity requirements are frequently 99.9 % for most CVD applications, with purities of 99.999 % typically required for the fabrication of microelectronic materials. Ideally, precursor complexes should be air and moisture-stable, non-toxic liquid materials. However, the use of most organometallic species frequently requires compromises in these ideal standards.

The necessity of a relatively high vapour pressure of the precursor complex is important in order to provide adequate concentration of the organometallic species in the vapour phase so that a reasonable deposition rate may be attained. The generally high vapour pressure required for most CVD applications is particularly critical in the formation of sharp boundary heterostructures. Liquid source complexes are the most desirable due to their relative ease in delivery, control in the deposition chamber and elimination of problems such as sublimation onto reactor components. High volatility in a precursor molecule can also be achieved chemically by: [1-3]

(i) Controlling the molecular weight.

(ii) Introducing weak intermolecular interactions

(iii) Employing bulky substituents and/or fluorinated ligands.

For a clean decomposition pathway and high film purity it is necessary for the metal-ligand bond to cleave during the deposition and for the unassociated ligand, or fragment, to be stable enough for elimination from the reaction chamber without contamination of the film. Organic ligands are especially prone to gas-phase and surface-mediated decomposition pathways leading to significant film contamination. Other ligand systems such as phosphines and boranes are also frequently co-deposited with the film under CVD reaction conditions. However, new complexes have been designed to overcome this type of problem. These provide low-energy decomposition pathways leading to clean metal depositions that are both thermodynamically and kinetically favourable. For example, in the deposition of metal containing films from metal alkyls the free metal is formed along with either or both saturated and unsaturated hydrocarbons derived from the alkyl ligand. One of the primary decomposition mechanisms for metal alkyl complexes is referred to as β-elimination and will be discussed in the next section.

CVD precursor complexes must exhibit sufficient thermal stability to be handled and to exist in the gas phase as discrete complexes prior to epitaxial processes. Low temperature CVD conditions are especially important in pattern deposition, deposition on thermally sensitive substrates such as plastics and in the formation of complex heterostructures. Higher temperature depositions can cause severe problems relating to interlayer diffusion, impurity mobility and broad structural features. [1-3]

Precursor Decomposition Pathways

In the overall β-elimination reaction, a metal alkyl complex is converted into a metal hydride and either a co-ordinated or a free alkene. The proposed mechanism is shown schematically in **Fig. 1.10**. [3]

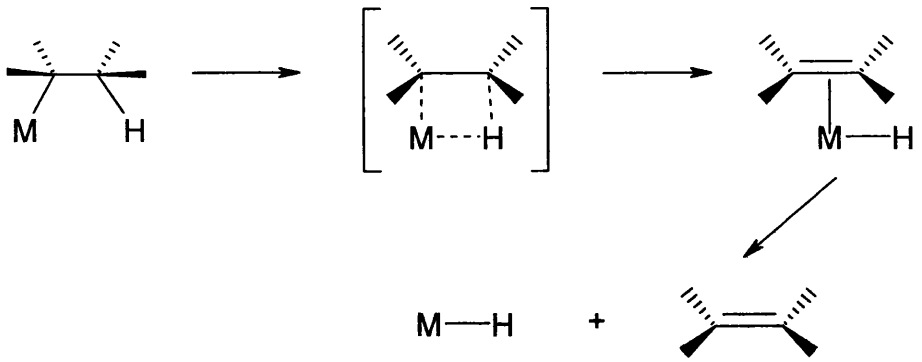

Fig.1.10 β-Hydrogen elimination pathway.

The reaction is thought to proceed through a planar, four co-ordinate metal-alkene hydride intermediate. The hydrogen atom on a β-carbon of a co-ordinated alkyl group is then transferred to the metal centre, forming a hydrido-metal alkene complex. This complex can, in turn, lose either an alkene by dissociation or displacement or an alkane by a reductive elimination step. A typical example of this chemistry is shown in **Fig.1.11**. This reaction sequence typically leads to clean decompositions of metal films.

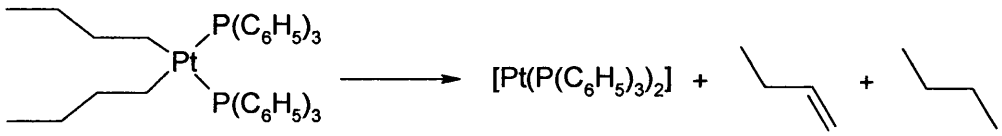

Fig.1.11

Traditionally, the alkyl groups attached on to the metal centre had to be relatively small with just a few carbon atoms in order to avoid carbon incorporation in the depositing film. Tertiary butyl groups, although bulky and hence contributing to minimise molecule aggregation, had the potential to incorporate carbon in the growing film. However, the β-hydrogen elimination mechanism is particularly favourable for tertiary butyl groups since they have three β-hydrogen sites. In addition, the hydrido-metal alkene complex is further stabilised by the electron donating nature of the alkyl groups (**Fig.1.12**) and hence clean decomposition is enhanced for complexes containing tertiary butyl groups on the metal.

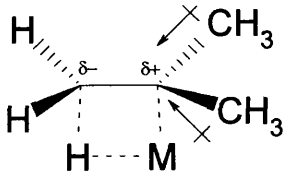

Fig.1.12 The β-hydrogen elimination intermediate where the ligand attached on the metal centre is a tertiary butyl group. The arrows illustrate the stabilising effect of the alkyl groups on the β-carbon on the four-centre intermediate.

The β-elimination process can only occur when a complex has β-hydrogens available for transfer, a co-planar intermediate can be formed and has a vacant *cis* co-ordination site on the metal centre. If these criteria are not met then an α-elimination may result instead.

In a typical α-elimination reaction a hydrogen atom in the α position to the metal centre is transferred to a second alkyl group via a four-centred planar intermediate. The alkane formed is then eliminated to generate a metal alkylidene. This process is summarised in **Fig.1.13.** [3]

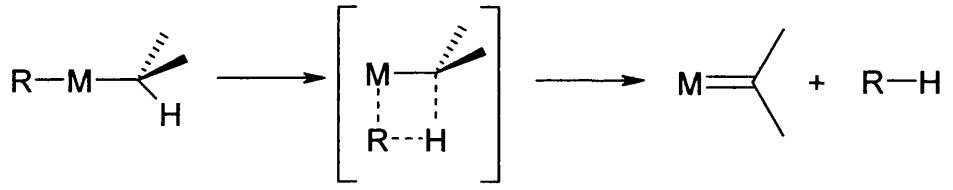

Fig.1.13 α-Hydrogen elimination pathway.

In CVD reactions, the α-elimination process typically leads to large amounts of carbon incorporation into the films because of the formation of surface bound alkylidene analogues.

In some systems the two elimination pathways have been found to compete with one another. It is also believed that many other gas-phase reactions may take place under CVD conditions, such as radical and fragment coupling reactions. [3]

Single-source Precursors

Films containing more than one element are often required. Metal silicides, M_xSi_y, metal nitrides, M_xN_y and mixed metal alloys, $M_xM'_y$ are examples of such materials that are used as contact layers, diffusion barrier layers, and interconnects. The general form of the reactant is MR_x where M is a group II, III, IV, V or VI element and R is the radical, which fractures from the depositing metal. The most common approach for the CVD of these materials is to use two or more different precursors that react individually on the growing film. For example, for group II and III metals the ligands were generally methyl or ethyl radicals, while for group IV, V and VI complexes were primarily metal hydrides:

$$AsH_{3(g)} + Ga(CH_3)_{3(g)} \longrightarrow GaAs_{(s)} + 3\ CH_{4(g)}$$

However, using this strategy makes it difficult to control film stoichiometry. [2] Furthermore, other complications can occur as in the case of InP deposition. A pre-reaction occurs at room temperature, before the reactants reach the decomposition chamber, resulting in the formation of a polymeric liquid. The following diagram summarises the process: [18, 19]

$$InMe_3 + RPH_2 \longrightarrow InP + [MeIn\text{-}PR]_n$$

This is also true for systems depositing GaN (e.g. $Ga(CH_3)_3$ with NH_3). [17] The solution to the pre-reaction problem comes as a modification in the reactor layout. Before the main reactant gas mixture flows in to the reaction chamber, the gas source is separated into two flows, one that carries one reactant and a second flow carrying the other, hence minimising contact before deposition occurs. [17]

Another approach is to use single-source precursors that contain two or more elements (e.g. two metals), in the same molecule. For simplicity, the single-source precursor described (**Fig.1.14**), for the formation of mixed M-M' films, contains the two desired elements (M and M') bonded to each other, with

several ligands attached to each metal centre (L_nM-$M'L'_m$). The desired reaction pathway involves adsorption of the precursor with loss of the supporting organic ligands, L and L', without breaking the M-M' bond. The potential advantages of this approach are: [2]

(i) The stoichiometry of the precursor can be retained in the film.
(ii) The precursor delivery system can be simplified.
(iii) Better homogeneity can be obtained because the desired elements are effectively premixed at the molecular level.

The disadvantages are:

(i) Single-source precursors often have lower vapour pressures than sources of the individual elements, so that delivery and deposition rates are lower.
(ii) The stoichiometry of the precursor is not always retained in the film (depending on the film under consideration).
(iii) Single-source precursors are often commercially unavailable.

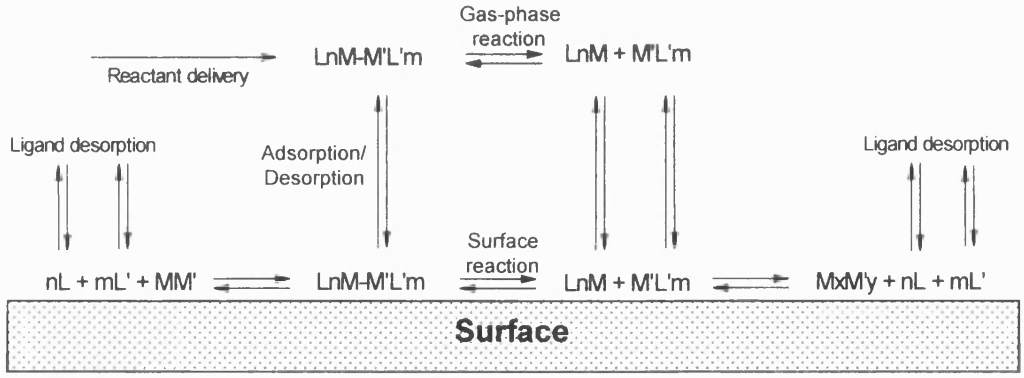

Fig.1.14 Reaction pathways for single-source precursor leading to conservation and loss of precursor stoichiometry. [2]

Fig.1.14 shows how a single-source precursor can form films with non-integral stoichiometry if the M-M' bond breaks to form separate volatile species containing M and M' which desorb at different rates before reacting. This makes it difficult to control film stoichiometry because composition can vary with temperature.

Other complications can occur: the stoichiometry may be achieved even though all the M-M' bonds are broken. In such cases, the elements contained in a single source precursor are not necessarily those found in the final material. For example, labelling studies show that in the deposition of TiN from $Ti(NMe_2)_4$ and NH_3, the N is derived from ammonia rather than the amide ligands ($-NMe_2$). Under these conditions, $Ti(NMe_2)_4$ is only a convenient source of one of the constituent elements of the final film.

$$6\ Ti^{IV}(NMe_2)_4 + 8\ NH_3 \longrightarrow 6\ Ti^{III}N + 24\ HNMe_2 + N_2$$

In other cases, the stoichiometry in the precursor molecule might not be the desired one for the deposited film. However, the loss of one or more metal atoms from the precursor may result in the formation of a film with the desired stoichiometry. For example, $Ga(AsMe_2)_3$ thermally decomposes to form GaAs films, with loss of the corresponding diarsine, As_2Me_4, according to the equation below. [2]

$$Ga(AsMe_2)_3 \longrightarrow GaAs + As_2Me_4 + \text{other products}$$

1.3 Tin Sulfide Materials Chemistry

1.3.1 Introduction

Due to the versatile co-ordinating characteristics of tin and sulfur, tin sulfide-based solid-state materials exhibit a rich structural chemistry. Tin atoms can take a co-ordination number of 2 to 9 and as a result the environment around tin embraces many geometrical arrangements. The most common ones are trigonal pyramidal for divalent tin, tetrahedral, trigonal bipyramidal and octahedral for tetravalent tin. In addition, sulfur chemistry is adorned by its ability to catenate. The catenation length can be as short as in S_2 and as long as in a polymeric sulfur chain, which may contain more than 200 000 sulfur atoms. [6]

As a result of the synthesis of new tin sulfide and polysulfide-based solid-state materials, many new 1D chain, 2D sheet and 3D frameworks have emerged and some of them present interesting optical and electrical properties for device applications. Furthermore, it has proven possible to incorporate other elements into the tin sulfide and polysulfide structures to form ternary or quaternary structures. [6] SnS has an optical band gap of 1.3 eV and its films have potential applications as photovoltaic materials, holographic recording systems and solar control devices. Because of its layered structure it has also found application as a solid-state lubricant. SnS_2, a wider band gap (2.07-2.18 eV) n-type semiconductor, has been much less intensely studied, but it is known that its layered structure (in contrast to the rutile structure of SnO_2) permits

intercalation of alkali metals and metallocenes with resulting increase in conductivity. Sn_2S_3 is a direct forbidden semiconductor with a band gap of 0.95 eV and has highly anisotropic conduction band. However, all of the tin sulfides have excited interest as semiconductors although SnS has elicited most attention, as its electronic band gap is midway between that of silicon and GaAs. [15, 16]

1.3.2 Tin Sulfide Layers – SnS, SnS_2

The German mineralogist R. Herzenberg first reported tin monosulfide, also called herzenbergite. Tin sulfide is a 14-16 semiconductor and has been prepared by the CVD of a mixture of tetramethyl tin, $(Sn(CH_3)_4)$ and H_2S as well as by the bulk decomposition of the cyclic compound $(Ph_2SnS)_3$. [5] It can also be prepared in the laboratory by reacting stoichiometric Sn and S elements over a temperature range of 600-750 °C.

The structure of tin monosulfide corrugated double layers is shown in **Fig 1.15**.

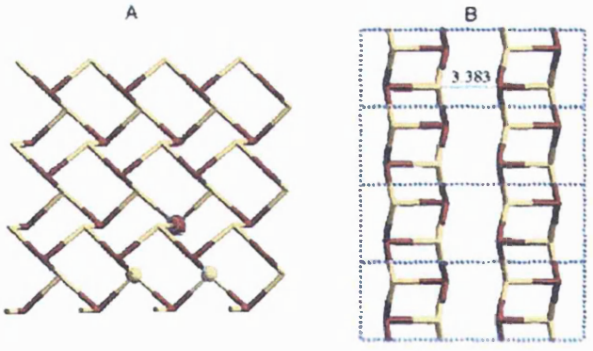

Fig.1.15 The layered structure of SnS with one distorted SnS_6 octahedron highlighted (the sixth sulfur apex on the neighbouring tin sulfide layer is not shown). [6]

Each tin atom is co-ordinated by six sulfurs in a highly distorted octahedral geometry with the tin actually displaced towards one of the octahedral faces (**Fig1.15a**). This leads to three short (*ca.* 2.7 Å) and three long (*ca.* 3.4 Å) Sn-S

bonds. In addition, there are two SnS layers in the unit cell and one of the long distance sulfurs actually resides on the neighbouring SnS layer. This weak Sn-S interaction binds the two sulfide layers together to form a double-layer structure (**Fig 1.15b**).

Tin disulfide is probably the first known tin sulfide material and its laboratory synthesis can be traced back over two hundred years. It can be prepared by the chemical vapour transport technique (CVT) at a temperature range of 600-800 ^{o}C, using I_2 as a transport agent. Tin disulfide adopts the PbI_2/CdI_2 layered structure with a hexagonal unit cell in which the tin atoms are located in the octahedral sites between two hexagonally close-packed sulfur slabs to form a sandwich structure, as shown in **Fig 1.16**.

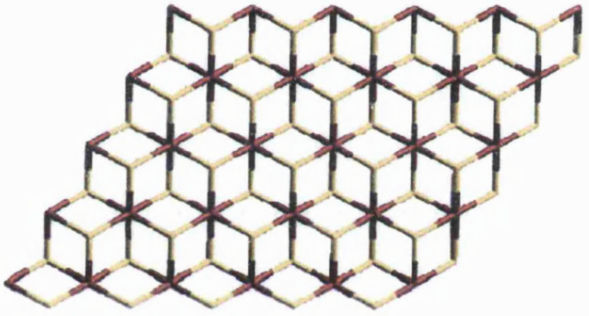

Fig.1.16 The dense-packed layered structure of SnS_2. [6]

The SnS_2 layer can be viewed as composed of all-edge-sharing octahedral SnS_6 building blocks with the sulfur atoms being three co-ordinate and exhibiting local trigonal pyramidal geometry. The layers are then stacked on top of each other along the crystallographic *c*-axis and held together by weak Van der Walls forces. [6]

There are many ways to stack SnS_2 layers together leading to various polytypes. More than 70 polytypes have been identified via single crystal structure analysis. All of the polytypes have the same hexagonal close-packed structure within the layer and therefore have identical unit cell parameter *a* (3.647 Å). However, they exhibit a different parameter *c* orthogonal to the layer. One

crystallite of SnS_2 often contains domains of different polytypes and the structural details have to be extracted from a mixed-phase crystal, making therefore the determination of SnS_2 polytype structure a difficult task. [6]

In view of the many stoichiometries of tin and sulfur in stable sulfide materials, like SnS, SnS_2, Sn_2S_3 and Sn_4S_5, it has been suggested that it is the versatile bonding nature of tin and sulfur that is responsible for the many stoichiometric, non-stoichiometric and lattice site-deficient structures of tin sulfides and the occurrence of polytypes. [6]

1.3.3 Tin Sulfide Chains - Sn_2S_3

Tin sesquisulfide, Sn_2S_3, is one of the tin sulfide minerals. It was named ottemannite after its discovery by the German mineralogist J.Ottemann. Sn_2S_3 is the best-known mixed-valence tin sulfide and has an aesthetic ribbon structure as shown in **Fig 1.17**.

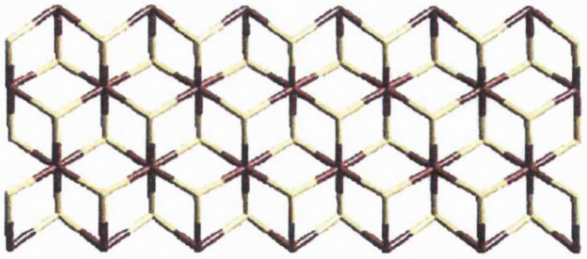

Fig.1.17 The ribbon structure of Sn_2S_3, trigonal pyramidal Sn (II) located at the edge and octahedral Sn (IV) at the centre of the ribbon. [6]

The tin (IV) sites in the ribbon are octahedrally co-ordinated with Sn-S distances of 2.459-2.604 Å. The tin (II) sites on the edge of the ribbon have typical trigonal pyramidal geometry with two Sn-S distances of 2.645 and 2.765 Å. At least three polytypes of Sn_2S_3, *i.e.* α-$Sn_{2\pm x}S_3$, β-$Sn_{2\pm x}S_3$ and γ-Sn_2S_3, have been identified. [6]

1.3.4 Tin Sulfide Film Production

Tin sulfide thin films have received scant attention compared to the extensive thin film technology of materials such as silicon and gallium arsenide. In the past three decades various synthetic approaches including solid-state reactions, hydrothermal or organothermal synthesis and molten salt (flux) methods have been employed in the search for new tin sulfide and/or polysulfide-based solid state materials, especially those with open-framework structures. [6] Tin sulfide films have been prepared by spray pyrolysis, melt growth, electrodeless deposition and chemical baths, while bulk SnS has been prepared *inter alia* by thermal decomposition of the molecular precursors $(Ph_3Sn)_2S$ (300 °C) and $(BzSnS)_3$ (450 °C). However, in contrast to the preparation of tin oxide films where chemical vapour deposition (CVD) from an appropriate precursor(s) is common, this methodology has been largely ignored for tin sulfide films. [16]

Chemical baths have been used to deposit a range of tin sulfide films. A bath containing $SnCl_2$, $Na_2S_2O_3$ and EDTA in aqueous solution has been used to deposit SnS on glass and titanium substrates. A solution of $SnCl_2$, ammonia, thioacetamide and glacial acetic acid has been used to grow films on the sides of suspended glass slides at 75 °C. A dipping method has been used to form tin sulfide films by the alternating immersion of glass slides into solutions containing Na_2S and $SnCl_2$. Tin (IV) sulfides have also been grown by dip-coating. Tin sulfide films produced from chemical baths showed the presence of significant impurities, required post treatment to produce crystalline films and were poorly adhesive. Improved tin sulfide films have been grown at the anode in cyclic voltammetry experiments and from spray-pyrolysis using $SnCl_2$ and dimethylthiourea. Furthermore, gas-phase deposition methods have included limited examples of low pressure and plasma assisted CVD. Plasma enhanced CVD reaction of $SnCl_4$ and H_2S at 100-350 °C produced SnS films on small silica substrates but were contaminated with chlorine and elemental sulfur. Organometallic precursor routes to tin sulfide films on CaF_2/MgF_2 substrates were reported by reaction of tetraalkyltin species (Me_4Sn, Et_4Sn) with hydrogen sulfide and hydrogen at 600 °C. Although the materials were only characterised

by thickness measurements and colour, the authors speculated that SnS formed because of the reducing conditions employed in the experiment. [15, 16]

Molloy and Parkin et al. have instituted an intensive study of tin sulfide film deposition on glass substrates by atmospheric pressure (APCVD) and aerosol-assisted (AACVD) CVD. Reaction of tin tetrahalides ($SnCl_4$, $SnBr_4$) [7-9] with H_2S under APCVD conditions provided a facile route to high quality, phase-pure, uniform, conventional sulfides on glass substrates. The tin sulfides deposited in the experiments were directly related to the substrate temperature and were invariant of the precursor concentration. At 300-500 °C single-phase SnS_2 was deposited, at 525 °C Sn_2S_3 was formed, while at 550 °C and above single-phase SnS was observed. The study was then expanded to other tin sources involving organotin carboxylates ($Bu_3SnO_2CCF_3$) [10] from which only one phase of tin sulfide (SnS) was produced at 300-550 °C using H_2S as a co-reagent.

The next goal was to produce single-source precursors to tin sulfide coatings. A range of volatile precursors such as $Sn(SCH_2CF_3)_4$ and $Sn(SPh)_4$ [11, 13] were investigated. These homoleptic materials contain an all sulfur primary co-ordination sphere and would be expected to form tin sulfide films under CVD conditions. Unfortunately, all of these single source systems failed to deposit tin sulfides in the absence of H_2S. Ultimately, this failure was tracked to the facile disulfide (RSRS) elimination pathway. Subsequent molecular orbital calculations revealed that the general class of $M(SR)_4$ (M = Group IV elements) molecules suffer significant distortions from tetrahedral geometry because of the non-covalently bonded S···S interactions. This distortion and the *cis*-annular interaction promoted the disulfide elimination pathway. However, all of the single-source precursors could be made to deposit tin (II) sulfide coatings by employing a minimal flow of H_2S in the system. [15] In this view, chelating dithiolates e.g. $Sn(SCH_2CH_2S)_2$ were also used to deposit tin sulfide films and were found to obviate the need for H_2S as a co-reagent. [12]

1.4 Production and Properties of Other Metal Sulfides

Numerous metal sulfides possess valuable opto-electronic properties, including semiconductivity, photoconductivity and luminescence. CVD is a promising technique for the preparation of metal sulfide films and has been widely employed. [2]

1.4.1 Transition Element Sulfides

There is a great deal of work concerning II-VI materials but it is out of the scope of this thesis to examine these materials in detail. Therefore, only a brief insight on their uses is mentioned here. Group II-VI materials are presently important for optoelectronics in device applications at opposite spectral regions, as well as photovoltaics. The two applications are the blue and near UV emitters (ZnS, ZnSe) and the near to far IR detectors (HgCdTe). [5] Thin layers of mercury(II) sulfide have been prepared by evaporation and sputtering methods. They are useful in ultrasonic transducers, image sensors, electrostatic imaging materials and photoelectric conversion devices. The formation of ternary alloys between HgS and PbS has also been established and is well investigated. [20]

Titanium disulfide, TiS_2, is a desirable cathode material for lithium batteries. It is also used as a catalyst in the hydrodesulfurization process and as a lubricating component in titanium alloys. CVD has been employed widely for the preparation of TiS_2 thin films. [5]

The compound can be prepared by the CVD of $TiCl_4$ and H_2S or by an activated reactive evaporation process, consisting of sublimation of elemental titanium into a plasma containing H_2S. The decomposition of a mixture of $TiCl_4$ and t-butylthiol also has been used to deposit TiS_2. Other alkyl thiols are equally effective in this reaction, however, the vapour pressure of t-butylthiol rendered it to be the best suited for this experiment. Titanium tetrachloride reacts with cyclohexylthiol to form the adduct $[TiCl_4(C_6H_{11}SH)_2]$. This compound decomposes at temperatures between 200 and 600 °C to yield TiS_2. The titanium

thiolate compound $Ti(^tBuS)_4$ decomposes at temperatures as low as 100 °C to give TiS_2. [5]

Several diverse markets have been proven for MoS_2, as a combination of its physical and chemical characteristics. As a consequence of its layered structure, MoS_2 possesses properties that make it an important solid lubricant material. Its lubricating properties extend over a large range of temperatures and pressures and make MoS_2 an ideal lubricant for high temperature and low-pressure applications, whenever the use of liquid lubricants becomes impractical. Molybdenum disulfide is a semiconductor and its band gap is in the optimum range for solar energy conversion. Additionally, its layers can be intercalated with lithium atoms making it a promising material for solid-state secondary lithium batteries.

Molybdenum disulfide can be prepared by CVD using $MoCl_5$, MoF_6 or $Mo(CO)_6$ as the molybdenum source. The sulfur source in each case is hydrogen sulfide. The molybdenum tetrakis(thiolate) compound, $Mo(S^tBu)_4$, is a unimolecular precursor to MoS_2 and decomposes at temperatures as low as 100 °C. [5]

Tungsten disulfide shows properties similar to MoS_2 and has been prepared by the CVD of $W(CO)_6$ in the presence of H_2S. [5]

1.4.1 Main Group Element Sulfides

Rare earth element-doped alkaline earth sulfides are employed in luminescence-based devices like thin film electroluminescent displays and devices for optical data storage. Strontium sulfide, SrS, thin films have been prepared by atomic layer epitaxy from [Sr(tmhd)$_2$ in the presence of H_2S. [5] CaS thin films have been deposited by aerosol-assisted CVD from the polyether adduct single-source precursor $Ca(SOCMe)_2 \cdot 15$-crown-5. [21] Barium is a constituent of some technologically important thin film materials such as high T_c superconductor YBa_2CuO_{7-x} and ferroelectric $BaTiO_3$ and $Ba_xSr_{1-x}TiO_3$. In addition, BaS is a

potential though scarcely examined phosphor host material for thin film electoluminescent (TFEL) displays. [22]

The composition C_3S is an organic semiconductor, which follows Ohm's law up to a temperature-dependent threshold voltage (1-10 V). The compound is prepared by passing CS_2 vapour over an incandescent tungsten filament. [5]

Silicon sulfide is the base material for a novel class of fast Li^+ conductors for use in solid-state battery applications. The material can also be used in infrared transparent fibres and films. A compound of the composition SiS_x:H (x=1.6-2.5) has been prepared by remote plasma enhanced chemical vapour deposition using SiH_4 and H_2S as precursors. [5]

Amorphous germanium disulfide shows a photoinduced change of its chemical and physical properties when exposed to light. The changes are caused by structural transformations and lead to a shift of the absorption edge to lower or higher energy (photodarkening / photobleaching). Applications of such materials include media for optical imaging or storage, IR-transparent films and employment as an inorganic photoresist. Amorphous Ge_xS_{1-x} has been prepared by plasma-enhanced CVD of a mixture of GeH_4 and H_2S. [5]

Lead sulfide is a photoconductor with an exceptionally high response in the near IR region. It has been prepared by atomic layer epitaxy using lead halides, lead acetate or lead bis(β-diketonate) compounds as the lead source and H_2S as the sulfur source. Another route to PbS is atomic layer epitaxy using $Pb_4O(O^tBu)_6$ or polymeric $[Pb(O^tBu)_2]$ and H_2S as precursors. [5]

Amorphous As_2S_3 is a chalcogenide semiconductor. Like GeS_2 it shows structural transformations when exposed to light and is employed in optical imaging and storage devices. Arsenic sulfide has been prepared by CVD of a mixture of arsine (AsH_3) and hydrogen sulfide. [5]

Bismuth(III) sulfide has attracted considerable interest in the recent years due to its potential application in thermoelectric coolers and photodiode arrays. Thin films of Bi_2S_3 have been prepared by the drip-dry method, chemical deposition from solution and spray pyrolysis. Furthermore, single-source precursors (e.g. $Bi(S_2CNEt)_3$ and $Bi(S_2CNMe^nHex)_3$) have been employed in LP-MOCVD to produce Bi_2S_3 thin films. [23]

1.5 Aims

The specific aim of the study reported in this thesis was to prepare and characterise compounds that might be useful in the deposition of metal sulfides. So far, as it has been discussed in the introduction, the precursors synthesised for the deposition of tin sulfide films do so by a temperature-controlled mechanism, often requiring H_2S. As decomposition temperatures increased tin sulfides were obtained according to the following series SnS_2, Sn_2S_3 and finally SnS. There is the need however for single-source precursors that deposit different types of tin sulfides directly, by control of the decomposition mechanism rather than by control of the decomposition temperature. Hence, in search for new single-source precursors to tin sulfide films a study was undertaken during which tin dithiocarbamate derivatives were utilised for the deposition of SnS_x-type of materials. [16] The results of this study are presented in chapter two of this thesis.

Furthermore, the second aim of this research project was to investigate the synthesis of mixed organotin/transition metal sulfides as precursors for mixed-metal, ternary Sn-M-S thin films. The goal was to produce single-source precursors to transition metal-doped tin sulfide coatings. The precursors were designed with the assertion that on decomposition the required coating would be formed by maintaining the metal-S-Sn fragment. [16] The design of such molecules was inspired by the fact that doping of semiconductors enhances their conductivity. Therefore, by introducing a transition metal (i.e. doping) within the layered structure of the organotin sulfides a novel material with enhanced semiconducting properties could potentially be obtained. [14]

1.6 References

[1] J. Vossen, W. Kern, 'Thin Film Processes', Academic Press, New York, 1978, Ch III-2.

[2] T. Kodas, M. Hampden-Smith, 'The Chemistry of Metal CVD', VCH, 1994, Ch 1, 3, 6, 8, 9.

[3] K. D. Karlin, *Prog. Inorg. Chem.*, 1994, **41**, 145.

[4] A.C. Jones, P. O'Brien, 'CVD of Compound Semiconductors', VCH, 1997, Ch 1, 7.

[5] W. S. Rees, Jr., 'CVD of Nonmetals' VCH, 1996, Ch 4, 7.

[6] T. Jiang, G. A. Ozin, *J. Mater. Chem.*, 1998, **8**, 1099.

[7] L. S. Price, I. P. Parkin, A. Hardy, R. Clark, T. G. Hibbert, K. C. Molloy, *Chem. Mater.*, 1999, **11**, 1792.

[8] L. S. Price, I. P. Parkin, T. G. Hibbert, K. C. Molloy, *Adv. Mater.*, 1998, **4**, 222.

[9] I. P. Parkin, L. S. Price, A. Hardy, R. Clark, T. G. Hibbert, K. C. Molloy, *J. Phys. IV.*, 1999, **9**, Pr8.

[10] L. S. Price, I. P. Parkin, M. Field, A. Hardy, R. Clark, T. G. Hibbert, K. C. Molloy, *J. Mater. Chem.*, 2000, **10**, 527.

[11] G. Barone, T. G. Hibbert, K. C. Molloy, M. F. Mahon, L. S. Price, I. P. Parkin, A. Hardy, M. Field, *J. Mater. Chem.*, 2000, **11**, 464.

[12] I. P. Parkin, L. S. Price, T. G. Hibbert, K. C. Molloy, *J. Mater. Chem.*, 2001, **11**, 1486.

[13] T. G. Hibbert, M. F. Mahon, K. C. Molloy, I. P. Parkin, L. S. Price, *J. Mater. Chem.*, 2001, **11**, 469.

[14] T. G. Hibbert, A. T. Kana, M. F. Mahon, K. C. Molloy, L. S. Price, I. P. Parkin, M. M. Venter, *Main Group Met. Chem.*, 2001, **24**, 633.

[15] A. T. Kana, T. G. Hibbert, M. F. Mahon, K. C. Molloy, I. P. Parkin, L. S. Price, *Polyhedron*, 2001, **20**, 2989.

[16] G. Barone, T. Chaplin, A. T. Kana, T. G. Hibbert, M. F. Mahon, K. C. Molloy, I. D. Worsley, I. P. Parkin, L. S. Price, *J. Chem. Soc., Dalton Trans.*, 2002, 1085.

[17] C. C. Yang, C. K. Huang, G. C. Chi, M. C. Wu, *J.Cryst.Growth*, 1999, **200**, 39.

[18] H. H. Abdulridha, J. E. Bateman, R. C. Crowte, P. Hoye, A. C. Jones, R. Padda, D. G. Patrikarakos, M. E. Pemble, *J.Cryst.Growth*, 1994, **145**, 485.

[19] H. H. Abdulridha, J. E. Bateman, G. H. Fan, M. E. Pemble, I. M. Povey, *J. Electrochem. Soc.*, 1994, **141**, 1886.

[20] M. Z. Najdoski, I. S. Grozdanov, S. K. Dey, B. B. Siracevska, *J. Mater. Chem.*,1998, **8**, 2213.

[21] K. Kunze, L. Bihry, P. Atanasova, M. J. HampdenSmith, E. N. Duesler, *Chem. Vap. Deposition.*, 1996, **2**, 105.

[22] V. Saanila, J. Ihanus, M. Ritala, M. Leskelä, *Chem. Vap. Deposition.*, 1998, **4**, 227.

[23] O. C. Monteiro, T. Trindade, J. H. Park, P. O'Brien, *Chem. Vap. Deposition*, 2000, **6**, 230.

CHAPTER TWO

The Synthesis, Characterisation and CVD Properties of Homo- and Heteroleptic Tin(IV) Thiolates and Dithiocarbamates.

2.1 Introduction

As mentioned in the introduction chapter, in the search for the ideal single-source precursor for the deposition of tin sulfide films compounds such as $(PhS)_4Sn$ and $Sn(CH_2CF_3)_4$ were tested. It was found that they required the presence of H_2S during deposition in order to avoid tin oxide formation. However, when a precursor incorporating a chelating disulfide ligand, $Sn(SCH_2CH_2S)_2$, [6] was tested it was found that it deposited mostly SnS, most importantly in the absence of H_2S. However, while $Sn(SCH_2CH_2S)_2$ does not need the presence of H_2S in producing tin sulfide films, the final product is, as for previous precursors, solely determined by temperature (*i.e.* SnS_2 is obtained at lower temperatures while SnS at higher). Hence, a precursor is sought after which will have such a decomposition mechanism that will directly result in the formation of a specific type of tin sulfide without the need for temperature control. An alternative method of tailoring the decomposition pathway of single-source precursors is by using dithiocarbamate (chelating) ligands, both homoleptically and in conjunction with thiolates.

Dithiocarbamate complexes are good candidates as precursors for metal sulfide preparations since their lower alkyl derivatives are generally crystalline solids but significantly volatile. Furthermore, it is well known that the solid-state pyrolysis of dithiocarbamate complexes, under an inert atmosphere, generally gives the corresponding metal sulfide. However, the stoichiometry and phase of metal sulfide deposited are strongly dependent on the pyrolysis conditions. [14]

In this chapter the preparation, characterisation and properties of a number of further CVD candidates is evaluated. Dithiocarbamate derivatives of tin were considered the most promising species, as analogous compounds have been used effectively in other areas of metal chalcogenide deposition (see chapter one). In addition to homoleptic tin dithiocarbamates, heteroleptic species containing both dithiocarbamate and thiolate ligands have also been considered, i.e. $(R_2NCS_2)_n(RS)_{4-n}Sn$, as possible precursors. From the CVD perspective the use of hybrid alkoxide/β-diketonates is widespread [15] but an analogous strategy

for hybrid thiolate/dithiocarbamates has not been exploited in the metal sulfide preparation. These materials, $(R_2NCS_2)_n(RS)_{4-n}Sn$, contain an all-sulfur primary co-ordination sphere and would be expected to form tin sulfides under CVD conditions.

2.2 Results and Discussion

2.2.1 Synthesis and Characterisation

During this study a selected range of compounds was synthesised and tested for their suitability as CVD precursors. Tetrakis-(diethyldithiocarbamato)tin(IV) (**1**) was synthesised by a literature route from $SnCl_4$ and $[Et_2NCS_2]Na$. [7] The structure of this compound is known showing that two of the dithiocarbamate ligands are bidentate, while the other two monodentate (see **Eq. 2.1**).

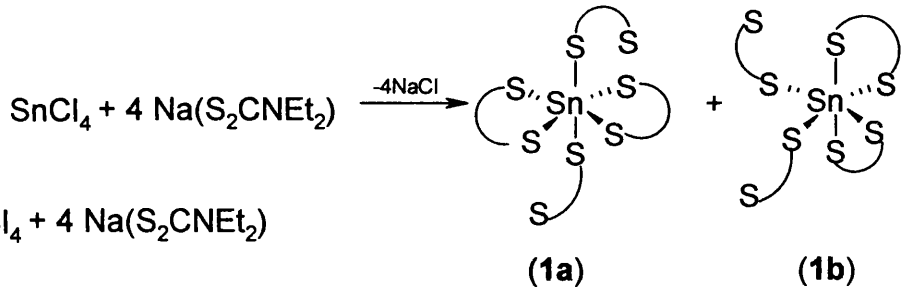

Eq. 2.1 *trans*-(**1a**) and *cis*-(**1b**) isomers of $Sn(dtc)_4$ (**1**) in solution.

The ^{119}Sn NMR spectrum of an analytically pure sample of (**1**), $(Et_2NCS_2)_4Sn$, showed three, closely spaced resonances at -766 (100%), -764 (30%) and -768 (32%) ppm that can be assigned to the presence of both *trans*-(**1a**) and *cis*-(**1b**) isomers of (**1**). Speculatively, the major resonance can be assigned to isomer (**1a**) whose solid state structure has been determined. One of the remaining species is likely to be isomer (**1b**), while the third is probably one of (**1a**) or (**1b**) in which the orientation of the dative and covalent Sn-S bonds in the two monodentate dithiocarbamate groups differ.

$Sn(dtc)_4$ (**1**) dissolved in either $CHCl_3$ or CH_2Cl_2 undergoes decomposition on standing even at room temperature. This is evidenced by the consequent colour change from bright orange to pale yellow. The process can be accelerated by heating. (**Eq. 2.2**).

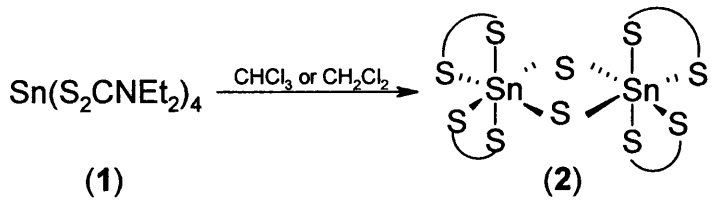

Eq. 2.2 Decomposition of (**1**) in chlorinated solvents.

After 24 hours at room temperature the ^{119}Sn NMR of (**1**) shows a new resonance at -736 ppm which is identical to that shown by a solution of crystals of the dimeric sulfide $[(Et_2NCS_2)_2SnS]_2$ (**2**). However, a second species also appears in the NMR spectrum ($\delta(^{119}Sn)$= -705 ppm) and although this has not been identified, it is not *cis*-$(Et_2NCS_2)_2SnCl_2$ ($\delta(^{119}Sn)$= -519 ppm). [9]

The mechanism of formation of (**2**) is of importance, since the appearance of the signal due to (**2**) in the ^{119}Sn NMR spectrum of (**1**) is accompanied by a decrease in the intensity of the minor signal at -768 ppm, which was assigned to the *cis*-(**1b**) isomer of compound (**1**). The decrease in intensity of the signal for (**1b**) can be attributed to the fact that the *cis*-arrangement of the dithiocarbamate ligands is vital in the formation of (**2**), since (**2**) has the same *cis* stereochemistry as isomer (**1b**). Therefore, in the conversion of (**1**) into (**2**) the minor isomer (**1b**) appears to act as an intermediate.

The existence of a *cis*-(**1b**) isomer of (**1**) can be further suggested by comparing the above observations to the chemical behaviour of the unsymmetrical dithiocarbamate $[^nBu(Me)NCS_2]_4Sn$. ^{119}Sn NMR data for $[^nBu(Me)NCS_2]_4Sn$, show only one resonance at -786 ppm due to the fact that the dithiocarbamate ligands are all bonded in the same manner to tin. [1] In addition, the unsymmetrical dithiocarbamate $[^nBu(Me)NCS_2]_4Sn$ fails to react with either

$(RS)_4Sn$ [1] or to undergo decomposition in chlorinated solvents to give a sulfide-bridged dimer analogous to (**2**). Therefore, since a *cis*-stereochemistry of the dithiocarbamate ligands is vital for the formation of (**2**), it is the absence of a *cis* isomer of $[^nBu(Me)NCS_2]_4Sn$ that is responsible for its unreactivity.

Compound (**2**) can also be synthesised by adding sublimed sulfur to a THF solution of $Sn(dtc)_2$ and stirring at room temperature. **Eq 2.3** summarises the process. The yields for both methods are comparable and modest, ranging from 33 to 40%.

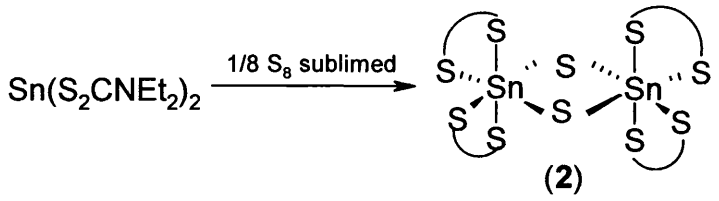

Eq. 2.3 Synthesis of (**2**) from $Sn(dtc)_2$.

Pale yellow crystals of (**2**) were isolated from chloroform and were identified by X-ray crystallography as the dimeric sulfide $[(Et_2NCS_2)_2SnS]_2$ (**2**). **Fig. 2.1** shows the structure of (**2**) and **Table 2.1** summarises relevant bond lengths and angles. Crystals of (**2**) were grown from both chloroform and THF.

The sulfide bridges enforce a *cis*, *cis*, *cis* geometry around the tin atom. The Sn-S (sulfide) bonds (2.4454(5), 2.4550(5) Å) are typical of other dimeric organotin sulfides containing six-co-ordinate tin, e.g. $\{[CyNC(Me)NCy]_2Sn\}_2S$ with sulfide bond lengths of 2.434 and 2.476 Å. [10] However, the bridging Sn-S bonds are longer than in other analogous dimers in which tin is only four-co-ordinate, e.g. $(^tBu_2SnS)_2$ with bond lengths of 2.419 and 2.441 Å. [11]

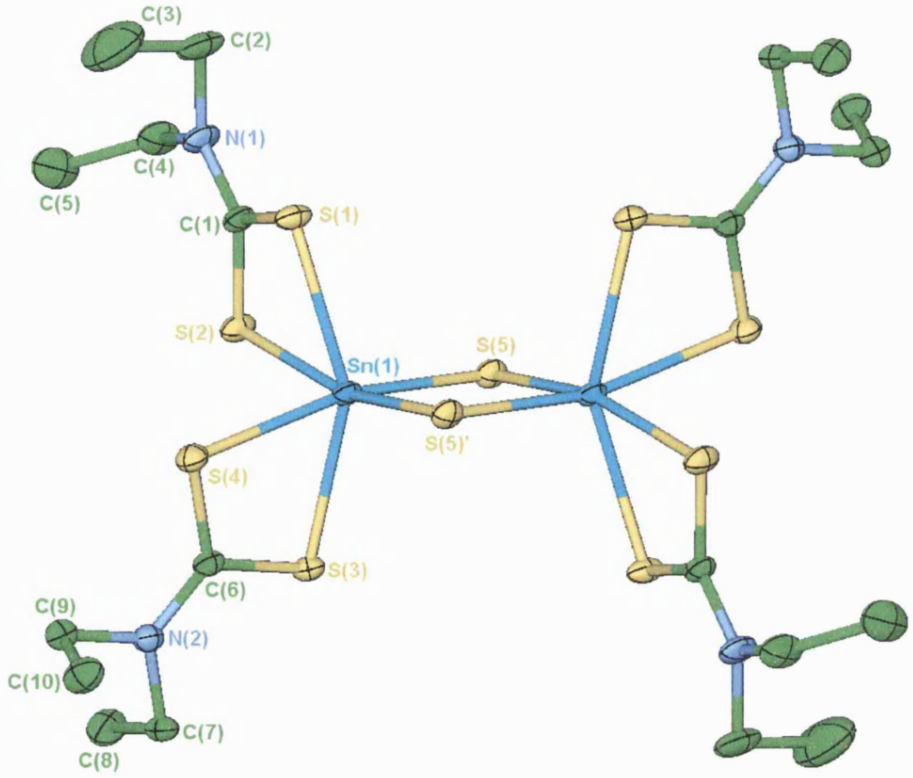

Fig. 2.1 The molecular structure of (**2**). Thermal ellipsoids are at the 30% probability level. Primed atoms are related to their unprimed counterparts in the asymmetric unit by -x+2, -y, -z+1.

The two dithiocarbamate groups chelate in an anisobidentate manner, i.e. one of the Sn-S bonds of the chelating dithiocarbamate is longer than the other. The bond lengths for each pair of ligands are, respectively, 2.5676(5), 2.5986(5) and 2.5772(5), 2.6075(5) Å, with the longer Sn-S bond in each dithiocarbamate being *trans* to a bridging sulfur.

Bonds (Å)		Angles (°)	
Sn(1)-S(1)	2.5676(5)	S(1)-Sn(1)-S(2)	69.84(2)
Sn(1)-S(2)	2.5986(5)	S(1)-Sn(1)-S(3)	89.30(2)
Sn(1)-S(3)	2.6075(5)	S(1)-Sn(1)-S(4)	150.03(2)
Sn(1)-S(4)	2.5772(5)	S(1)-Sn(1)-S(5)	98.96(2)
Sn(1)-S(5)	2.4454(5)	S(1)-Sn(1)-S(5')	100.74(2)
Sn(1)-S(5')	2.4550(5)	S(2)-Sn(1)-S(3)	88.74(2)
		S(2)-Sn(1)-S(4)	88.21(2)
		S(2)-Sn(1)-S(5)	168.75(2)
		S(2)-Sn(1)-S(5')	89.60(2)
		S(3)-Sn(1)-S(4)	69.44(1)
		S(3)-Sn(1)-S(5)	92.31(1)
		S(3)-Sn(1)-S(5')	168.56(2)
		S(4)-Sn(1)-S(5)	102.65(2)
		S(4)-Sn(1)-S(5')	99.19(2)
		S(5)-Sn(1)-S(5')	91.53(2)

Table 2.1 Summary of selected metric data for compound (**2**).

In order to increase the variety of compounds available for CVD trials mixed thiolate/dithiocarbamate derivatives of tin(IV) were synthesised. Compound (**1**) was stirred at room temperature with $(RS)_4Sn$ in toluene giving the product $(Et_2NCS_2)_2(RS)_2Sn$. This was the only product obtained from this reaction regardless of the stoichiometric quantities used (**Eq. 2.4**)

$$(Et_2NCS_2)_4Sn + (RS)_4Sn \longrightarrow 2\ (Et_2NCS_2)_2(RS)_2Sn$$

R = Cy (**3**), Ph (**4**)

Eq. 2.4

Compound (**4**) has also been obtained from the reaction of $(PhS)_4Sn$ with $Cu(dtc)_2$

In addition (**4**) has also been prepared previously by the reaction of $[Ph_4P^+][(PhS)_3Sn^-]$ with tetraethyldithiuram disulfide. [1] **Eq. 2.5** summarises the process.

$$[Ph_4P^+][(PhS)_3Sn^-] + (Et_2NCS_2)_2 \longrightarrow (Et_2NCS_2)_2(PhS)_2Sn + [Ph_4P^+][PhS^-]$$

Eq. 2.5

Compounds (**3**) and (**4**) are characterised by large upfield shifts in their ^{119}Sn NMR resonances (-649 and -666 ppm, respectively), in contrast to the downfield shifts of the four co-ordinate species $(RS)_4Sn$, e.g. $(CyS)_4Sn$ ($\delta(^{119}Sn)$ = 109.0 ppm) [13] and $(PhS)_4Sn$ ($\delta(^{119}Sn)$ = 48.2 ppm). [5]

The crystal structure of (**3**) is shown in **Fig. 2.2** and **Table 2.2** summarises relevant bond lengths and angles.

It can be seen that the dithiocarbamate ligands in (**3**) adopt a *cis* conformation in contrast to the *trans* conformation found for (**1**), while the thiolate ligands are also mutually *cis*. The Sn-S (thiolate) bond lengths are identical (2.450(1) Å), but somewhat longer than those in four co-ordinate $(CyS)_4Sn$ (2.382(1) Å). [13] The two dithiocarbamate ligands are also equivalent, both being slightly anisobidentate and the Sn-S (dithiocarbamate) bond lengths being 2.570(1) and 2.618(1) Å. In all comparable diorganotin bis(dithiocarbamate) structures the bidentate dithiocarbamates are also anisobidentate, but with a greater difference in bond lengths than the one observed for (**3**). Furthermore, the S-Sn-S angle involving the two thiolate ligands is quite large (100.68(8)°).

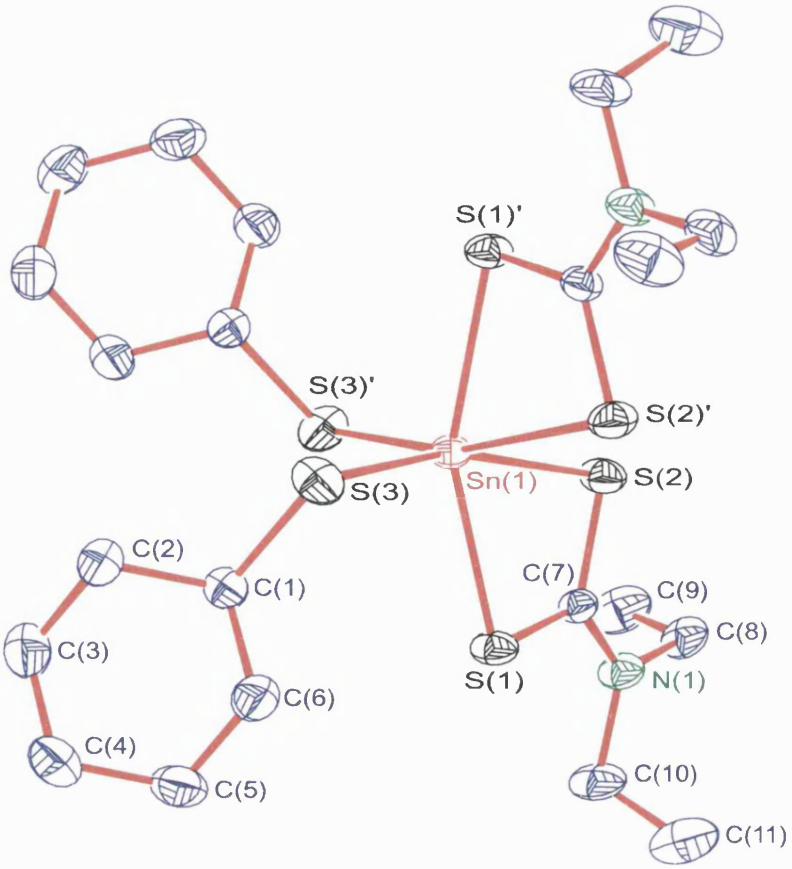

Fig. 2.2 The molecular unit of (**3**). Thermal ellipsoids are at the 30% probability level. Primed atoms are related to their unprimed counterparts in the asymmetric unit by 1-x, y, 1/2-z.

Bonds (Å)		**Angles (°)**	
Sn(1)-S(3)	2.450(1)	S(3')-Sn(1)-S(3)	100.68(8)
Sn(1)-S(1)	2.570(1)	S(3')-Sn(1)-S(1)	98.88(5)
Sn(1)-S(2)	2.618(1)	S(3)-Sn(1)-S(1)	95.29(5)
		S(1')-Sn(1)-S(1)	157.72(7)
		S(3)-Sn(1)-S(2')	87.49(5)
		S(1)-Sn(1)-S(2')	94.60(4)
		S(3)-Sn(1)-S(2)	163.46(4)
		S(1)-Sn(1)-S(2)	69.07(4)
		S(2')-Sn(1)-S(2)	88.44(7)

Table 2.2 Summary of selected metric data for compound (**3**).

Compound (**4**) (**Fig. 2.4**) also adopts a *cis*, *cis* arrangement for both the thiolate and dithiocarbamate groups. In general, the electron withdrawing C_6H_5 group generates features such as weakening of the Sn-S (thiolate) bond (2.473(1), 2.480(1) Å) and making chelation more symmetrical, for at least one ligand (2.573(1), 2.639(1) Å), due to enhancement of the Lewis acidity of tin. Furthermore, the inter-thiolate bond angle S-Sn-S (88.85(4)°) is lower than that for compound (**3**) (100.68(8)°) and the dihedral S-Sn-S-C angles are (-83.1, 154.8 or -178.3° due to some disorder in the thiolate unit – C17). **Table 2.3** summarises selected metric data for compound (**4**).

The difference of the inter-thiolate bond angles between compound (**3**) and (**4**) can be attributed to the different conformations of the C-S-Sn-S units. In the case of compound (**3**) the C-S-Sn-S units approach a *gauche*, *gauche* conformation (*sc*, *sc*; dihedral angle: 51.9, 51.9°) while for (**4**) the conformations are consistent with a distorted *trans*, *gauche* arrangement. The significance of this is in the alignment of sulfur lone pairs along the C-S-Sn-S-C moiety. In the case of compound (**3**) there are two lp/bp combinations in an eclipsed conformation, while the third eclipsed lp/lp pair-combination point away from each other and does not affect the angle (S-Sn-S). For compound (**4**) there are one lp/lp and one lp/bp pair-combinations which are both in an eclipsed conformation. Note again that for compound (**4**) the third eclipsed bp/lp pair-combination point away from each other and do not affect the S-Sn-S angle. [13]

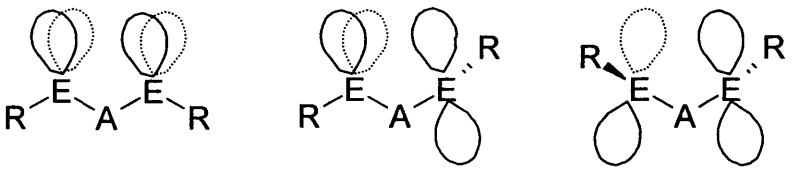

Fig. 2.3 The conformational preferences adopted by the R-E-A-E-R unit, (A=C, Si, Ge, Sn. E=O, S, Se) [13]

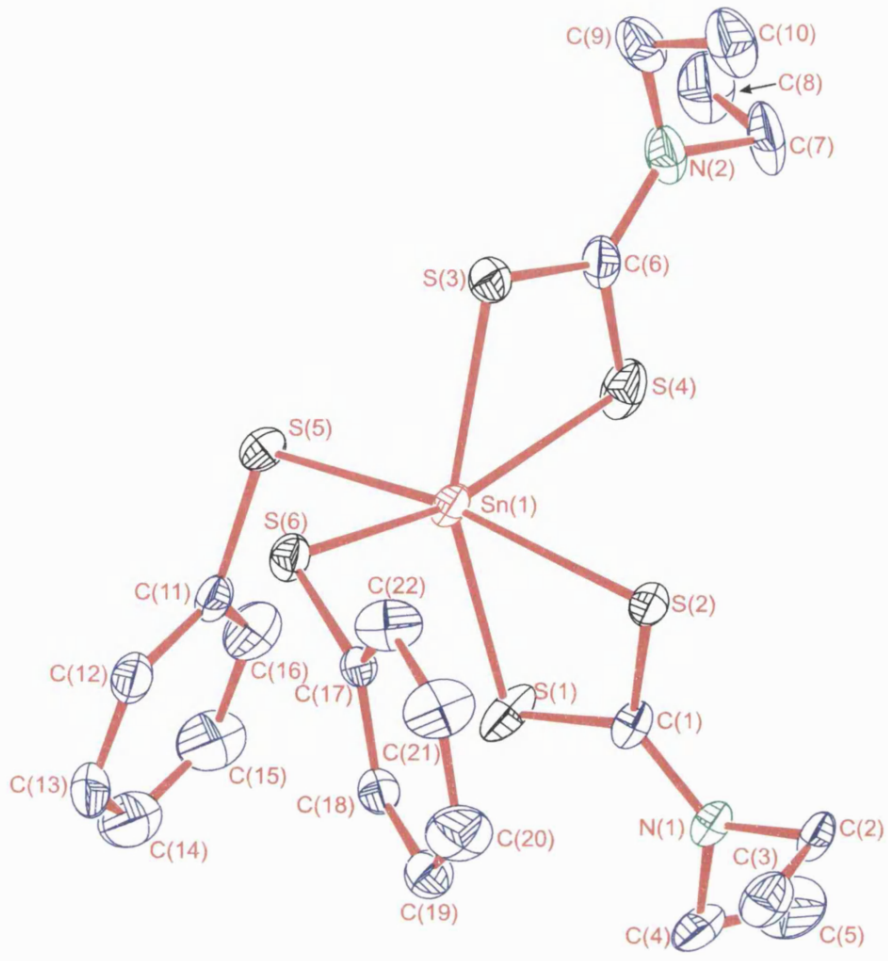

Fig. 2.4 The asymmetric unit of (**4**). Thermal ellipsoids are at the 30% probability level.

Bonds (Å)		Angles (°)	
Sn(1)-S(1)	2.546(1)	S(1)-Sn(1)-S(2)	70.83(4)
Sn(1)-S(2)	2.573(1)	S(1)-Sn(1)-S(3)	156.30(5)
Sn(1)-S(3)	2.552(1)	S(1)-Sn(1)-S(4)	89.60(5)
Sn(1)-S(4)	2.639(1)	S(1)-Sn(1)-S(5)	97.11(4)
Sn(1)-S(5)	2.473(1)	S(1)-Sn(1)-S(6)	105.71(5)
Sn(1)-S(6)	2.480(1)	S(2)-Sn(1)-S(3)	96.36(4)
		S(2)-Sn(1)-S(4)	87.57(4)
		S(2)-Sn(1)-S(5)	167.94(4)
		S(2)-Sn(1)-S(6)	94.17(4)
		S(3)-Sn(1)-S(4)	69.51(5)
		S(3)-Sn(1)-S(5)	95.01(4)
		S(3)-Sn(1)-S(6)	94.80(4)
		S(4)-Sn(1)-S(5)	92.67(5)
		S(4)-Sn(1)-S(6)	164.32(5)
		S(5)-Sn(1)-S(6)	88.85(4)

Table 2.3 Summary of selected metric data for compound (**4**).

In order to obtain a variety of compounds with an all-sulfur primary co-ordination sphere around the tin centre, complexes $[(RS)_2SnS]_2$ were considered. The synthesis of $[(RS)_2SnS]_2$ was envisaged *via* (**5a**) with the view of substituting- the labile amide groups with thiolate ligands (**Eq. 2.6**). Compound (**5a**) is known and was synthesised according to literature. [3]

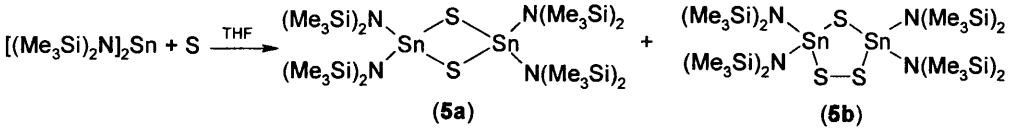

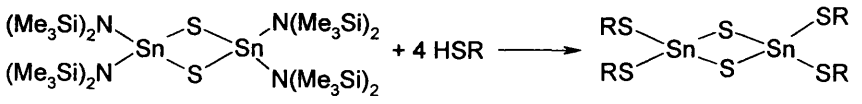

Eq. 2.6

The purpose of this study was to produce solely (**5a**) (analogous to compound (**2**)) via a synthetic route described in literature. [3] However, as it is revealed later, the synthesis proved to be very difficult because (**5b**) was always formed as a by-product, regardless the stoichiometric ratios of the starting materials.

Two synthetic methods were followed. Firstly, sonication was employed to drive the reaction to completion. Sublimed sulfur was first suspended in THF and sonicated for an hour. To the mixture the Sn(II) complex, bis[bis(trimethylsilyl)amido]tin(II), was added. The reaction took place in both stoichiometric quantities and slight excess of sulfur. However, the result was the same in both cases, producing (**5a**) and (**5b**) in a 0.9:1 ratio. Extended sonication of the reactants in THF was then tried (~5 hrs) resulting to 1:1 ratio of products. Grater excess of sulfur only produced up to 2:1 ratio of (**5b**):(**5a**).

Secondly, reflux was employed. The Sn(II) complex was added to a suspension of sublimed sulfur (1:1 ratio) under a nitrogen atmosphere and the mixture was refluxed for five hours. The resulting product was mostly (**5a**) by comparison of NMR and known crystallographic data. [3] However, when the same reaction was repeated with greater amounts of reactants (100% excess sulfur) the product ratio resulted in a 2:1 ratio of (**5a**):(**5b**).

Upfield chemical shifts in the ^{119}Sn NMR spectrum are also observed for compounds (**5a**) ($\delta(^{119}Sn)$= -105.0 ppm) and (**5b**) ($\delta(^{119}Sn)$= -55.0 ppm), while a downfield shift is observed for the $Sn(NR)_2$ starting material [3] ($\delta(^{119}Sn)$ = 776.0 ppm). In addition, through bond coupling is observed between the ^{119}Sn and ^{117}Sn nuclei in the ^{119}Sn NMR spectrum. The coupling constants for (**5a**) and (**5b**) are respectively: ($^2J(^{119}Sn\text{-}^{117}Sn)$ = 607.3 and 323.6 Hz).

The structure for compound (**5b**) is shown in **Fig. 2.6** and **Table 2.4** summarises metric data. The X-ray structure of (**5a**) [3] is illustrated in **Fig. 2.5** for comparison.

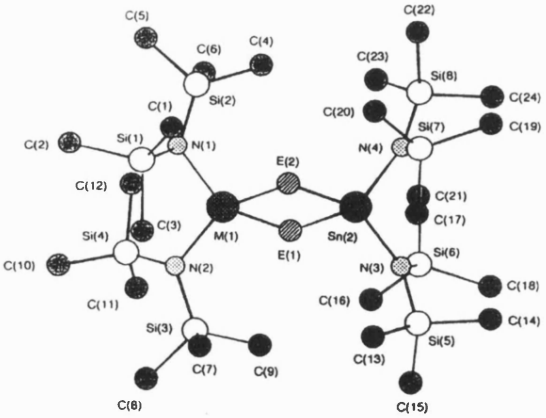

Fig. 2.5 The molecular structure of (**5a**). [3]

The two products were isolated by recrystallisation from hexane where two types of crystals were formed. Colourless crystals of complex (**5b**) were isolated and used for X-ray analysis, while yellow crystals of (**5a**) were analysed to verify its identity.

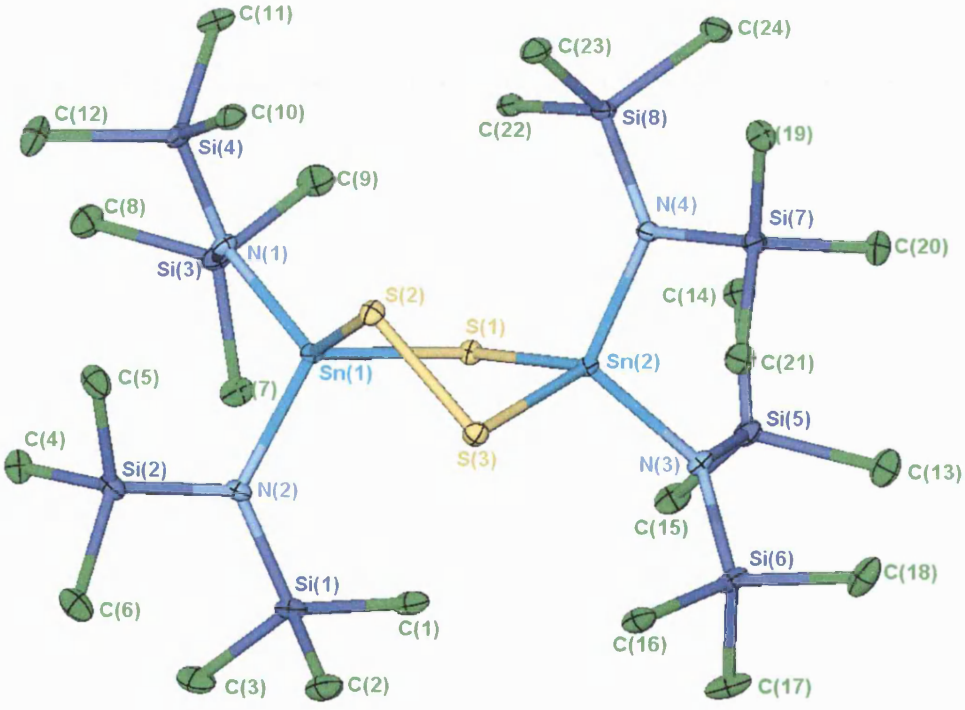

Fig. 2.6 The asymmetric unit of (**5b**). Thermal ellipsoids are at the 30% probability level.

In comparison with (**5a**), compound (**5b**) forms a 5-membered ring core, which has both mono-and disulfide bridges in between two tin atoms. The Sn-S distances in the monosulfide bridge (**5b**) are practically identical (2.4037(6), 2.4025(6) Å) but shorter than in (**5a**) (2.409(5)-2.427(6) Å). [3] The Sn-S distances in the disulfide bridge (**5b**) (2.4336(6), 2.4298(6) Å) are longer than those in the monosulfide bridge, while the S-S bond in the disulfide bridge (2.0816(9) Å) is similar to the values reported for various polysulfides (S-S 2.07 Å). [2] The S-Sn-S angles in compound (**5b**) (100.93(2), 101.01(2)°) are bigger than in (**5a**) (93.5(2), 93.3(2)°) [3] which is in accordance with the formation of a less strained 5-membered ring.

Bonds (Å)		**Angles (°)**	
Sn(1)-N(1)	2.0408(18)	N(1)-Sn(1)-S(1)	104.45(5)
Sn(1)-N(2)	2.0340(19)	N(1)-Sn(1)-S(2)	115.89(5)
Sn(2)-N(3)	2.0448(19)	N(2)-Sn(1)-N(1)	111.37(8)
Sn(2)-N(4)	2.099(18)	N(2)-Sn(1)-S(1)	114.81(6)
Sn(1)-S(1)	2.4037(6)	N(2)-Sn(1)-S(2)	109.02(5)
Sn(1)-S(2)	2.4336(6)	S(1)-Sn(1)-S(2)	101.01(2)
Sn(2)-S(1)	2.4025(6)	N(3)-Sn(2)-S(1)	104.47(5)
Sn(2)-S(3)	2.4298(6)	N(3)-Sn(2)-S(3)	115.85(6)
S(2)-S(3)	2.0816(9)	N(4)-Sn(2)-N(3)	111.53(8)
		N(4)-Sn(2)-S(1)	114.84(5)
		N(4)-Sn(2)-S(3)	109.91(5)
		S(1)-Sn(2)-S(3)	100.93(2)
		Sn(2)-S(1)-Sn(1)	98.94(2)
		S(2)-S(3)-Sn(2)	94.50(3)
		S(3)-S(2)-Sn(1)	95.07(3)

Table 2.4 Summary of selected metric data for compound (**5b**).

Alkyl/aryl thiols were added to a mixture of 1:1 ratio of (**5a**):(**5b**) in an attempt to substitute the labile amide groups on tin with thiolate ones. **Eq. 2.7** summarises the reactions that were attempted:

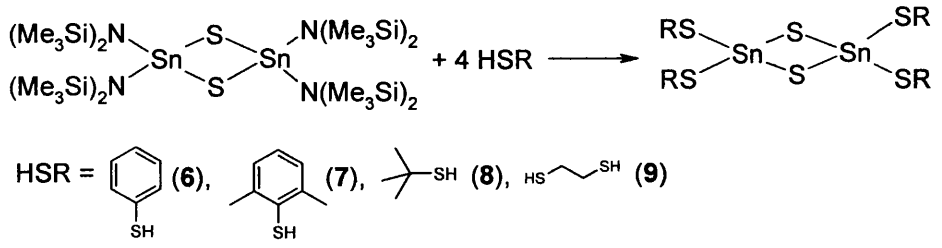

Eq. 2.7

For the syntheses of (**6**)-(**9**) similar conditions were applied. The reaction mixtures were stirred in either THF or toluene at room temperature under a nitrogen atmosphere. Furthermore, the reaction products were also very similar. In most cases insoluble, yellow to dark orange, precipitates were formed. In addition, by interpretation of the elemental analysis results the fact that these insoluble solids are types of short polymer chains similar to SnS_2 can be concluded.

These insoluble materials formed are very unlikely to be constituted of just a single product. However, from the elemental analyses obtained the following products can speculatively be attributed. In particular, the product of **Eq. 2.8** was identified as the hexamer (**6**) (Calculated: C 18.3, H 2.93, N 1.78%, Found: C 17.6, H 2.36, N 1.74%). The product of **Eq. 2.9** as the octamer (**7**) (Calculated: C 16.8, H 2.70, N 1.40%, Found: C 16.2, H 2.06, N 1.88%). The product of **Eq. 2.10** as the pentamer (**8**) (Calculated: C 16.9, H 3.52, N 1.10%, Found: C 17.7, H 4.06, N 1.66%). The product of **Eq. 2.11** as the trimer (**9**) (Calculated: C 20.6, H 4.21, N 1.2%, Found: C 21.2, H 4.60, N 0.42%). The following diagrams summarise the products for each of the thiols employed.

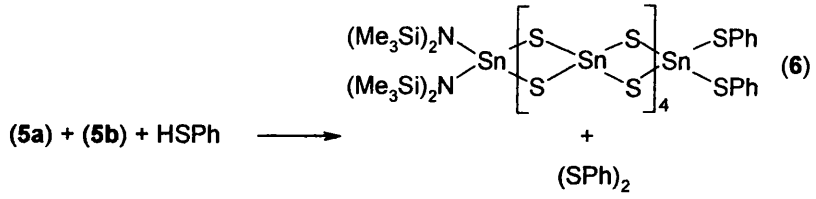

Eq. 2.8

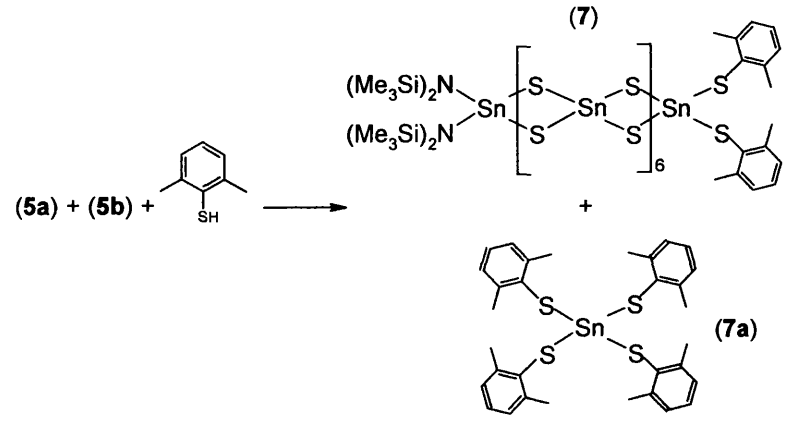

Eq. 2.9

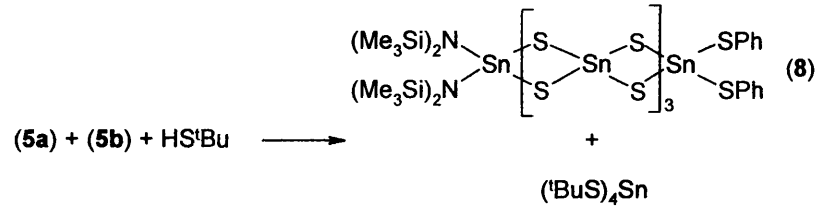

Eq. 2.10

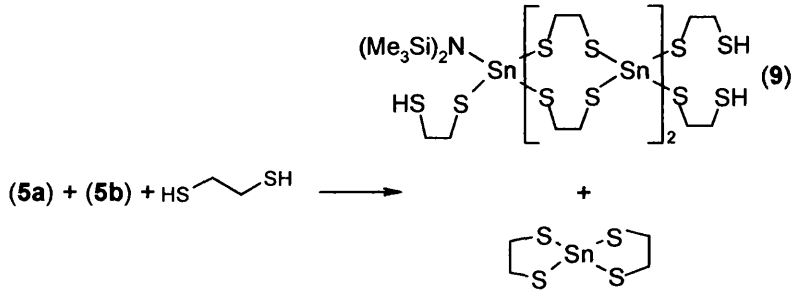

Eq. 2.11

Since compounds (**6**)-(**9**) were insoluble no NMR data were obtained. However, Mössbauer spectra were recorded for all (**6**)-(**9**). Mössbauer data of the compounds synthesised in this chapter are summarised in **Table 2.6**. **Eq. 2.12** describes a possible mechanism for the formation of the polymeric materials (**6**)-(**9**).

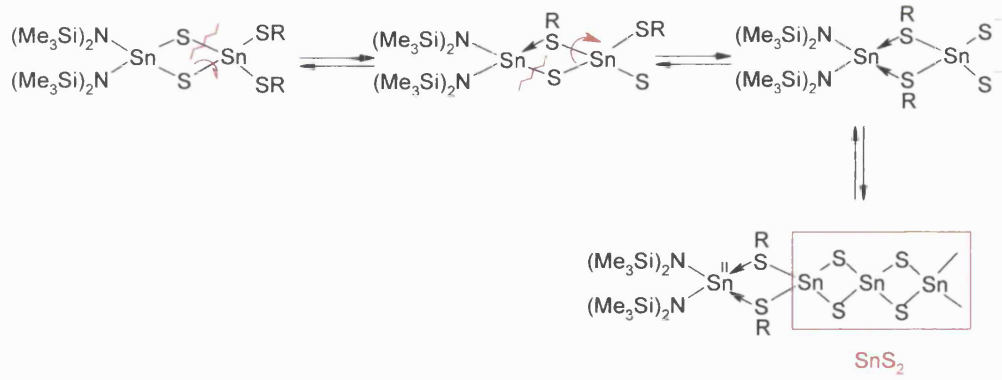

Eq. 2.12

The by-products formed in the synthesis of (**6**) (PhSSPh), (**8**) [(^{t}BuS)$_4$Sn], and (**9**) [Sn(SCH$_2$CH$_2$S)$_2$] are all known compounds. They were identified by either NMR spectroscopy or by comparison of crystallographic parameters from obtained crystals. However, for the synthesis of (**7**) the by-product tetrakis tin(2,6-dimethylphenyl thiolate) (**7a**) is a new compound and its structure is shown in **Fig. 2.7**. **Table 2.5** summarises selected metric data.

Bonds (Å)		**Angles (^{0})**	
Sn(1)-S(1)	2.4074(4)	S(1)-Sn(1)-S(2)	105.85(2)
Sn(1)-S(2)	2.4171(4)	S(1)-Sn(1)-S(3)	117.32(2)
Sn(1)-S(3)	2.4128(5)	S(3)-Sn(1)-S(2)	106.15(2)
Sn(1)-S(4)	2.3980(4)	S(4)-Sn(1)-S(1)	104.80(2)
		S(4)-Sn(1)-S(2)	117.10(2)
		S(4)-Sn(1)-S(3)	106.15(2)

Table 2.5 Summary of selected metric data for compound (**7a**).

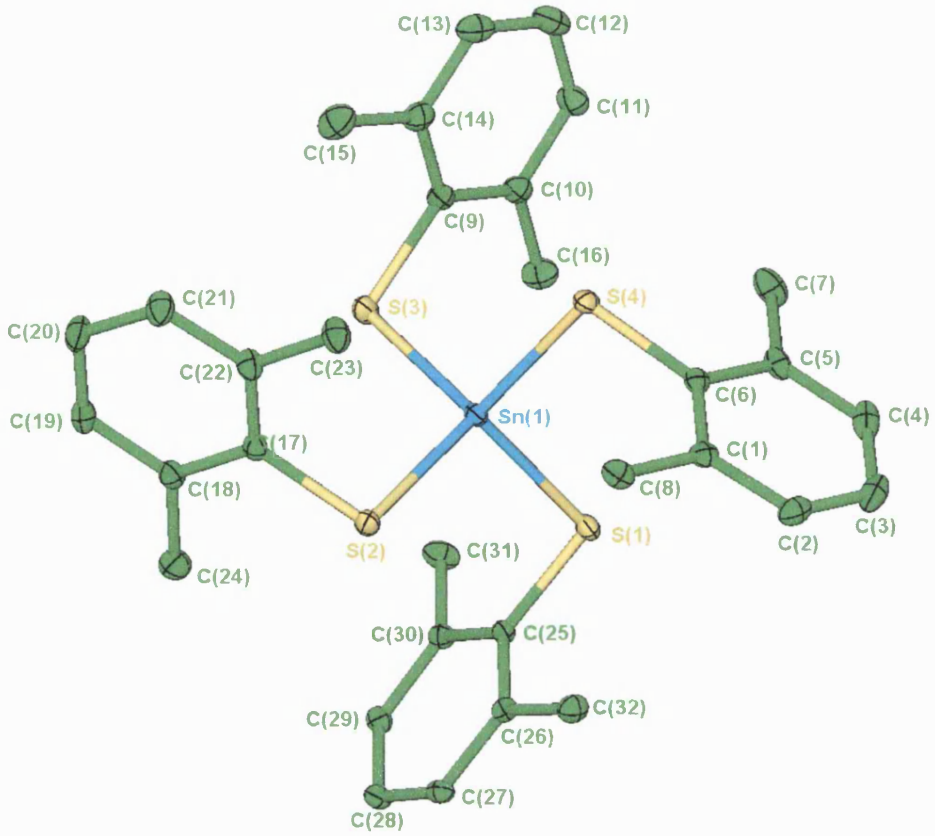

Fig. 2.7 The asymmetric unit of (**7a**). Thermal ellipsoids are at the 30% probability level.

As in other structurally characterised $Sn(SR)_4$ compounds the co-ordination around tin is tetrahedral although slightly distorted. The S-Sn-S angles in compound (**7a**) are in the range of 104.8-117.3°, while the angles in the structure of $Sn(SPh)_4$ are smaller ranging from 98.2 to 114.9°. [5] This is in accordance with the fact that the 2,6-dimethylphenyl thiolate ligands are bulkier than the phenyl ones and hence more space is needed to accommodate them. Furthermore, this can also be explained by the fact that the R-S-Sn-S-R unit adopts (as for $(PhS)_4Sn$ [5] and $(^tBuS)_4Sn$ [13]) a distorted *trans*, *gauche* conformation [*t*, *g*, (*ap*, *sc*)], with one lp/lp and one lp/bp eclipsed combination and this is in accordance with the dihedral angles (**Table 2.6**) observed for the R-S-Sn-S-R (very distorted S_4 point group).

	S-Sn-S Angles (°)					
	105.85(2)	117.32(2)	106.15(2)	104.80(2)	117.10(2)	106.15(2)
Dihedral	32.5	-85.7	147.5	156.9	92.0	-149.7
Angles (°)	-151.0	-94.4	-25.7	-24.9	92.6	22.2

Table 2.6 Summary of the dihedral angles for compound (**7a**).

Sn-S bond lengths in compound (**7a**) are approximately 2.40 Å, almost identical to the ones in $Sn(SPh)_4$ (2.379(4), 2.401(4) Å), and $Sn(SCy)_4$ (2.382(1) Å) and $(^tBuS)_4Sn$ (2.397(2) Å). [5, 13]

All isomer shift values for the compounds synthesised in this chapter correspond to a Sn(IV) centre ($\delta < 2$ mms^{-1}), while the quadrupole splitting values for (**2**) and (**3**) are typical for a tetrahedral environment around tin. However, for compounds (**4**)-(**9**) the quadrupole splitting is zero (a singlet is observed in the Mössbauer spectrum), which means that the tin atoms in each case have an almost perfect spherical electronic environment as for example in Me_4Sn. This for at least compounds (**6**)-(**9**) corroborates the speculation that they are polymeric materials similar to SnS_2.

Compound	**Isomer Shift** δ **(mm** s^{-1}**)**	**Quadrupole Splitting** ΔE_Q **(mm** s^{-1}**)**
(**2**)	0.96	0.55
(**3**)	1.05	0.55
(**4**)	1.01	0
(**6**)	1.04	0
(**7**)	0.69	0
(**8**)	1.11	0
(**9**)	1.12	0

Table 2.7. Summary of Mössbauer parameters.

2.2.2 Thermal Analysis

In order to asses the potential of compounds (**1**), (**2**), and (**3**) for the formation of tin sulfides under CVD conditions, their thermal decompositions, along with that of the tin(II) species $(Et_2NCS_2)_2Sn$ (**10**), have been assessed by a combination of TGA and Mössbauer methods. The resulting Mössbauer spectra were compared with those of the starting materials and known spectra of SnS (δ=3.26, ΔE_Q=0.57 mms^{-1}), SnS_2 (δ=0.87, ΔE_Q=0.00 mms^{-1}), and Sn_2S_3 (δ=1.21, 3.31, ΔE_Q=0.00, 0.70 mms^{-1}). [46] Additional XRD and Raman analyses have also been carried out to identify the nature of the decomposition products. The Raman spectra for each of the three common tin sulfides are SnS_2 317, 209 cm^{-1}, Sn_2S_3 307, 251, 234, 183, 71, 60, 52 cm^{-1}, SnS 288, 220, 189, 163, 96 cm^{-1}. [4]

Compound (**1**) $(Et_2NCS_2)_4Sn$ decomposed at 250 °C leaving a species with δ = 0.97, ΔE_Q = 0.66 mms^{-1} which can be assigned to compound (**2**), rather than SnS_2, on the basis that SnS_2 has no quadrupole splitting. Decomposition of (**1**) at 375 °C, under N_2, resulted to SnS_2 being formed and this has been confirmed by XRD and Raman spectroscopy. XRD revealed that the residue sample was primarily berndtite (*ca.* 90%) mixed with traces of the SnS_2-4H polytype. The measured crystallographic data [hexagonal, a=3.64(1), c=5.89(1) Å] compare well with literature values for SnS_2 (a=3.62-3.65, c=5.85-5.90 Å). Furthermore, the deposition of SnS_2 was confirmed by Raman bands at 316 and 210 cm^{-1}. In addition, SnS (herzenbergite) was also present at *ca.* 10%. The sample also contained some residual organic matter (C: 5.45, H: 0.36, N: 0.95%). In contrast, decomposition at 600 °C led to the formation of nanocrystalline SnO_2 (XRD: cassiterite) with no evidence for the formation of any tin sulfides. The residual organic matter at 600 °C was low (C: 1.12, H: 0.34, N: 0.00%).

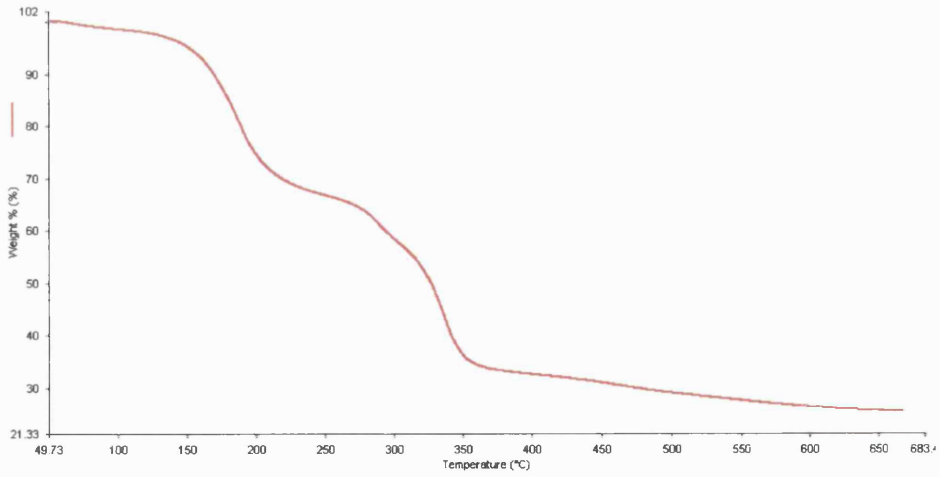

Fig. 2.8 TGA of $(Et_2NCS_2)_4Sn$ (**1**).

For comparison, TGA analyses of (**1**) and (**2**) were carried out at atmospheric pressure under a N_2 flow. The TGA of compound (**1**) (**Fig. 2.8**) shows the formation of (**2**) by 250 °C (observed mass loss: 33.0, theoretical: 38.0%). In addition, between 250 and 375 °C further decomposition leads to SnS_2 (observed residual mass: 33.0, theoretical: 38.0%). Finally, a species with mass corresponding to either SnS or SnO_2 is formed by 650 °C (observed residual mass: 25.6, theoretical: 21.2%). These findings are consistent with the decomposition of bulk samples under static N_2 described above.

There are conflicting reports in the literature as to the mechanism of decomposition of (**1**). Bratspies *et al.* [12] have claimed by TGA that (**1**) decomposes initially to give $(Et_2NCS_2)_2Sn$ (**10**) along with tetraethylthiuram disulfide $[Et_2NC(S)SS(S)CNEt_2]$ (**11**). Perry *et al.* [47] have claimed that (**10**) decomposes in dry N_2 to give tin metal and thus in air would provide a mechanism for the formation of SnO_2. This has also been noted in this study, present as a minor component in the Mössbauer spectra of compound (**1**) when heated to *ca.* 300 °C. Furthermore, SnO_2 is the final decomposition product of a bulk sample of (**1**) heated to 600 °C.

However, Bratspies *et al.* [48] have repeated the TGA of pure (**10**) and have claimed the formation of SnS, CS_2 and $(Et_2N)_2C{=}S$. To complicate matters,

Bratspies *et al.* have also claimed that $(dtc)_2$ (**11**) formed in the decomposition of (**1**) undergoes sulfur elimination to form the monosulfide $[Et_2NC(S)S(S)CNEt_2]$ and that the eliminated sulfur oxidises (**10**) to $[(Et_2NCS_2)_2SnS]_2$ (**2**) *in situ*, which then further decomposes through a series of unidentified intermediates to leave SnS by 400 °C. [12]

In contrast, the TGA of commercially available tetraethylthiuram disulfide (**12**) shows it loses almost all its mass (*ca.* 95%) in a single step between 250 and 325 °C (**Fig. 2.9**), with no evidence for the stepwise elimination of sulfur.

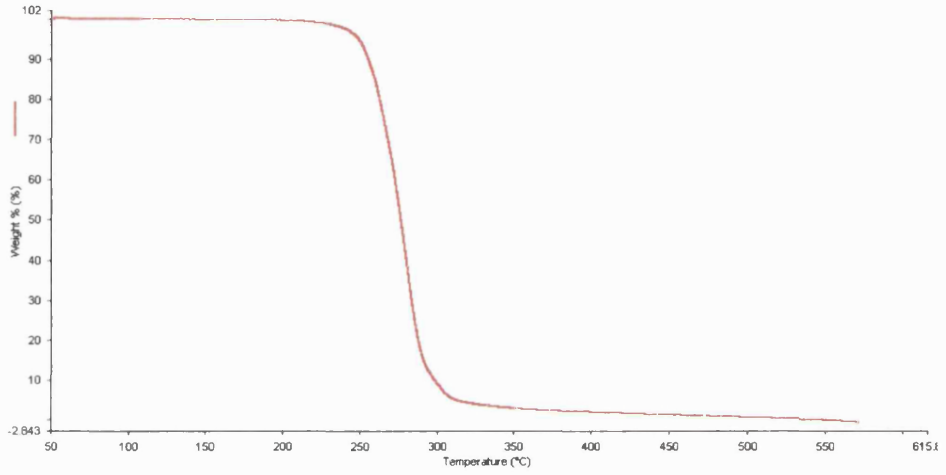

Fig. 2.9 TGA of tetraethylthiuram disulfide $(Et_2NCS_2)_2$ (**11**).

Furthermore, it should be noted that in all of the above analysis SnS and SnO_2 are indistinguishable in just simple mass terms and in order to identify correctly the type of material obtained simple mass calculations are insufficient.

To rationalise all the above findings the following theory can be proposed (**Eq. 2.13**). The decomposition of (**1**) appears to go by the sequential elimination of two equivalents of tetraethylthiuram disulfide (**11**). After one equivalent is lost, the $Sn(dtc)_2$ (**10**) remaining will readily react with, or abstract sulfur from, (**11**) to form (**2**), provided the temperature is below *ca.* 325 °C at which point the volatility of the disulfide causes its separation from the tin-containing residue.

At 325 °C and below:

$$Sn(dtc)_4 \xrightarrow{-(dtc)_2} \underset{\textbf{(10)}}{Sn(dtc)_2} \xrightarrow{(dtc)_2} \underset{\textbf{(2)}}{[Sn(dtc)_2S]_2}$$

At 600 °C:

$$Sn(dtc)_4 \xrightarrow{-2(dtc)_2} Sn\ (o) \xrightarrow{O_2} SnO_2$$

Eq. 2.13

In contrast, decomposition of (**1**) at 600 °C seems to promote the elimination of two equivalents of (**11**) and its removal from the residue before sulfur abstraction takes place. The remaining tin metal combines with oxygen from either the glass surface or the N_2 to generate SnO_2. In this respect, the decomposition of (**1**) follows what has been described previously for homoleptic thiolates $(RS)_4Sn$, *i.e.* the deposition of tin oxide films in the absence of a secondary sulfur source. [5]

The sulfide-bridged dimer (**2**) appears to be a key intermediate in the thermal decomposition of (**1**). However, the facile formation of this species from (**1**) in solution is not consistent with the formation of (**10**) as an intermediate. Therefore, the formation of (**2**) by a concerted mechanism seems more likely to happen in solution. While previous TGA studies on the thermal decomposition of $Sn(dtc)_4$ have claimed elimination of $(dtc)_2$ followed by sulfur extrusion (giving $(Et_2NCS)_2S$) and subsequent oxidative addition to $Sn(dtc)_2$ as the route by which species such as (**2**) are formed, [12] the fact that decomposition can take place at room temperature suggests this is unlikely, at least for chlorinated solvents. Therefore, it can be concluded that it is the *cis*-arrangement of monodentate dithiocarbamate groups around tin, which allows the formation of (**2**), by the concerted mechanism shown in **Fig. 2.10**.

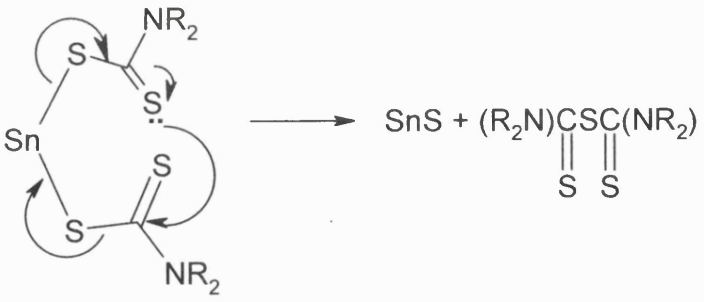

Fig. 2.10 Formation of (**2**) by a concerted mechanism (chelating groups omitted for clarity).

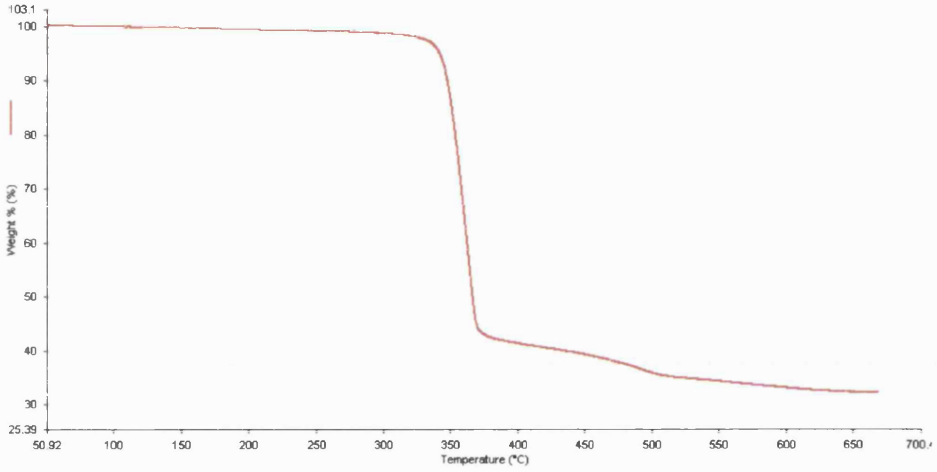

Fig. 2.11 TGA of the sufide-bridged dimer $[Sn(dtc)_2S]_2$ (**2**).

The TGA of (**2**) (**Fig. 2.11**) shows clean decomposition between 325 and 375 °C, which corresponds to the elimination of $[Et_2NC(S)]_2S$ and leaves SnS_2 (observed residual mass: 42.0, theoretical: 40.9%). This is in accordance with the identified residue from decompositions taken place at 400 °C under static N_2 (Raman: 317, 210 cm^{-1}). Further heating to 550 °C affords SnS as prismatic plates (observed residual mass: 34.0, theoretical: 33.7%). Again this finding is in agreement with the results obtained from decompositions at 600 °C (Raman: 288, 218, 182, 161, 94 cm^{-1}). Furthermore, in the decomposition residue at 600 °C some traces of Sn_2S_3 (Raman: 307 cm^{-1}) were identified.

The heteroleptic compounds $(Et_2NCS_2)_2(RS)_2Sn$ (R = Cy (**3**), Ph (**4**)) behave similarly. It appears that both compounds decompose *via* a common intermediate $Sn(dtc)_2$ (**10**) by loosing RSSR. Thus, this behaviour parallels the homoleptic thiolates $(RS)_4Sn$, which have been found to consistently produce Sn_3O_4 films unless H_2S is present. [5] It appears that (**4**) decomposes *via* loss of PhSSPh to give first $(dtc)_2Sn$ and subsequently tin metal, which then gets oxidised to either an oxide or a sulfide depending on conditions. [1]

The Mössbauer spectrum of the product of the decomposition of (**3**) at 200 °C confirms the formation of (**10**) (δ = 3.23, ΔE_Q = 1.78 mms^{-1}). Microanalysis of the residue is also consistent with the formation of (**10**) [Found (Calculated for $C_{10}H_{20}N_2S_4Sn$): C 29.9 (28.9), H 5.17 (4.87), N 4.81 (6.75)%]. Formation of SnS at temperatures higher than 375 °C has been confirmed by the decomposition of (**3**) under static N_2 at 400 °C. The XRD pattern of the residue at 400 °C correlates with that of the mineral herzenbergite (orthorhombic, a = 4.33, b = 11.2, c = 3.98 Å). The formation of SnS has also been confirmed by Raman Spectroscopy (observed bands at 289, 218, 182, 162, and 96 cm^{-1}). However, the decomposition residue still contained some organic matter (C 2.0, H 0.06, N 0.03%).

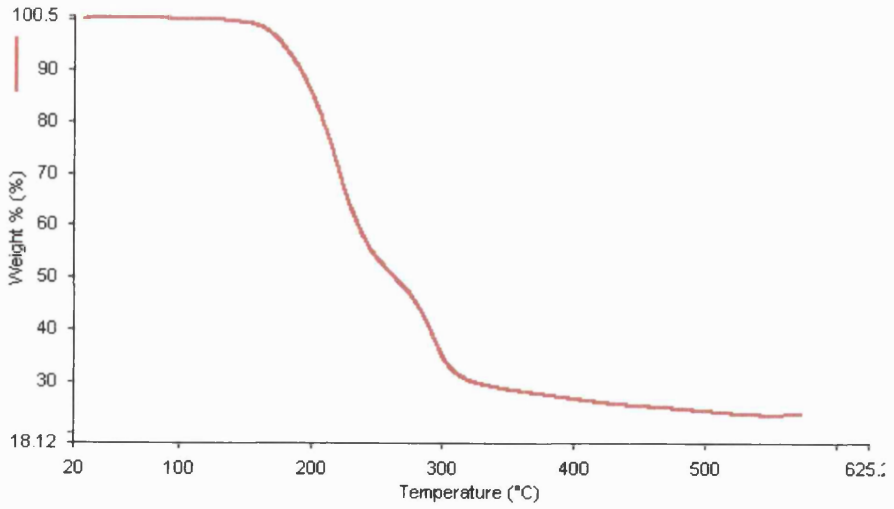

Fig. 2.12 TGA of $(CyS)_2Sn(dtc)_2$ (**3**).

The TGA of (**3**) shows a two-stage decomposition (**Fig. 2.12**). Initial decomposition between 145 and 250 °C (*ca.* 55%) with a second stage at 270-325 °C resulting in a residual mass of 29.0% attributed to SnS_2 (observed residual mass: 29.0, theoretical: 28.3%). Further decomposition occurs up to 550 °C resulting to the final product SnS (observed residual mass: 23.9, theoretical: 23.4%). Again the TGA results match the findings for the bulk decomposition of (**3**).

2.3 Film Growth Results

2.3.1 Introduction

Compounds (**2**) and (**3**) were tested for their suitability to produce tin sulfide films under CVD conditions. Experiments took place by either LPCVD or APCVD under a static nitrogen atmosphere.

2.3.2 Deposition Conditions

Films were deposited on standard borosilicate glass slides. The substrate was heated at temperatures ranging from 540 to 550 °C. For each growth experiment approximately 0.2 g of complex was used. For the experiments at low pressure (LPCVD) the precursor was held at low pressure (ca. 0.1 mm Hg) and heated in a tube furnace until evaporation was complete. At the same time external to the furnace the deposition substrate (glass slide) was placed and was independently heated by a ceramic infrared heater to the desired decomposition temperature. Any volatile material produced from heating the precursor would be expected to decompose and deposit on the glass slide. For the atmospheric pressure experiments (APCVD) the same set-up was used (see **Appendix Two**) but the precursor was held under a static nitrogen atmosphere throughout the duration of the deposition run. The deposition conditions for the films obtained are summarised in **Table 2.7**.

Compound	(2)	(2)	(2)	(3)	(3)	(3)
CVD Method	LP	AP	AP	LP	AP	AP
Tube Furnace Temp (°C)	350	400	600	375	200	400
Substrate Temp (°C)	550	550	550	450	550	550
Film ID	**(F1)**	**(F2)**	**(F3)**	**(F4)**	**(F5)**	**(F6)**

Table 2.7 CVD conditions for experiments with compounds (**2**) and (**3**).

2.3.3 Film Analysis

Films were examined using a number of techniques: Visual inspection, Energy Dispersive X-Ray Analysis (EDAX), Scanning Electron Microscopy (SEM) and Raman Spectroscopy.

The films obtained from precursor (**2**) were all similar in appearance, yellow-brown with visible refrigence patterns. However, no Raman analysis was performed for any of (**F1**)-(**F3**) films and hence the exact type of tin sulfide deposited is not known. Film (**F1**) was obtained under LPCVD conditions and EDAX analysis showed it contained tin and sulfur. Scanning electron microscopy was also used to analyse this film, which showed a uniform coverage consisting of small spheres (**Fig. 2.13**).

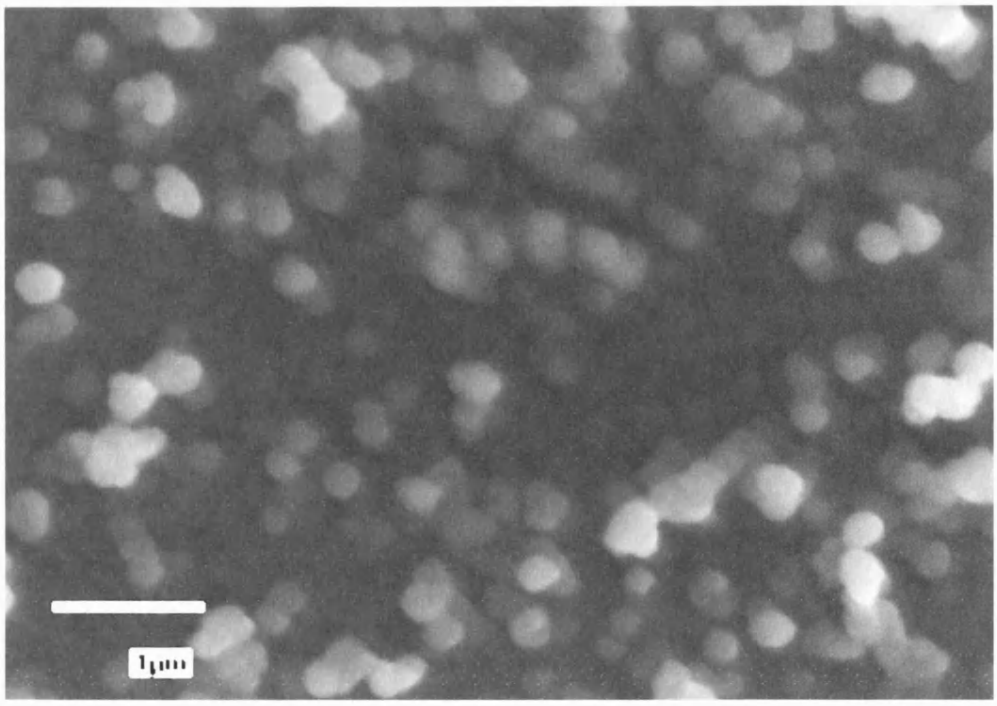

Fig. 2.13 0^{o} tilt SEM image of film (**F1**), precursor (**2**).

Films (**F2**) and (**F3**) were both deposited by APCVD but under a static nitrogen atmosphere. EDAX analysis reveals that both contain tin and sulfur. In addition, Scanning Electron Microscopy used to analyse film (**F3**) revealed a uniform coverage of small crystallites with some areas of preferred orientation (**Fig. 2.14**, **Fig. 2.15**).

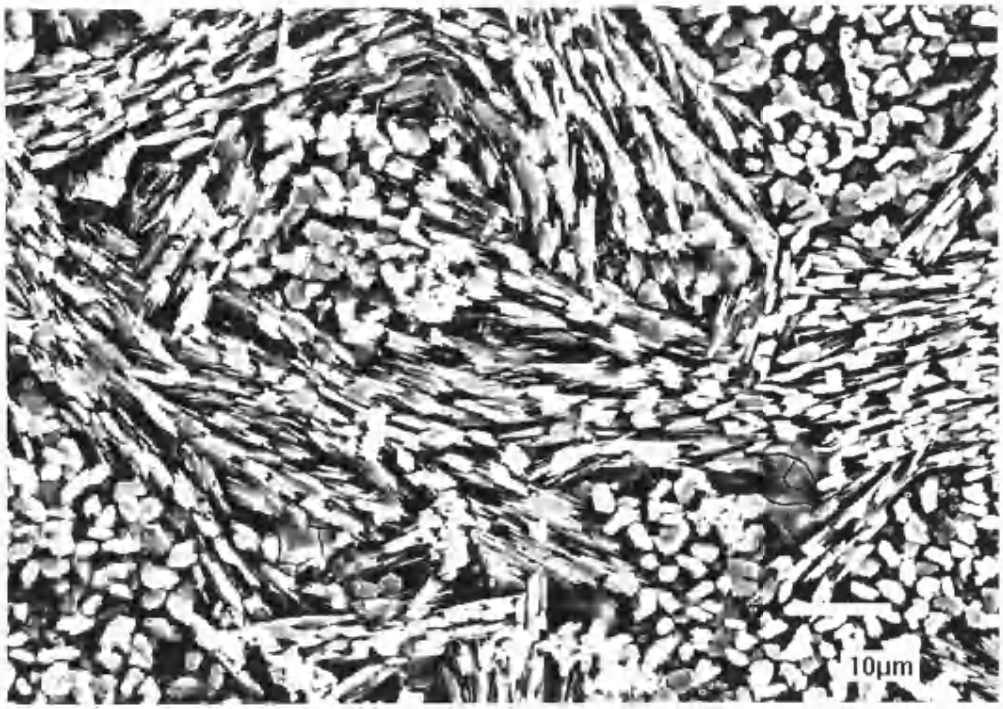

Fig. 2.14 0^{o} tilt SEM image of film (**F3**), precursor (**2**).

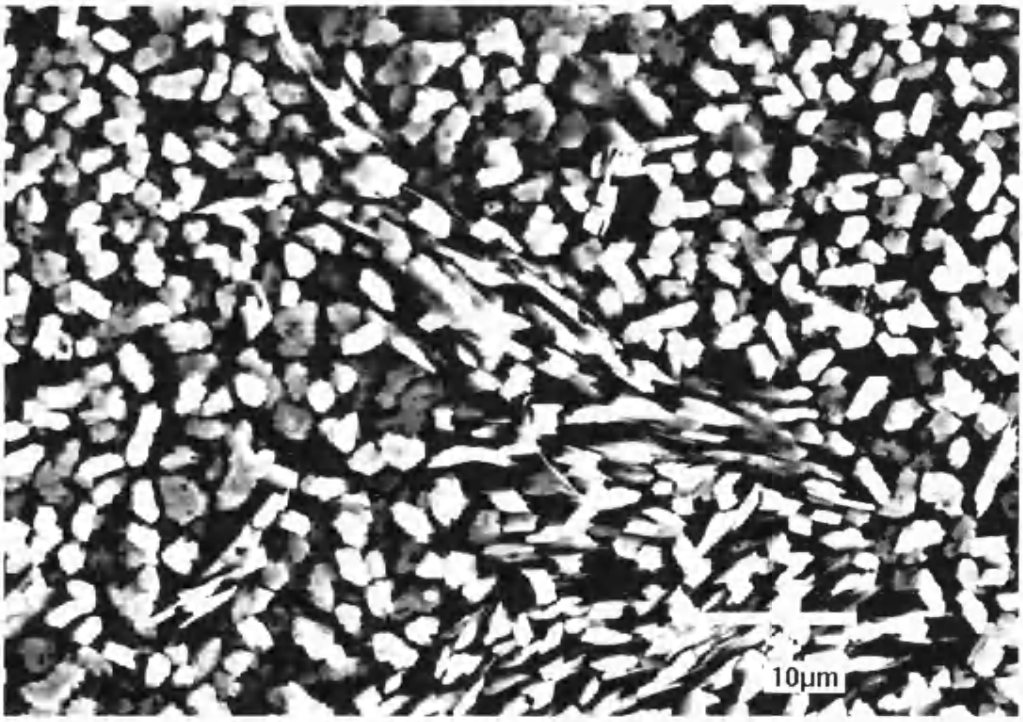

Fig. 2.15 0^{o} tilt SEM image of film (**F3**) at higher magnification, precursor (**2**).

Film (**F5**) was deposited by APCVD from precursor (**3**) under the conditions described in **Table 2.7** above. The film had a yellow appearance and its Raman analysis indicated SnS_2 (Raman: 315 cm^{-1}). In contrast, when (**3**) was heated to 400 °C under N_2 and decomposed at 550 °C film (**F6**) was produced. This consisted of a leading edge of yellow material analysed as SnS_2 (Raman: 311-314 cm^{-1}), followed by a large area of grey/black film, which was mainly SnS (Raman: 221, 185, 159, 95 cm^{-1}). Film (**F6**) also contained traces of Sn_2S_3 (Raman: 306 cm^{-1}) incorporated in the grey/black area.

The quality of the SnS_2 film was enchanced by repeating the experiment at low pressure (LPCVD) and with the precursor (**3**) heated to 375 °C (substrate at 450 °C). The hard transparent coating deposited (**F4**) showed refrigence patterns due to the significant thickness of the film. Raman analysis verified the fact that film (**F4**) was SnS_2 (Raman: 315 cm^{-1}). This is in itself a significant result because previous attempts to deposit SnS_2 films from either single- or dual-source precursors had always generated soft, powdery films typical of formation of the film components in the gas phase and subsequent diffusion to the substrate surface. However, the SnS_2 deposited in film (**F4**) under LPCVD conditions is more typical of a surface controlled reaction, which is probably formed by a different mechanism than that observed in bulk decompositions, where formation of SnS is observed.

2.4 Conclusions

Decomposition of $(Et_2NCS_2)_4Sn$ (**1**) to SnS_2 takes place via $[(Et_2NCS_2)_2SnS]_2$ (**2**) by effectively losing $[Et_2NC(S)]_2S$, while at higher temperature complete removal of two equivalents of $(dtc)_2$ leads to *in situ* formation of Sn(0) and consequently SnO_2.

The synthesis of mixed-ligand species $(Et_2NCS_2)_2(RS)_2Sn$, (**3**) and (**4**), has been achieved. These heteroleptic species decompose to SnS by initial elimination of RSSR to afford $(dtc)_2Sn$ and subsequent loss of $[Et_2NC(S)]_2S$.

Hence, the two types of compound, $(dtc)_4Sn$ and $(dtc)_2(RS)_2Sn$, can be considered as single-source materials for bulk SnS_2 and SnS, respectively, by virtue of their differing decomposition pathways. The formation of SnS directly from $(dtc)_2(RS)_2Sn$ at temperatures as low as 350 °C is in contrast with other deposition routes in which SnS is formed from the subsequent decomposition of the previously formed SnS_2 and at temperature higher than 500 °C, *i.e.* decomposition to SnS by a temperature controlled deposition.

From the CVD perspective, experiments with compounds $(dtc)_2(CyS)_2Sn$ and $[(Et_2NCS_2)_2SnS]_2$ show that tin sulfide films can be grown particularly at low pressure. However, for $(dtc)_2(CyS)_2Sn$ in particular the CVD experiments show different results from those in the bulk decomposition experiments. Under CVD conditions SnS_2 is the primary deposition product rather that SnS, possibly due to a different growth mechanism than that observed in the bulk.

2.5 Experimental

Starting materials were commercially obtained (e.g. Aldrich) and were used without further purification unless otherwise stated. Standard Schlenk line techniques were employed where applicable. For further details about instrumentation see **Appendix One.**

The synthesis of tetrakis(diethyldithiocarbamato) tin(IV) $Sn(dtc)_4$ (1). [7]

This was prepared by a known route and exhibited spectroscopic properties identical to those reported in literature. Sodium diethyldithiocarbamate trihydrate (10.37 g, 46 mmol) was dissolved in ethanol (*ca.* 30 ml) and tin tetrachloride (1.35 ml, 11.5 mmol) was added dropwise to the solution. On addition, a bright orange precipitate formed and the mixture was left stirring for two hours. The mixture was then filtered to remove the precipitated sodium chloride. Condensation of the filtrate and subsequent addition of ether yielded a

bright orange solid. The product was then suction filtered, washed with ether and dried *in vacuo*. Yield 7.1 g, 68%.

Elemental Analysis:

Found (Calculated for $C_{20}H_{40}S_8N_4Sn$): %C 27.7 (29.6); %H 5.12 (5.02); %N 6.45 (6.77).

^{1}H NMR [δ (ppm), $CDCl_3$]:

1.01 [t, 6H, CH_3-Et]; 3.54 [q, 4H, CH_2-Et].

^{13}C NMR [δ (ppm), $CDCl_3$]:

12.1 [CH_3, Et]; 42.4 [CH_2, Et]; 49.9 [CS_2].

^{119}Sn NMR [δ (ppm), $CDCl_3$]:

-766 [*trans*]; -764; -768.

The synthesis of bis(diethyldithiocarbamato)tin (II) $Sn(dtc)_2$. [8]

Tin dichloride dihydrate (4.0 g, 17.8 mmol) and sodium diethyldithiocarbamate trihydrate (8.02 g, 35.5 mmol) were dissolved in deoxygenated water (ca. 100 ml), with the immediate formation of a yellow precipitate. After 30 mins stirring at RT the precipitate was isolated by filtration and dried in vacuo giving the product as a yellow solid. Yield 6.71g, 91%. Spectroscopic properties were identical to those reported in literature.

The synthesis of bis[bis(diethyldithiocarbamato)tin(IV) sulfide] $[(dtc)_2SnS]_2$ (2).

Method One

A two-necked round-bottom flask was charged with tetrakis (diethyldithiocarbamato)tin (1.50 g, 1.99 mmol) dissolved in dichloromethane (50 ml). The solution was refluxed under nitrogen for 24 hours resulting to a colour change from red-orange to yellow and the formation of a small amount

of white precipitate. Further reflux (24 hrs), subsequent filtration and slow evaporation of the solvent in air yielded colourless crystals of the product (0.50 g, 33%), mp 272 °C.

Method Two

A Schlenk tube was charged with bis(diethyldithiocarbamato)tin(II) (0.5 g, 1.20 mmol) dissolved in tetrahydrofuran (ca. 30 ml). To the solution was added sublimed sulfur (0.04 g, 1.20 mmol). The mixture was left stirring and after 30 minutes the colour changed from pale yellow to orange and a precipitate was formed. The precipitate was then isolated by filtration and dried *in vacuo*. Yield 0.2 g, 40%.

Elemental Analysis:

Found (Calculated for $C_{20}H_{40}S_{10}N_4Sn_2$): %C 27.0 (26.8); %H 4.56 (4.47); %N 6.22 (6.26).

^{1}H NMR [δ (ppm), $CDCl_3$]:

1.49 [t, 6H, CH_3-Et; J=7.3 Hz]; 3.04 [q, 4H, CH_2-Et; J=7.3 Hz].

^{13}C NMR [δ (ppm), $CDCl_3$]:

10.9 [CH_3, Et]; 42.2 [CH_2, Et]; 50.4[CS_2].

^{119}Sn NMR [δ (ppm), $CDCl_3$]:

-736.

Mössbauer [mms^{-1}]:

δ=0.96, ΔE_Q =0.55.

The synthesis of bis(diethyldithiocarbamato) bis(cyclohexylthiolato)tin (IV) $(dtc)_2(CyS)_2Sn$ (3). [1]

A conical flask was charged with tetrakis(diethyldithiocarbamato)tin (992 mg, 1.39 mmol) dissolved in toluene (ca. 50 ml) and tetrakis(cyclohexylthiolato)tin (808 mg, 1.39 mmol) dissolved in toluene (ca. 50 ml). The solution was stirred at room temperature for 8 hrs, resulting to a colour change from orange to yellow. The solution was then concentrated *in vacuo*. Standing at –30 °C

overnight gave bright yellow crystals of the product, (1.20 g, 67%), which were isolated by filtration, mp 114-114.5 °C.

Elemental Analysis:

Found (Calculated for $C_{22}H_{42}S_6N_2Sn$): %C 41.4 (40.9); %H 6.59 (6.56); %N 4.34 (4.34).

^{1}H NMR [δ (ppm), C_6D_6]:

0.75 [t, 6H, CH_3-Et; *J*=7.1 Hz]; 1.47 [d, 4H, CH_2; *J*=10.8 Hz]; 1.80 [d, 4H, CH_2; *J*=10.7 Hz]; 2.47 [d, 2H, CH_2; *J*=9.6 Hz]; 3.07 [q, 4H, CH_2-Et; *J*=7.0 Hz]; 3.83 [m, 1H, CH].

^{13}C NMR [δ (ppm), C_6D_6]:

11.7 [CH_3, Et]; 26.1, 27.2, 38.9, 44.5 [CH_2, Cy]; 50.9 [CH_2, Et]; 198.8 [CS_2].

^{119}Sn NMR [δ (ppm), C_6D_6]:

-649.

Mössbauer [mms^{-1}]:

δ=1.05, ΔE_Q =0.55.

The synthesis of bis(diethyldithiocarbamato) bis(thiophenolato)tin (IV) $(dtc)_2Sn(SPh)_2$ (4). [1]

Method One

A conical flask was charged with tetrakis(diethyldithiocarbamato)tin (663 mg, 0.88 mmol) dissolved in toluene (ca. 50 ml) and tetrakis(thiophenolato)tin (490 mg, 0.88 mmol) dissolved in toluene (ca. 50 ml). The resulting solution was refluxed for 2 hrs, resulting to a colour change from orange to yellow. The solution was then concentrated *in vacuo*. Recrystallisation from diethyl ether (*ca.* 20 ml) gave bright yellow crystals of the product, (365 mg, 56%), which were isolated by filtration, mp 113 °C.

Method Two

Tetrakis(thiophenolato)tin (0.24g, 0.43 mmol) was dissolved in toluene (ca. 50 ml). Copper (II) (diethyldithiocarbamate) (0.16 g, 0.43 mmol) was added and

the resulting solution was refluxed for 2 hrs at 60 °C, causing a colour change from black-brown to yellow-brown. The solution was then stirred at RT overnight. The solvent was removed *in vacuo* and the residue dissolved in chloroform. Addition of cold pentane and immediate filtration yielded a yellow-orange solid, (0.07 g, 29%).

Elemental Analysis:

Found (Calculated for $C_{22}H_{30}S_6N_2Sn$): %C 41.8 (41.7); %H 4.79 (4.77); %N 4.54 (4.42).

^{1}H NMR [δ (ppm), $CDCl_3$]:

0.38 [t, 6H, CH_3-Et; *J*=7.1 Hz]; 2.65 [q, 4H, CH_2-Et; *J*=7.1 Hz]; 6.83 [m, 3H, C_6H_5]; 7.69 [d, 2H, C_6H_5; *J*=7.2 Hz].

^{13}C NMR [δ (ppm), $CDCl_3$]:

12.0 [CH_3, Et]; 51.3 [CH_2, Et]; 127.2, 137.6, 188.8 [C_6H_5]; 198.7 [CS_2].

^{119}Sn NMR [δ (ppm), $CDCl_3$]:

-666.

Mössbauer [mms^{-1}]:

δ=1.01, ΔE_Q =0.00.

The synthesis of bis[bis(trimethylsilyl)amido]tin(IV) cyclic sulfides [3]

$\{Sn[N(SiMe_3)_2]_2(\mu\text{-}S)\}_2$ (5a), $\{Sn[N(SiMe_3)_2]_2\}_2(\mu\text{-}S)_3$ (5b)

Method One

Sublimed sulfur powder (0.02 g, 0.73 mmol) was added to bis[bis(trimethylsilyl)amido]tin(II) (0.32 g, 0.73 mmol) in THF (*ca.* 50 ml) and the mixture was refluxed for 5 hrs. Some small amount of unreacted sulfur was filtered off and the pale yellow filtrate was condensed *in vacuo*. Dissolving in hexane then purified the residual solid and crystals of products (**5a**) and (**5b**) were grown.

Method Two

Sublimed sulfur powder (0.02 g, 0.73 mmol) was added to bis[bis(trimethylsilyl)amido]tin(II) (0.32 g, 0.73 mmol) in THF (*ca.* 50 ml) and the mixture was immersed in an ultrasonic cleaning bath for 1 hr. An almost instant change to a more intense yellow was observed. Some small amount of unreacted sulfur was filtered off and the yellow filtrate was condensed *in vacuo*. Dissolving in hexane then purified the residual solid and crystals of products (**5a**) and (**5b**) were grown.

^{1}H NMR [δ (ppm), $CDCl_3$] (**5a**):

0.05 [s, 72H, CH_3].

^{13}C NMR [δ (ppm), $CDCl_3$] (**5a**):

3.6 [CH_3, Me; $^{1}J(^{13}C\text{-}^{29}Si)$=12.27 Hz]

^{119}Sn NMR [δ (ppm), $CDCl_3$] (**5a**):

-105.0; $^{2}J(^{119}Sn\text{-}^{117}Sn)$=607.3 Hz

Elemental Analysis (**5b**):

Found (Calculated for $C_{24}H_{72}S_3N_4Sn_2$): %C 28.7 (29.6); %H 7.31 (7.39); %N 5.54 (5.75).

^{1}H NMR [δ (ppm), $CDCl_3$] (**5b**):

0.02 [s, 72H, CH_3].

^{13}C NMR [δ (ppm), $CDCl_3$] (**5b**):

3.9 [CH_3, Me; $^{1}J(^{13}C\text{-}^{29}Si)$=14.57 Hz]

^{119}Sn NMR [δ (ppm), $CDCl_3$] (**5b**):

-55.0; $^{2}J(^{119}Sn\text{-}^{119}Sn)$=323.6 Hz

2.6 References

[1] G. Barone, T. Chaplin, A. T. Kana, T. G. Hibbert, M. F. Mahon, K. C. Molloy, I. D. Worsley, I. P. Parkin, L. S. Price, *J. Chem. Soc., Dalton Trans.*, 2002, 1085.

[2] F. A. Cotton, G. Wilkinson, *Advanced Inorganic Chemistry (5th Ed.)*, John Wiley & Sons, 1988, 530.

[3] P. B. Hitchcock, E. Jang, M. F. Lappert, *J. Chem. Soc., Dalton Trans.*, 1995, 3179.

[4] L. S. Price, I. P. Parkin, A. Hardy, R. Clark, T. G. Hibbert, K. C. Molloy, *Chem. Mater.*, 1999, **11**, 1792.

[5] G. Barone, T. G. Hibbert, K. C. Molloy, M. F. Mahon, L. S. Price, I. P. Parkin, A. Hardy, M. Field, *J. Mater. Chem.*, 2000, **11**, 464.

[6] I. P. Parkin, L. S. Price, T. G. Hibbert, K. C. Molloy, *J. Mater. Chem.*, 2001, **11**, 1486.

[7] C. S. Harreld, E. O. Schlemper, *Acta Crystallogr., Sect. B*, 1971, **27**, 1976.

[8] B. F. Hoskins, R. L. Martin, N. M. Rohde, Aust. *J. Chem.*, 1976, **29**, 213.

[9] R. Selvaraju, K. Panchanatheswaran, K. Venkatasubramanian, *Polyhedron*, 1994, **13**, 903.

[10] Y. Zhou, D. S. Richeson, *J. Am. Chem. Soc.*, 1996, **118**, 10850.

[11] H. Puff, G. Bertram, B. Ebeling, M. Franken, R. Gattermeyer, R. Hundt, W. Schuh, R. Zimmer, *J. Organomet. Chem.*, 1989, **379**, 235.

[12] G. K. Bratspies, J. F. Smith, J. O. Hill, R. J. Magee, *Thermochim. Acta*, 1977, **19**, 361.

[13] T. G. Hibbert, M. F. Mahon, K. C. Molloy, I. P. Parkin, L. S. Price, I. Silaghi-Dumitrescu, *J. Chem. Soc., Dalton Trans.*, 2001, 3435.

[14] W. S. Rees, Jr., 'CVD of Nonmetals' VCH, 1996, Ch 4, 7.

[15] H. O. Davies, A. C. Jones, T. J. Leedham, M. J. Crosbie, P. J. Wright, N. M. Boag, J. R. Thompson, *Chem. Vap. Deposition*, 2000, **6**, 71.

CHAPTER THREE

The Synthesis, Characterisation and CVD Properties of Transition Metal Pentacarbonyl Complexes of Alkyltin (IV) Sulfides.

3.1 Introduction

Doping of semiconductors has an effect of enhancing their conductivity. Therefore, by introducing a transition metal (i.e. doping) within the layered structure of organotin sulfides, a novel material with enhanced semiconducting properties could potentially be obtained. In this chapter, the synthesis of mixed organotin/transition metal sulfides and their suitability as precursors for the deposition of mixed-metal thin films is examined. The precursors were designed using a strategy common for all single-source CVD precursors, which enshrines the assertion that on decomposition of a molecule in the gas-phase the required coating is formed by maintaining the metal-element bond.

As mentioned in chapter one, in order for the CVD process to yield high-quality films the suitability of a complex as a precursor is examined according to certain criteria. The choice for synthesising transition metal carbonyl complexes of tin sulfides can be justified by the fact that they meet most of these criteria.

Metal carbonyls, as CVD precursors, are very promising because they have potentially clean decomposition pathways. Since the carbonyl ligands are very labile they can be detached, under decomposition conditions, as CO and removed by the carrier gas away from the substrate. In addition, these particular single-source precursors contain the desired transition metal-sulfide fragment for the deposition of transition metal-doped tin sulfide films, as shown in the following diagram.

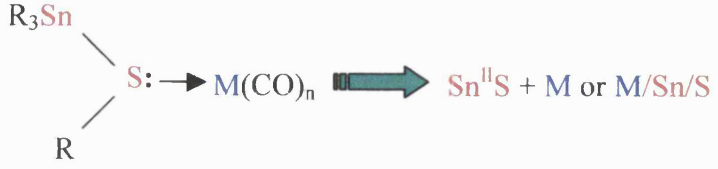

Metal carbonyl complexes have been studied extensively as precursors for CVD of Co, Fe, Mo, and Cr. In the cases of Co and Fe high-purity deposits can be obtained. In contrast, most other metal carbonyls produce films that are contaminated with metal carbides, metal oxides, and graphitic carbon. The

reason for this is that CO is dissociatively adsorbed on most metal surfaces and as a result carbon and oxygen are incorporated into the film. [2]

Reactions of many metal carbonyls lead to formation of metal carbides due to the catalytic dissociation on the metal. One example is the reaction of $Cr(CO)_6$:

$$Cr(CO)_{6(g)} \longrightarrow Cr_{(s)} + Cr_2O_{3(s)} + Cr_3C_{2(s)} + CO_{(g)}$$

These results suggest that metal carbonyls are a good precursor choice only for those elements that do not allow CO surface dissociation. In cases where dissociation occurs, it may be possible to remove some of the carbon and oxygen impurities by reaction with added reagents (e.g. H_2S, H_2O).

3.2 Results and Discussion

3.2.1 Synthesis

During this study a selected range of compounds were synthesised and tested for their suitability as CVD precursors. The hexacarbonyl complexes of the transition metals chromium and molybdenum were employed as starting materials. In addition, alkyltin thiolates were utilised as two-electron donor ligands. The alkyl groups on tin were either methyl or n-butyl, while on sulfur a t-butyl group. Transition metal pentacarbonyl complexes are relatively easy to obtain since their synthesis involves a simple elimination step during which one of the carbonyl ligands is replaced by a sulfide. The following equations summarise the syntheses:

$$R_3SnCl + NaS^tBu \longrightarrow R_3SnS^tBu + NaCl$$

Eq. 3.1

$$R_3SnS^tBu + M(CO)_6 \xrightarrow[-CO]{h\nu,\ THF} (CO)_5MS(^tBu)(R_3Sn)$$

M = Cr, R = ^{n}Bu (**14**), Me (**15**)

M = Mo, R = ^{n}Bu (**16**), Me (**17**)

Eq. 3.2

Complexes such as $[(CH_3)_3Sn]_2SCr(CO)_5$, $[(CH_3)_3Sn]S(C_6H_5)Cr(CO)_5$, $[(CH_3)_3Sn]_2SeW(CO)_5$, $[(CH_3)_3Ge]_2SW(CO)_5$, and $[(CH_3)_3Pb]_2SW(CO)_5$ have been synthesised by others and are well characterised. The crystal structure of $[(CH_3)_3Sn]_2SCr(CO)_5$ is shown in **Fig. 3.1**. [4] They were prepared by photochemical reaction between $M(CO)_6$ and the ligands. [4, 5, 8] However, none of the pentacarbonyl complexes reported here have been synthesised before.

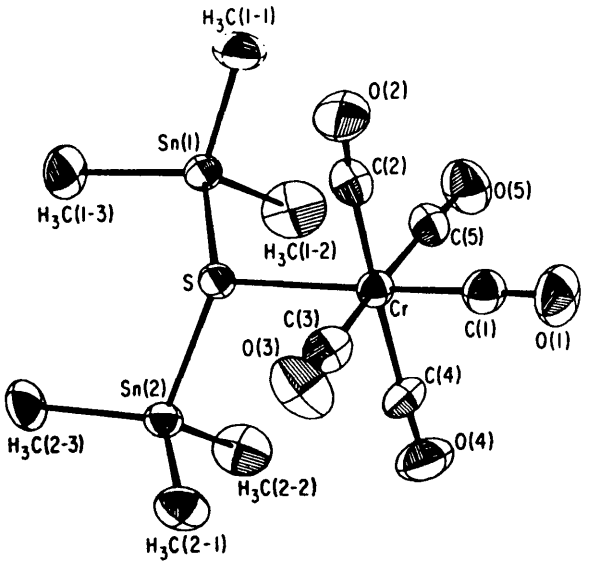

Fig. 3.1 The molecular structure of $[(CH_3)_3Sn]_2SCr(CO)_5$. [4]

Eq. 3.1 describes the synthesis of the trialkyltin sulfides, Bu_3SnS^tBu (**12**) Me_3SnS^tBu (**13**), used for the substitution of a CO group on the metal centre. Trialkyltin sulfides were synthesised by refluxing the sodium salt of tert-butyl thiol with trialkyltin chloride in toluene. The products were air-stable, clear viscous oils with pungent odour and were further purified by distillation. The yields recorded were 70% (**12**) and 65% (**13**), after distillation.

According to literature [13-18] trialkyltin thiolates can be synthesised by either employing the corresponding tin hydroxides or halides and the relevant thiol. The yields reported in literature are comparable with the ones reported here but more often than not these methodologies involve water as a solvent, making purification and drying of the product more tedious. Hence, in this study

trialkyltin halides and thiolate salts were employed for the synthesis of trialkyltin thiolates.

Eq. 3.2 demonstrates a two-step process. First, the dissolved metal hexacarbonyl is irradiated with UV light. Tetrahydrofuran, a highly co-ordinating solvent, displaces one of the CO groups forming a THF adduct, $M(THF)(CO)_5$, *in situ*. Consequently, substitution occurs when the sulfide ligand is added producing the tin sulfide metal pentacarbonyl complexes (**14**)-(**17**). [3-8] Complexes (**15**) and (**17**) were solids with low melting points (59 and 56 °C respectively), while (**14**) and (**16**) were oils.

All operations were carried out under an inert atmosphere (nitrogen or argon) since most metal carbonyl derivatives are sensitive to air, especially in solution. Their sensitivity strongly depends on the type of substituents on the transition metal and their lability. Furthermore, it has been shown experimentally [12] that relatively slight decomposition is sufficient to make isolation of a pure product difficult or impossible (poor crystallisation and great sensitivity of the crude product towards air). Purification of these complexes proved to be a laborious task since extensive sublimation was necessary in order to remove any unreacted hexacarbonyl complex. Furthermore, due to their low decomposition temperature (thermally unstable *ca.* 55 °C) [8] distillation, as a purification method, was rejected. Yields were comparable with those reported in literature, ranging from 42 to 53%.

3.2.2 NMR and Mössbauer Spectroscopy.

Since most of the naturally occurring isotopes of tin have I=0 a singlet is observed in the ^{1}H and ^{13}C NMR spectra, due to isotopes ^{116}Sn, ^{118}Sn and ^{120}Sn. In addition, it is also common to observe coupling between either ^{1}H or ^{13}C with isotopes ^{119}Sn, ^{117}Sn (sometimes ^{115}Sn) which have I=1/2. This is because the signal for either ^{1}H or ^{13}C is split into a doublet by the NMR active tin isotopes. These doublets appear as satellites on either side of the singlet and the coupling constants measured can give us important structural information. Furthermore,

the singlet is more intense since the NMR inactive tin isotopes are more abundant than the active ones. [1]

In the ^{119}Sn NMR spectrum a singlet is observed since the spectra are proton decoupled. However, satellites are also commonly observed in this case too. These are not due to coupling with other NMR active tin isotopes, unless a tin atom is directly bonded to another tin atom, but due to coupling with another NMR active nuclei, e.g. ^{13}C, ^{19}F.

For Bu_3SnS^tBu (**12**), ^1H and ^{13}C NMR spectra gave expected results. The methyl proton signal of the n-butyl is split into a triplet and the coupling constant is consistent with that predicted for alkyl groups. In the carbon spectrum we see the satellites from the NMR active isotopes of tin. Coupling constants give useful information about the co-ordination number for the particular element under investigation. Coupling constants ^1J, ^2J and ^3J were measured. The chemical shift in the tin spectrum is 49.9 ppm, clearly distinguishable from the chemical shift of the starting material Bu_3SnCl, (141.0 ppm). [1]

In the proton spectrum of Me_3SnS^tBu (**13**) the methyl protons attached on to tin give a singlet. Satellites were also resolved due to coupling with the ^{119}Sn isotope. In the $\{^1H\}^{13}C$ NMR spectrum all carbons were observed, as well as satellites (on the carbons closest to tin) from the NMR active isotopes of tin. The chemical shift in the tin spectrum is 58.2 ppm compared to 164 ppm for the starting material Me_3SnCl. [1] The coupling constants calculated are typical of tetrahedral tin compounds (e.g. ^{13}C NMR: 300-400 Hz, R_4Sn; ^1H NMR: 54 Hz, Me_4Sn). [1]All data are summarised in **Table 3.1**.

Mössbauer spectroscopy is a very useful technique to get structural information on a metal centre such as tin (^{119}Sn). For both compounds, (**12**) and (**13**), the Mössbauer isomer shifts correspond to a Sn(IV) centre ($\delta<2.70$ mms^{-1}) and the values for the quadrupole splitting are in accordance with tetrahedral compounds of the type R_3SnX (1.00-2.40 mm s^{-1}). [1]

R_3SnS^tBu

R	^1H NMR (Hz)	^{13}C NMR (Hz)	Mössbauer (mm s^{-1})
Me	$^2J(^{119}Sn^1H)$ 54.8	$^1J(^{119}Sn\text{-}^{13}C)$ 336.0	ΔE_Q=1.54 δ=1.24
^{n}Bu	$^3J(^1H\text{-}^1H)$ 14.5	$^1J(^{119}Sn^{13}C)$ 330.6 $^2J(^{119}Sn^{13}C)$ 36.9 $^3J(^{119}Sn^{13}C)$ 20.9	ΔE_Q=1.58 δ=1.26

Table 3.1. Coupling constants and Mössbauer parameters for R_3SnS^tBu.

In the ^{13}C NMR spectra *cis* and *trans* carbonyl groups were observed for all (**14**)-(**17**). In the ^{119}Sn NMR spectrum of $(CO)_5CrS(^tBu)(SnMe_3)$ (**15**) and $(CO)_5MoS(^tBu)(SnMe_3)$ (**17**) the chemical shifts are 120.1 and 116.0 ppm respectively. This is clearly distinguishable form that of the starting material Me_3SnS^tBu, 58.2 ppm. Furthermore, for $(CO)_5CrS(^tBu)(SnBu_3)$ (**14**) and $(CO)_5MoS(^tBu)(SnBu_3)$ (**16**) the chemical shift values in the ^{119}Sn NMR are 101.8 and 97.8 ppm respectively, compared to 49.9 ppm of the starting material Bu_3SnS^tBu.

Mössbauer data were only recorded for $Me_3Sn(^tBu)SCr(CO)_5$ (**15**) and $Me_3Sn(^tBu)SMo(CO)_5$ (**17**), since (**14**) and (**16**) were air-sensitive oils which made the recording of Mössbauer spectra very difficult. The parameters obtained for the chromium complex are ΔE_Q=2.06 mm s^{-1} and δ=1.30 mms^{-1}, while for the molybdenum complex ΔE_Q=2.04 mms^{-1} and δ=1.31 mms^{-1}. The isomer shift values correspond to a Sn(IV) centre, (δ <2 mms^{-1}), while the quadrupole splitting values are typical for a tetrahedral environment around tin. [1]

3.2.3 Infra-red Spectroscopy.

Infrared spectroscopy is a very useful technique for studying metal carbonyls. IR spectra are directly related to molecular symmetry and hence useful information can be derived about the structure and bonding of a carbonyl complex.

A metal hexacarbonyl has octahedral symmetry and therefore has only one carbonyl-stretching mode, which is IR active. For $Cr(CO)_6$ this is observed at 1983 cm^{-1}, while for $Mo(CO)_6$ at 1985 cm^{-1}. As reviewed in the literature, [7-11] there are four expected stretching frequencies for the CO in the $M(CO)_5$ moiety. The positions of the four CO-stretching vibrations for the $Cr(CO)_5$ skeleton are slightly dependent on the complex partner (ligand) and for $Cr(CO)_5L$ ($L=(CH_3)_3SnS(C_6H_5)$) are: [8]

2074 cm^{-1}
1996 cm^{-1}
1949 cm^{-1}
1926 cm^{-1}

The molecular symmetry in a pentacarbonyl metal complex is thought to approximate C_{4v} but this is highly dependent on the type of ligand (L). For a molecule with true C_{4v} symmetry only three IR active modes are observed. These are A_1, A_2 and E (doubly degenerate), while the B_1 and B_2 are only Raman active. However, since in a typical $M(CO)_5L$ the molecular symmetry is not truly C_{4v}, due to the influence of the unsymmetrical ligands, the IR spectra show four CO-stretching vibrations and this comes as a result of the removal of the degeneracy of the E vibration.

The actual values observed for the carbonyl complexes (**14**)-(**17**) are very similar to the ones reported in literature [7-11] and are summarised in the table below, **Table 3.2**.

$(R_3Sn)(^tBu)SM(CO)_5$

R	Cr (cm^{-1})	Mo (cm^{-1})	Values for $Cr(CO)_5L$ [8] L=$(CH_3)_3SnS(C_6H_5)$
Me	2062	2070	2074
	1976	1983	1996
	1934	1936	1949
	1919	1917	1926
^nBu	2062	2069	
	1978	1981	
	1935	1958	
	1928	1910	

Table 3.2 Infrared absorbances of $(R_3Sn)(^tBu)SM(CO)_5$.

3.2.4 Thermal Analysis

Compounds **(15)**-**(17)** were investigated using Thermal Gravimetric Analysis (TGA) in order to have an indication of the temperature at which decomposition may be expected to start. In this regard, the data also suggest information concerning the relative stability of the compounds. TGA analysis was carried out at atmospheric pressure under a N_2 flow.

The TGA of **(15)** **(Fig. 3.2)** shows the decomposition to begin at around 80 °C and complete at 650 °C. The first small step observed at 126 °C corresponds to only a 4.8% weight loss and is attributed to the elimination of a CO molecule, (observed mass loss: 4.8, theoretical: 6.3%). Between 135 and 250 °C further decomposition results to CrS_2 (observed residual mass: 27.2, theoretical: 26.1%). Finally, a species with mass corresponding to CrS is formed at 623 °C (observed residual mass: 17.3, theoretical: 18.9%).

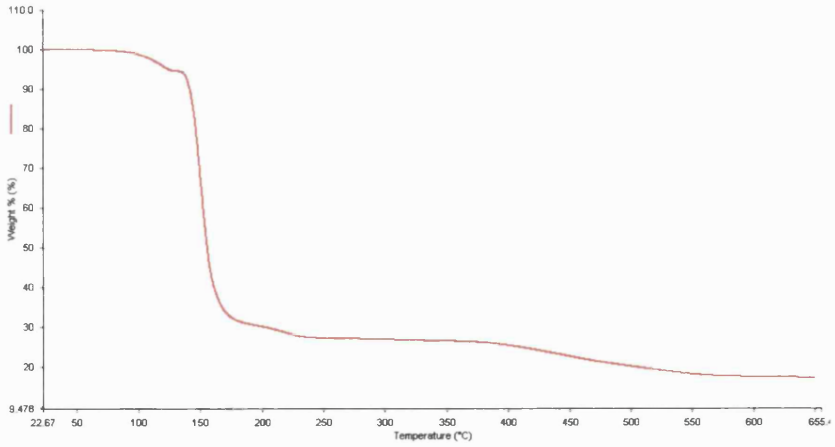

Fig. 3.2 TGA of $(CO)_5CrS(^tBu)(SnMe_3)$ (**15**)

The TGA of (**16**) (**Fig. 3.3**) shows the decomposition to begin at around 80 °C and complete at 400 °C. Precursor (**16**) is and oil and hence most volatile. Here decomposition seems to take place along with evaporation of the precursor, as almost no residue is left. The residual mass of 11.9% observed at the end of the decomposition is in fact less than that expected if the residue was the due to the lighter metal, *i.e.* Mo.

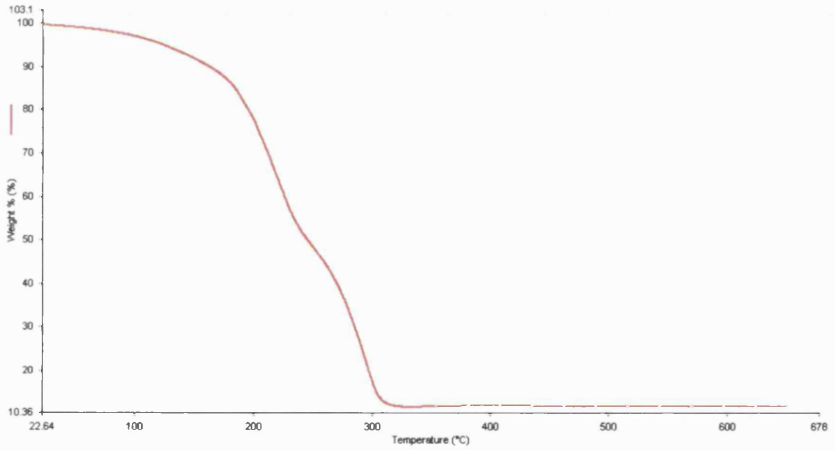

Fig. 3.3 $(CO)_5MoS(^tBu)(SnBu_3)$ (**16**)

The TGA of (**17**) (**Fig. 3.4**) shows the decomposition to begin at around 80 °C and is complete at 650 °C. The first step observed at 100 °C corresponds to a 28.3% weight loss and is consistent with the elimination of five CO molecules, (observed mass loss: 28.3, theoretical: 28.6). Between 168 and 222 °C further decomposition results to a species with mass corresponding to either MoSnS

(observed residual mass: 53.5, theoretical: 50.5), or $MoSnS_2$ (observed residual mass: 53.5, theoretical: 57.0). Finally, a species with mass attributed to MoS is formed at 606 °C (observed residual mass: 23.2, theoretical: 26.2).

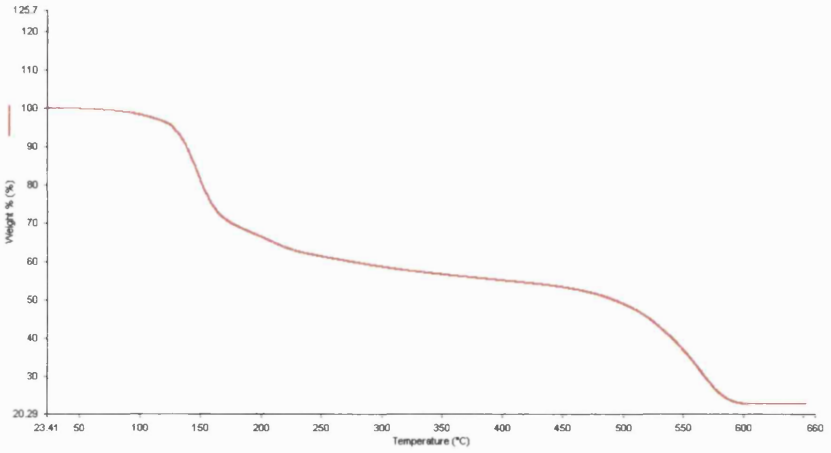

Fig. 3.4 $(CO)_5MoS(^tBu)(SnMe_3)$ (**17**)

3.3 Film Growth Results

3.3.1 Introduction

The primary reason for studying (**15**)-(**17**) was their volatility (low melting point) and their potentially clean decomposition pathway. However, due to the fact that their decomposition temperatures were also very low the method of APCVD was not suitable and hence the AACVD technique was employed instead.

Compounds (**15**)-(**17**) were tested for potential use as CVD precursors. They were screened using purpose-built equipment at the University of Bath (for reactor description see **Appendix Two**).

3.3.2 Deposition Conditions

Films were deposited by AACVD on standard borosilicate glass slides. The substrate was heated at temperatures ranging from 180 to 450 °C in order to deposit suitable films using these precursors. For each growth experiment, approximately 0.2 g of complex was used dissolved in THF.

Tetrahydrofuran was chosen as the solvent primarily because all compounds were very soluble in it. Furthermore, because of its relatively low boiling point, it evaporates quickly once it has entered the growth chamber minimising the danger of becoming incorporated in the growing film. THF, freshly distilled over sodium-benzophenone, was used to dissolve the precursors.

Because the precursors were all air-sensitive standard Schlenk-line techniques were required for the transportation of the precursor solution to the reactor and it was subsequently injected into the nebulising chamber under a flow of ultra-pure argon.

Deposition conditions for the films analysed are displayed in **Table 3.3**. Both low and high temperature runs were carried out for all the complexes in order to ascertain any differences in the films deposited.

Compound	**(15)**	**(15)**	**(16)**	**(16)**	**(17)**	**(17)**
Film ID	**556**	**557**	**565**	**566**	**562**	**563**
Reactor Temp. (°C)	250	180	450	300	300	270
Carrier Gas (Ar) Flow Rate (l/min)	1.0	1.0	1.0	1.0	1.0	1.0
Run Time (min)	30	30	30	30	30	30

Table 3.3 AACVD conditions for experiments with compounds **(15)**-**(17)**.

3.3.3 Film Analysis

Films were examined using a number of techniques: Visual Inspection, Glancing Angle X-Ray Diffraction, Energy Dispersive X-Ray Analysis (EDAX), Scanning Electron Microscopy (SEM) and Raman Spectroscopy.

*Visual Inspection, Scanning Electron Microscopy (SEM) and Raman Spectroscopy for Films **556** and **557***

Both films **556** and **557** were deposited from precursor (**15**) but at different temperatures. Film **557**, deposited at the highest temperature (250 °C), covered only the first slide of the eight constituting the glass substrate, while film **556** deposited at the lowest temperature (180 °C), covered all eight with an apparent colour change after the first slide.

The first slides of both films were clear with some interference fringes evident and were well adhered with no powdery surface layer. For film **556** however, the remaining slides showed a very different in visual appearance film, being brownish and having a powdery surface layer, which could easily be removed with a soft tissue.

Raman Spectroscopy was employed to analyse these films as well. Unfortunately, the films were very thin for the technique to give conclusive results. However, some graphitic carbon could potentially be identified as a broad peak in the region of 1400-1600 cm^{-1} in the spectrum of film **556** (slide 1).

Scanning electron microscopy (SEM) was used to analyse these thin films. SEM images of both films (**Fig. 3.5** to **Fig. 3.11**) showed a uniform coverage consisting of very small spheres. The islands seen on the film could indicate that it was deposited via the island growth mechanism.

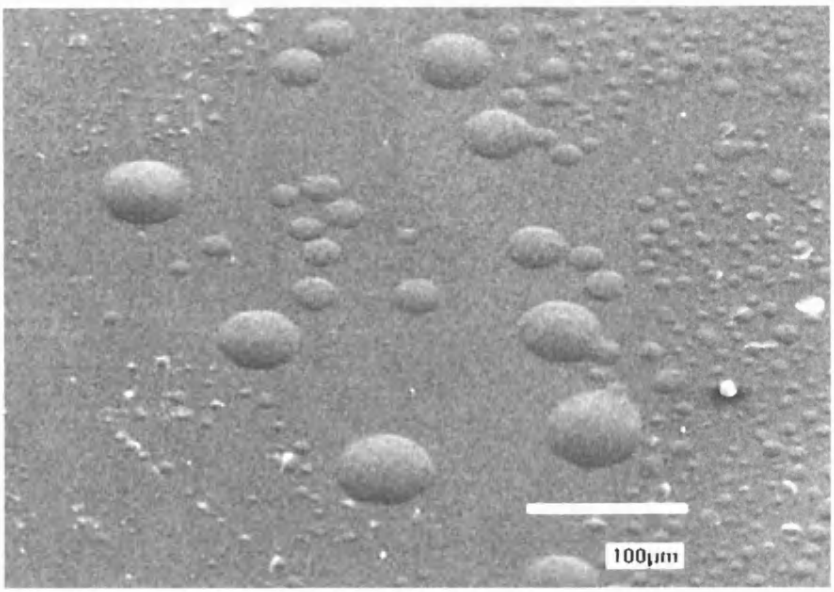

Fig. 3.5 45° tilt SEM image from film **557**, precursor (**15**), T=180 °C.

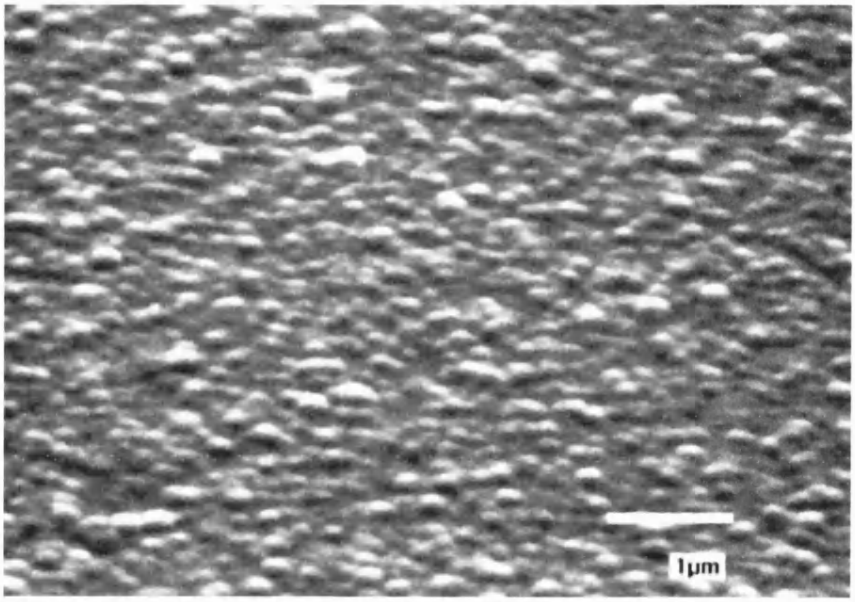

Fig. 3.6 45° tilt SEM image from film **557** at higher magnification.

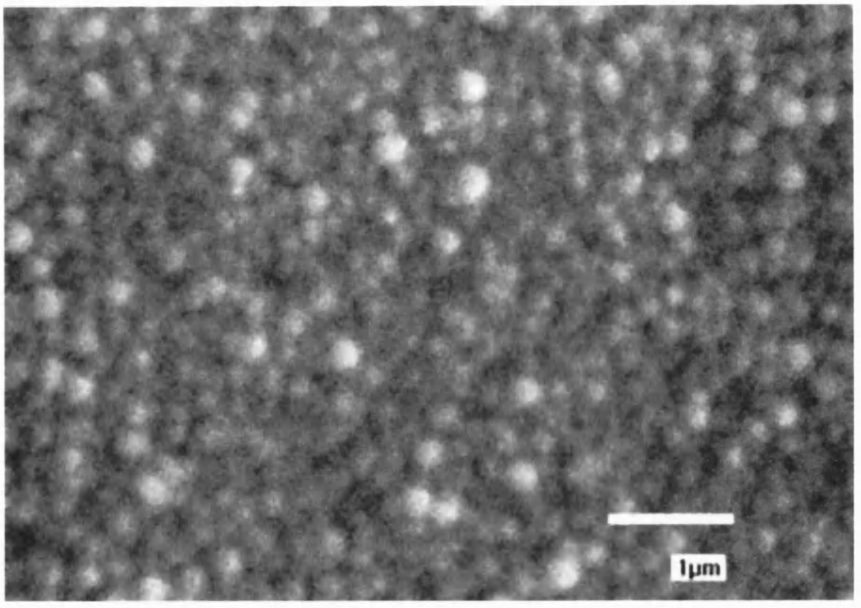

Fig. 3.7 0° tilt SEM image from film **557**.

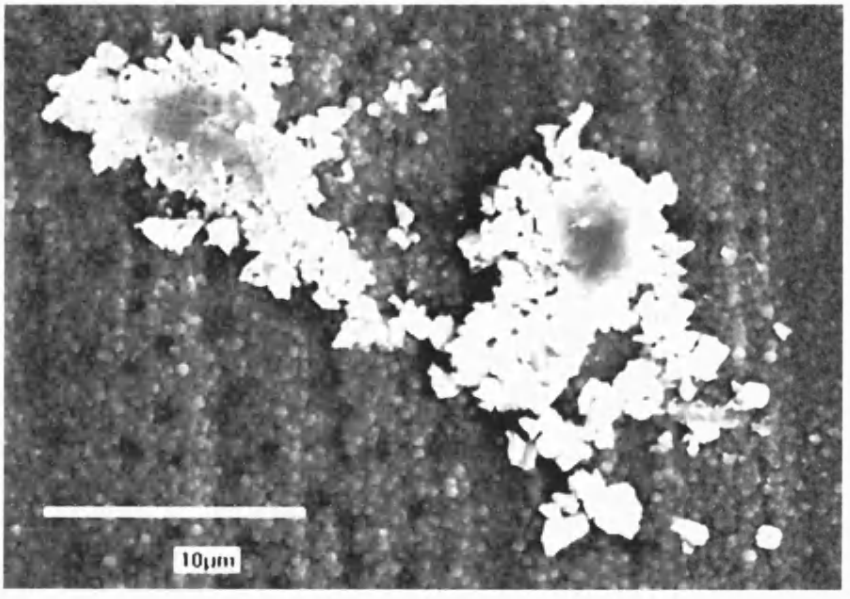

Fig. 3.8 0° tilt SEM image from film **556** (slide 1), precursor (**15**), T=250 °C. Some crystalline features are obvious. EDAX analysis suggested they were the same material as the bulk of the film.

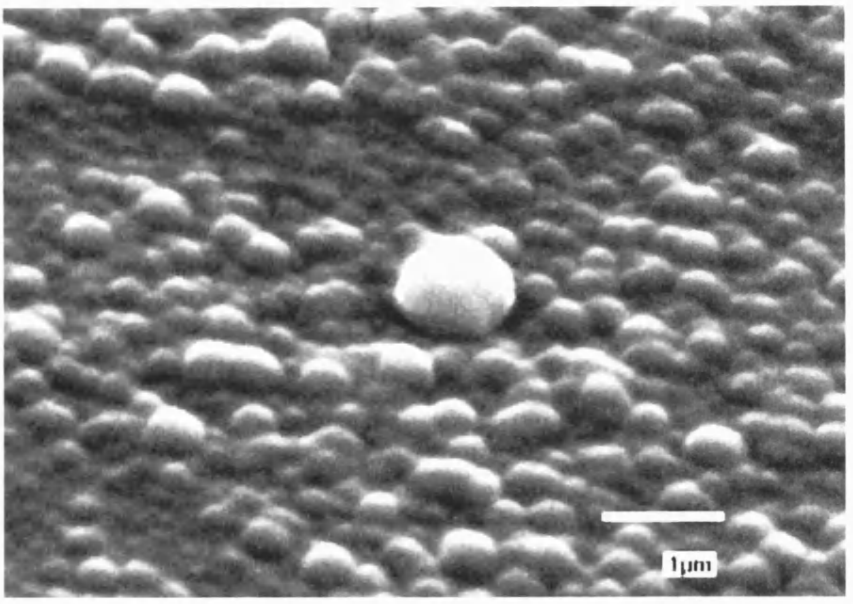

(a)

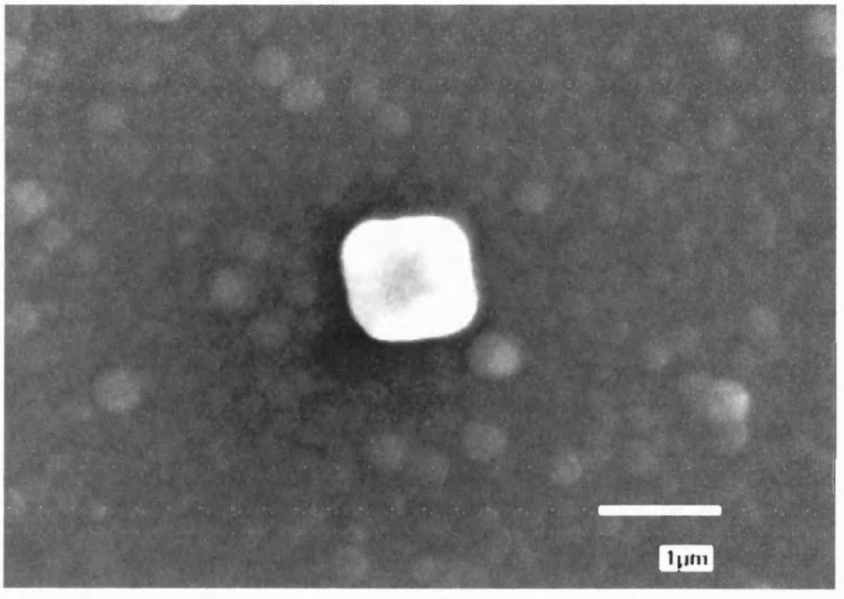

(b)

Fig. 3.9 (a) 45° tilt and **(b)** 0° tilt SEM image from film **556** (slide 1), at higher magnification and featuring a crystallite (same material as the bulk of the film).

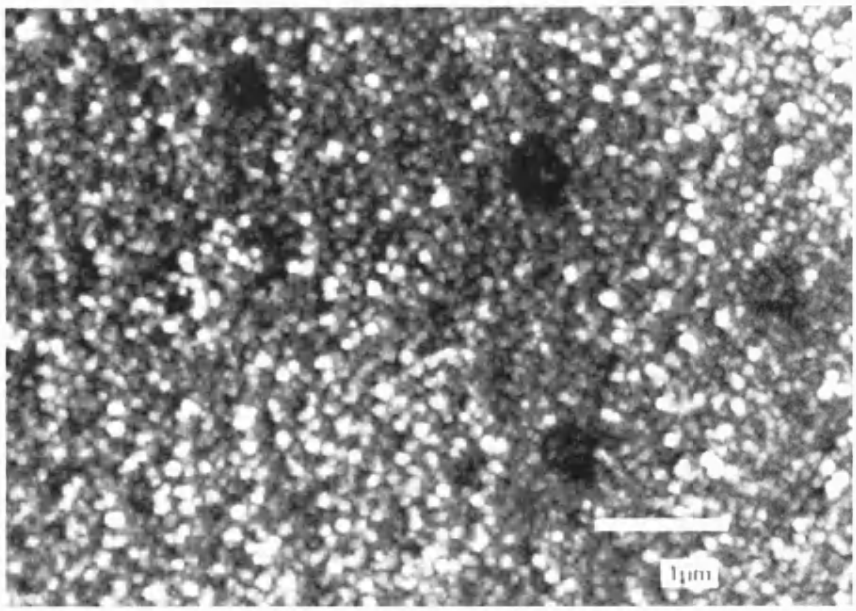

Fig. 3.10 0^{o} tilt SEM image from film **556** (slide 5), precursor (**15**), T=250 ^{o}C. The black areas shown on the film are shallow holes.

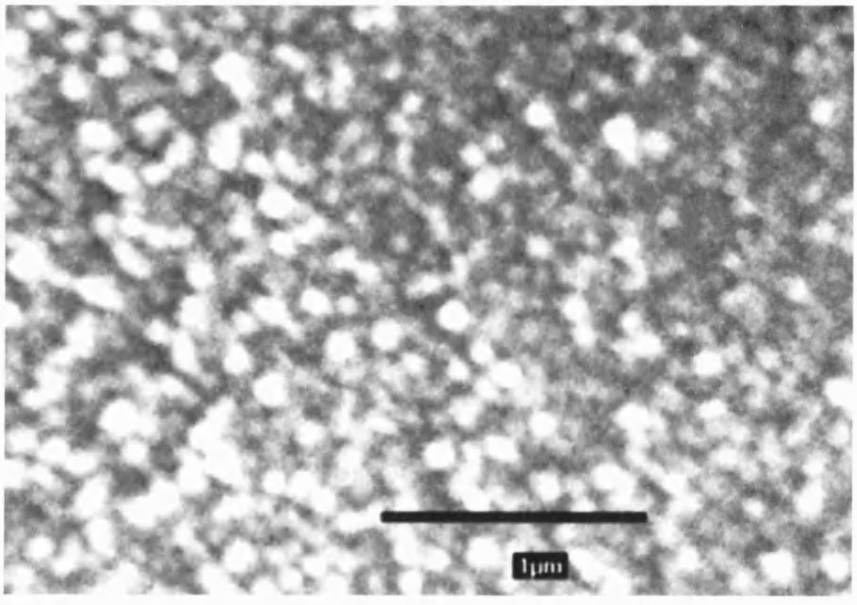

Fig. 3.11 0^{0} tilt SEM image from film **556** (slide 5) at higher magnification.

Energy Dispersive X-Ray Analysis (EDAX) For Films 556 and 557

EDAX analysis showed film **557** and the first slide of film **556** to contain chromium, tin and sulfur, while on the remaining slides of film **556**, where a brownish film appeared, the presence of mostly chromium and sulfur was verified. The findings for the brown film deposited (**556**) are in accordance with what would visually be expected for a type of chromium sulfide since CrS is black and Cr_2S_3 is brown-black. [19]

Glancing Angle X-Ray Diffraction for Films 556 and 557

Glancing Angle X-Ray Diffraction studies were performed to determine whether the films were crystalline or amorphous. This technique also gives information on the type of material deposited as well as its particular phase. The X-ray patterns were obtained with incident angle, ϑ (theta), locked at 2.5° and over the 2ϑ range of 0° to 75°.

The glancing angle X-ray diffraction patterns of the films **556** and **557** were amorphous (see **Fig. 3.12(a)** and **(b)**). The thin nature of the films allows the underlying amorphous glass to be observed as a broad hump in the range of 10-40°.

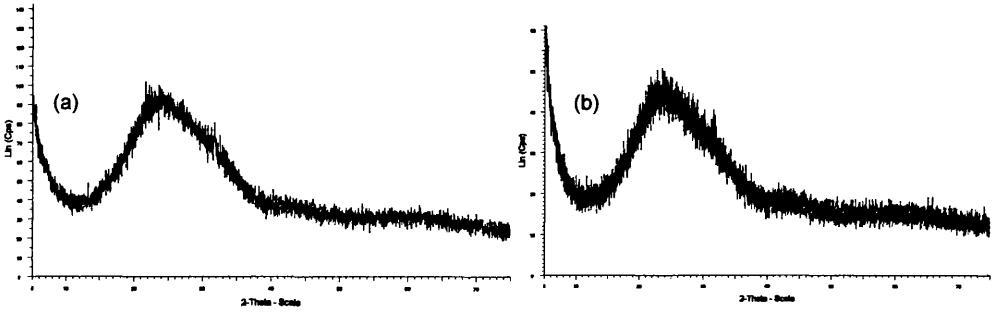

Fig. 3.12 Glancing angle X-ray pattern of film **556 (a)** and film **557 (b)**, precursor $(CO)_5CrS(^tBu)(SnMe_3)$ (**15**)

In summary, two different types of film were deposited from precursor (**15**). The film with brown appearance, deposited at higher temperature, (end-slides of film

556) is thought to be a type of chromium sulfide, possibly CrS. This view is supported by both EDAX (only chromium and sulfur present) and TGA analysis results. The other transparent film (**557** and **556** first slide), is determined to be a type of tin containing chromium sulfide as suggested by EDAX data (chromium, tin and sulfur present).

*Visual Inspection, Scanning Electron Microscopy (SEM) and Raman Spectroscopy for Films **562** and **563***

Films **562** and **563** had similar appearance, being dark brown with a metallic finish and very reflective. They covered on average half the length of the glass substrate and were very well adhered with no powdery surface layer.

Raman Spectroscopy used to analyse these films revealed that film **562** could potentially contain some graphitic carbon due to the broad hump observed in the Raman spectrum (between 1500-1700 cm^{-1}).

Scanning electron microscopy (SEM) was used to analyse these thin films. SEM images of both films (**Fig. 3.15** to **Fig. 3.15**) showed a uniform coverage. For film **562**, deposited at the highest temperature (300 °C) from precursor (**17**), the SEM image suggests a very smooth film, while for film **563**, deposited at the lowest temperature (270 °C) from precursor (**17**), the SEM images suggest a consistency of very small spheres and crystallites of various sizes.

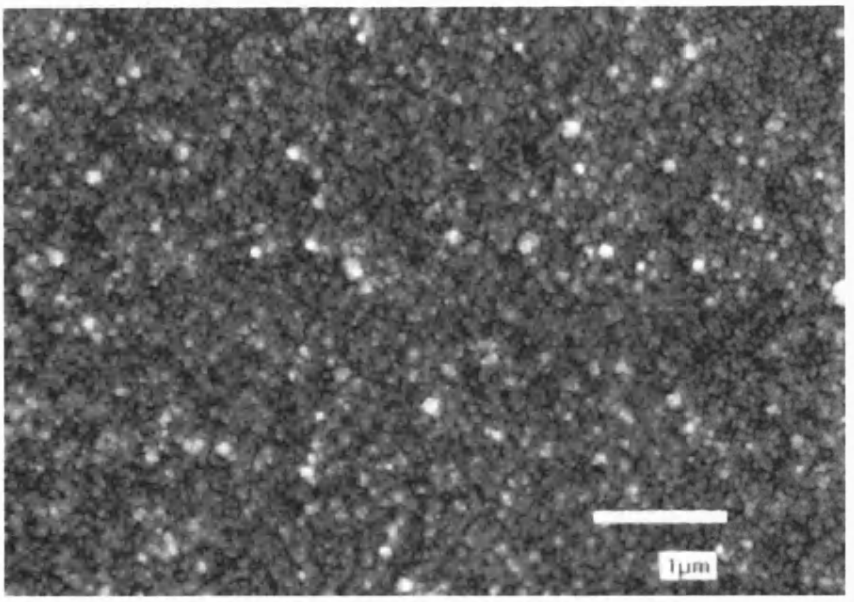

Fig. 3.13 0° tilt SEM image from film **562** (slide 1), precursor (**17**), T=300 °C.

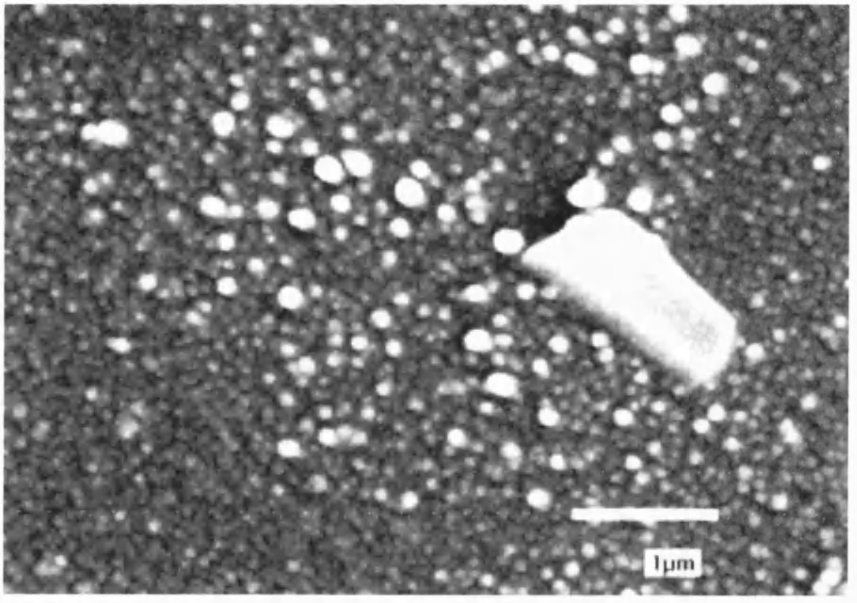

Fig. 3.14 0° tilt SEM image from film **563** (slide 3), featuring a crystallite, precursor (**17**), T=270 °C. EDAX analysis verified the fact that the crystallites were the same type of material as the bulk of the film.

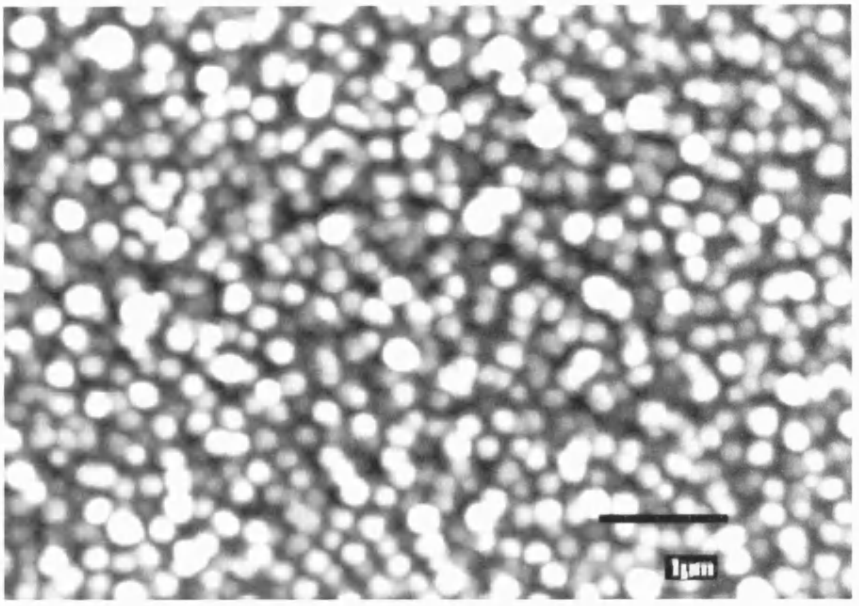

Fig. 3.15 0° tilt SEM image from film **563** (slide 1) at higher magnification.

*Energy Dispersive X-Ray Analysis (EDAX) For Films **562** and **563***

EDAX analysis showed both films **562** and **563** to contain molybdenum, tin and sulfur (**Fig. 3.16, Fig. 3.17**).

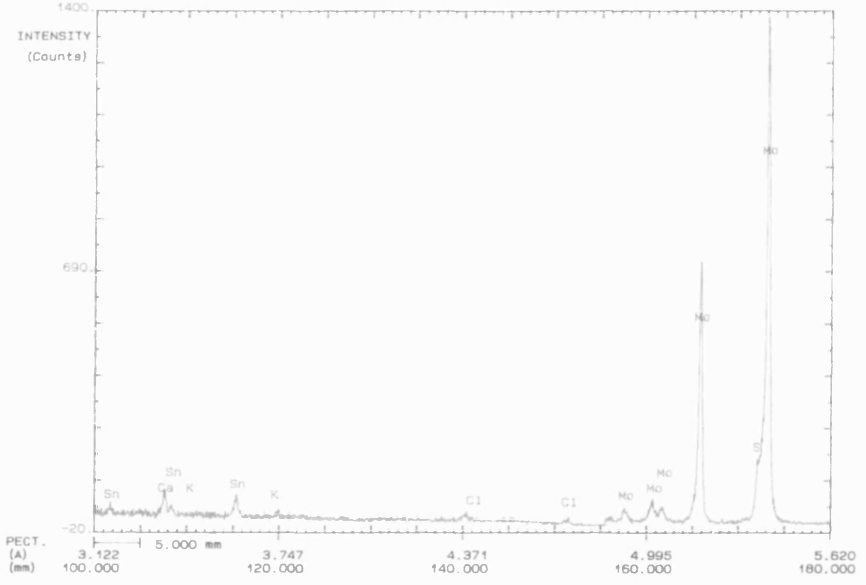

Fig. 3.16 EDAX qualitative analysis of film **562** (accelerating voltage 6.0 kV)

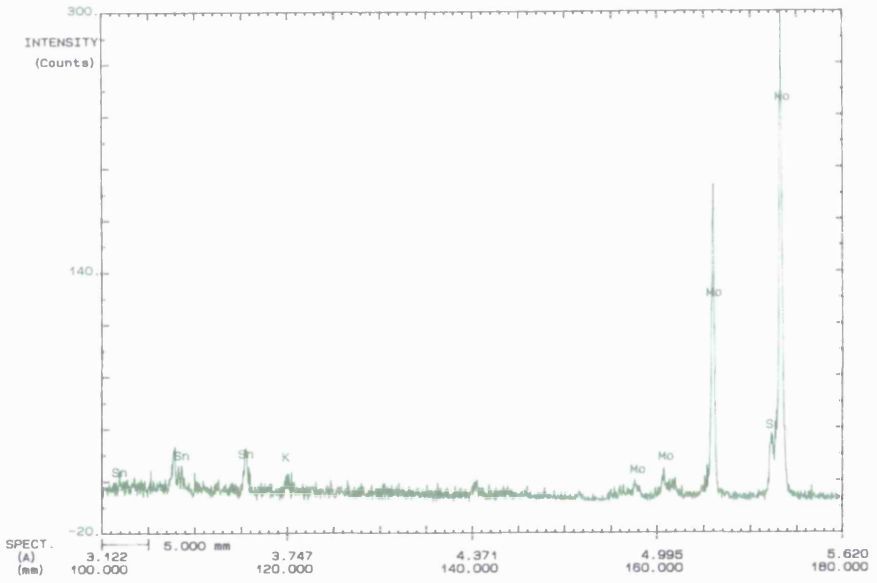

Fig. 3.17 EDAX qualitative analysis of film **563** (accelerating voltage 6.0 kV)

*Glancing Angle X-Ray Diffraction for Films **562** and **563***

The glancing angle X-ray diffraction patterns of the films **562** and **563** indicated that the films on some of the slides were crystalline while the rest were amorphous. This could be due to a possible temperature gradient throughout the heated substrate, which causes the deposition temperature to vary slightly from slide to slide resulting in varying crystallinity of the films. Another possible explanation for this effect could be the fact that either a temperature gradient and/or mass transport rate issues result in different types of films formed along the heated substrate.

Diffraction patterns were observed on slide 1 for both film **562** and film **563**. Due to the nature of this x-ray technique, the examination of crystalline films can be different from, for example, the examination of powders. The main difference is that crystalline films can have a preferred orientation towards the incident x-ray beam resulting in some of the reflections being enhanced while others being diminished. Therefore, the peaks shown in **Fig. 3.18** and **Fig. 3.19** are indicative of the types of materials present but their relative intensities are somehow untypical. Peak match software suggested tin molybdenum sulfide ($SnMo_6S_8$) as the possible deposited material for film **562** (**Fig. 3.18**) and **563**

(**Fig. 3.19**). However, β-Mo_2C and MoS_2 were also plausible candidates but the data fit was marginally worse (see **Table 3.4**).

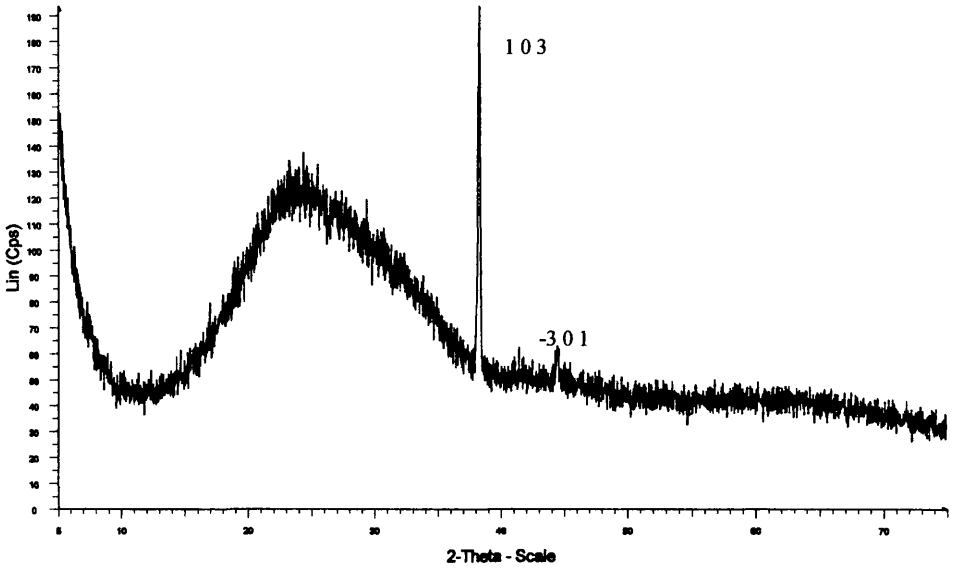

Fig. 3.18 Glancing angle X-ray diffraction pattern for film **562**.

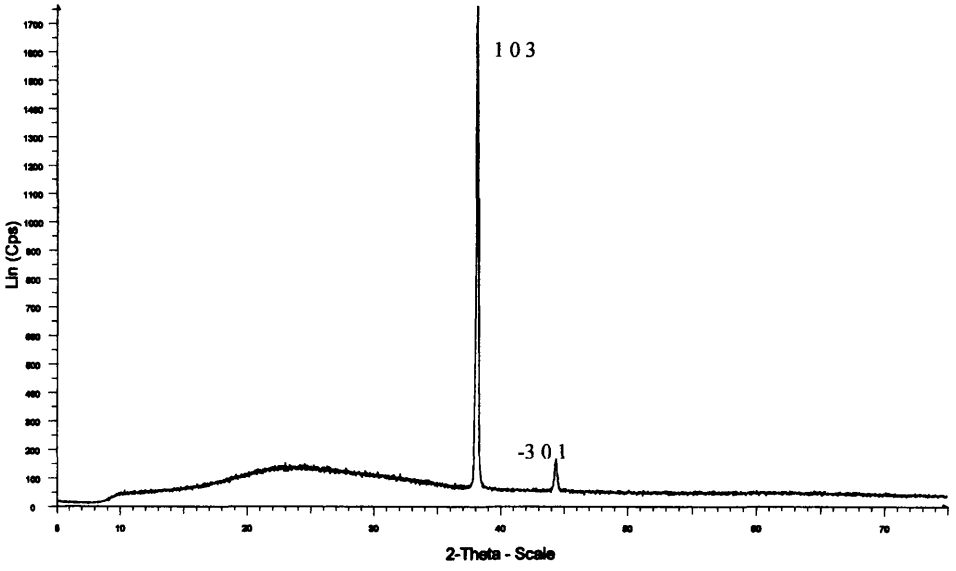

Fig. 3.19 Glancing angle X-ray diffraction pattern for film **563**.

In summary, both films **562** and **563** contain tin sulfur and molybdenum. Unfortunately, the films were very thin for a quantitative analysis X-ray

experiment therefore, the exact ratio of the elements in the deposited films is not known. However, one can safely assume (see **Fig. 3.16** and **Fig. 3.17**) that the amount of molybdenum in both films is more than the amount of tin. Furthermore, the X-ray diffraction patterns of both films are almost identical, indicating that they are likely to be the same material. Therefore, we can safely conclude that both the deposited films are tin containing molybdenum sulfides as verified by the peak match software, which indicates that $SnMo_6S_8$ is a possible material for the reflections observed. In addition, the appearance of the films supports this conclusion since most molybdenum sulfides match the colours observed on the slides (e.g. MoS_2 is black-lustre, MoS_4 brown, Mo_2S_3 steel grey and MoS_3 black). [19] Furthermore, the TGA analysis for precursor (**17**) concludes that a material such as MoSnS is formed at 220 °C, which upon heating to 600 °C eliminates tin to give MoS_2. Therefore, a CVD experiment between 220 and 600 °C would give results that could be consistent with loss of some tin from 'MoSnS' and hence producing a tin containing molybdenum sulfide such as $SnMo_6S_8$. However, for film **562** (deposited at higher temperature, 300 °C), molybdenum sulfide (MoS_2) is also suggested by the peak match software, but from the TGA data we conclude that this could only be possible at a much higher temperature than the one this film was deposited at. In addition, for film **563** the peak match software suggests the possibility of molybdenum carbide (β-Mo_2C). This could have been observed due to incorporation of carbon impurities resulting from the decomposition of the alkyl or carbonyl ligands present in the precursor.

The following table (**Table 3.4**) summarises the experimental and theoretical X-ray diffraction data for films **562** and **563**.

Film ID	d found (Å)	2theta (°)	$SnMo_6S_8$	MoS_2	β-Mo_2C
562	2.352	38.22	2.354 (1 0 3)	2.344 (1 0 4)	2.371 (14 5 1)
	2.037	44.44	2.036 (-3 0 1)	2.034 (0 0 9)	2.030 (6 6 4, 8 4 4)
563	2.366	37.10	2.354 (1 0 3)	2.344 (1 0 4)	2.371 (14 5 1)
	2.043	44.30	2.036 (-3 0 1)	2.034 (0 0 9)	2.030 (6 6 4, 8 4 4)

Table 3.4 Summary of the X-ray reflection data for films **562** and **563** and the data for the corresponding materials from the peak match software.

*Visual Inspection Scanning Electron Microscopy (SEM) and Raman Spectroscopy for Films **565** and **566***

Films **565** and **566** had the same appearance as films **562** and **563**. They were dark brown with a metallic finish and very reflective. They covered on average half the length of the glass substrate and were very well adhered with no powdery surface layer.

Raman Spectroscopy was employed to analyse films **565** and **566** as well. The incorporation of some graphitic carbon was evident as a broad band in the Raman spectra obtained (1500-1600 cm^{-1}) for both films. Furthermore, the existence of SnS was indicated in the spectrum of film **565** (sharp peaks at 187 and 211 cm^{-1})

Scanning electron microscopy (SEM) was used to analyse thin films **565** and **566** deposited from precursor (**16**). Film **565** was deposited at the highest temperature (450 °C) while film **566** at the lowest temperature (300 °C). SEM images of both films (**Fig. 3.20** to **Fig. 3.25**) showed a uniform coverage. For both films the SEM images suggest very smooth films consisting of very small spheres and various size crystallites.

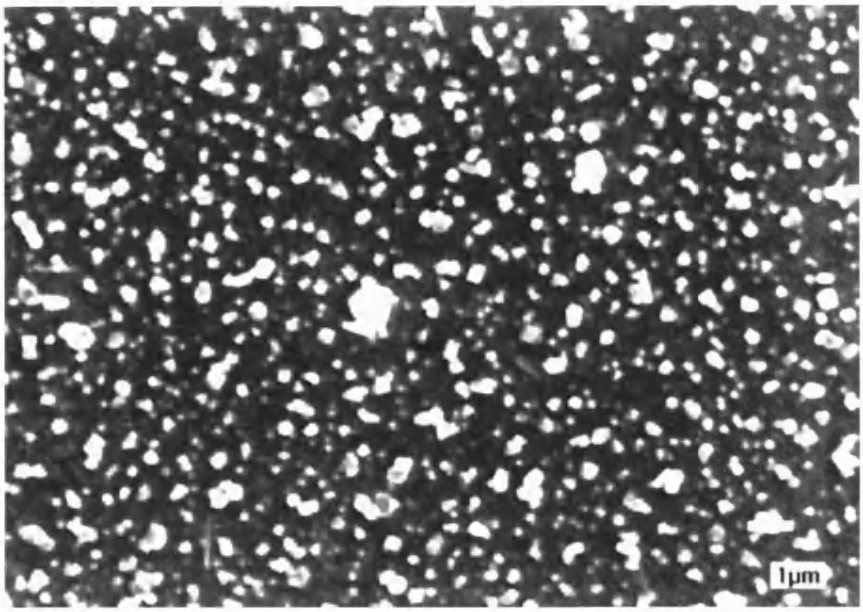

Fig. 3.20 0^0 tilt SEM image from film **565** (slide 1), precursor (**16**), T=450 ^oC

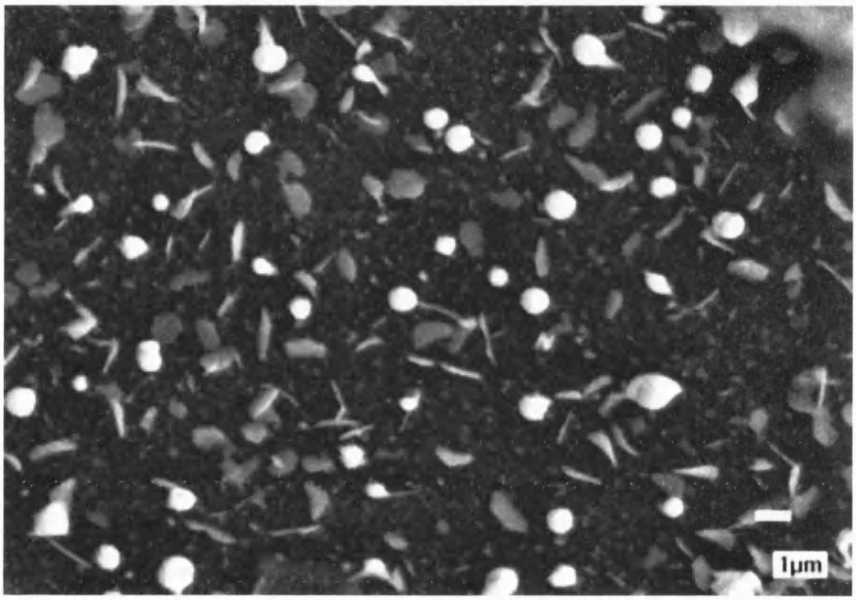

Fig. 3.21 0^o tilt SEM image from film **565** (slide 4).

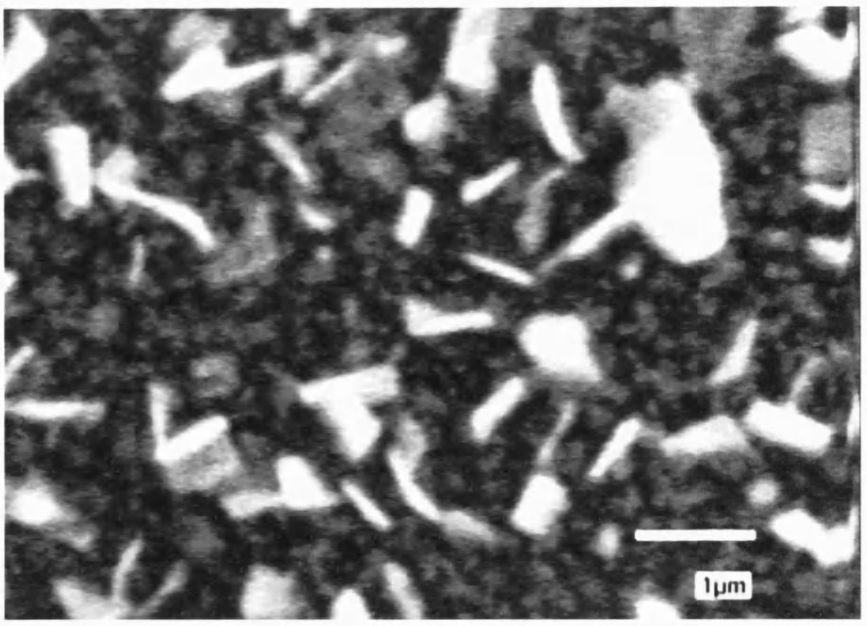

Fig. 3.22 0^{o} tilt SEM image from film **565** (slide 4) at higher magnification.

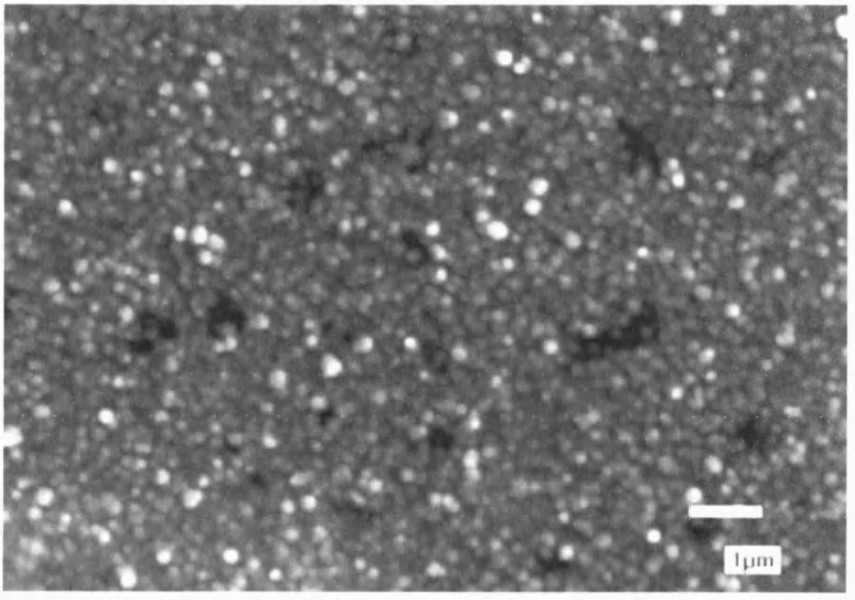

Fig. 3.23 0^{o} tilt SEM image from film **566** (slide 1), precursor (15), T=300 oC. The black areas shown on the film are shallow holes.

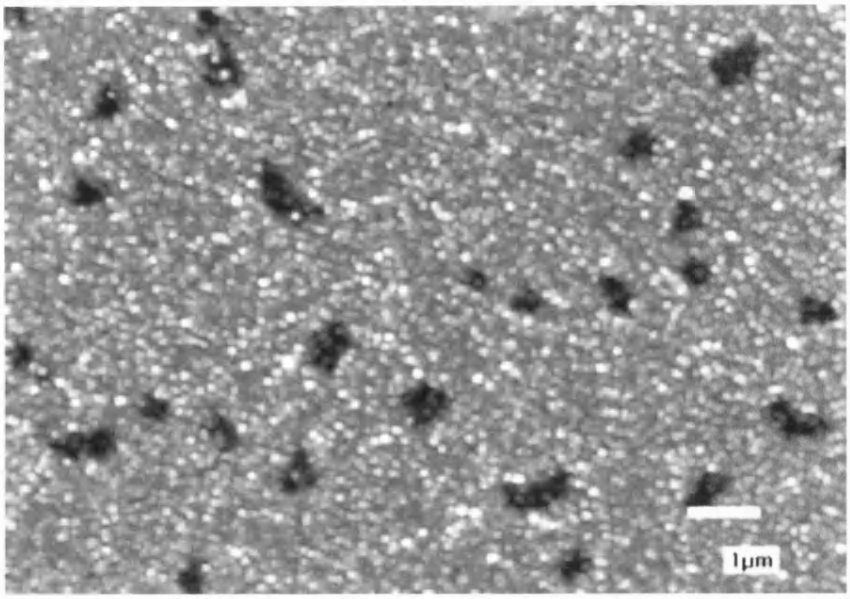

Fig. 3.24 0^{o} tilt SEM image from film **566** (slide 2)

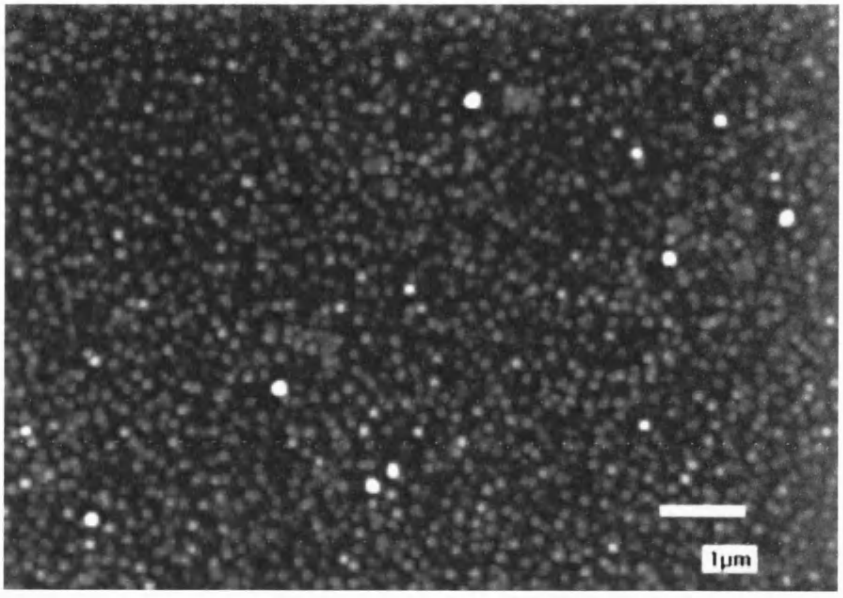

Fig. 3.25 0^{o} tilt SEM image from film **566** (slide 3)

*Energy Dispersive X-Ray Analysis (EDAX) For Films **565** and **566***

EDAX analysis showed both **565** and **566** films to contain molybdenum, tin and sulfur (**Fig. 3.26, Fig. 3.27**).

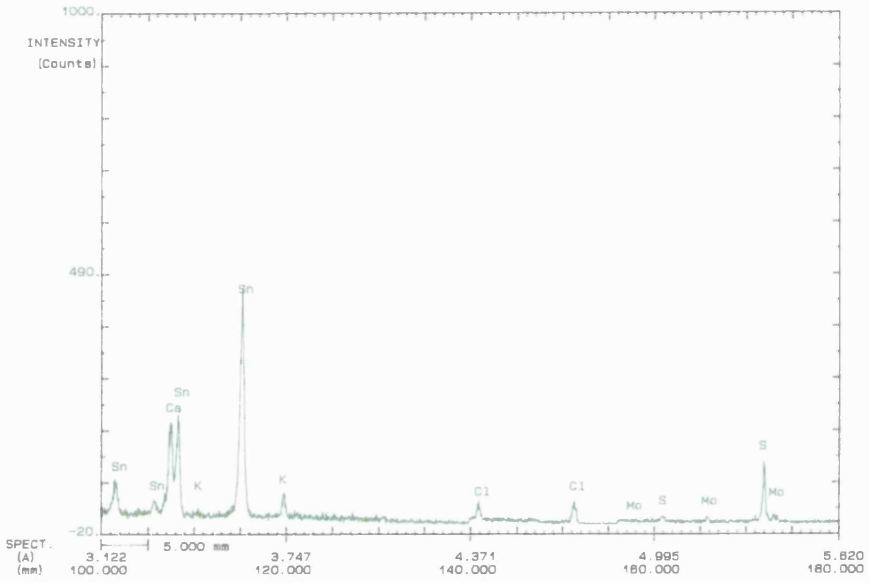

Fig. 3.26 EDAX qualitative analysis of film **565** (accelerating voltage 6.0 kV)

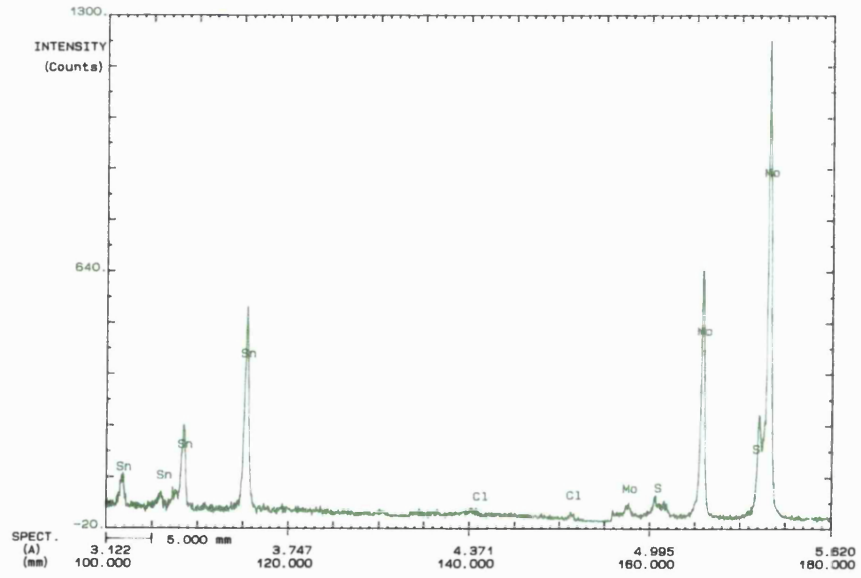

Fig. 3.27 EDAX qualitative analysis of film **566** (accelerating voltage 6.0 kV)

*Glancing Angle X-Ray Diffraction for Films **565** and **566***

Diffraction patterns were observed for film **565** (slide 4), while for film **566** (**Fig. 3.29**) all the slides were proved to be amorphous. **Fig. 3.28** shows the reflections obtained from film **565**.

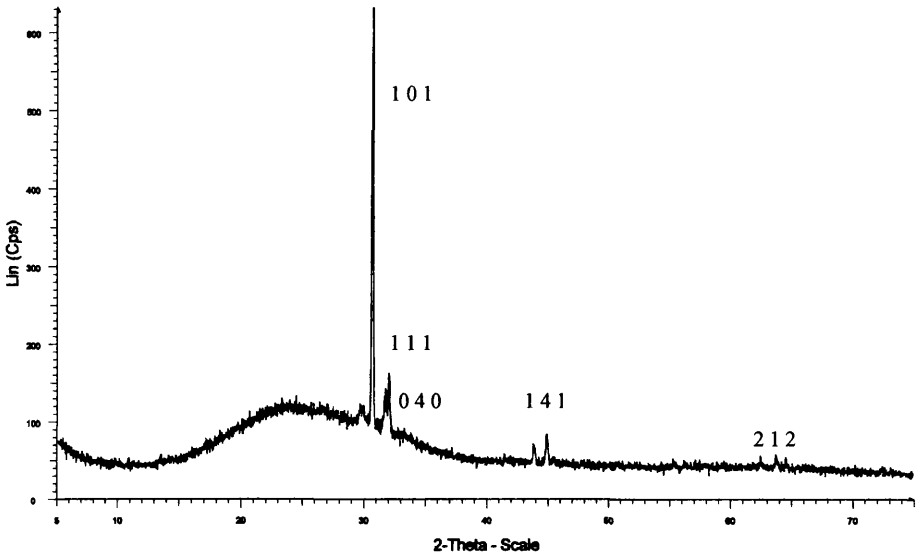

Fig. 3.28 Glancing angle X-ray diffraction pattern for film **565**

Peak match software suggested three possible types of materials for film **565**: SnS, γ-Sn_2S_3 and molybdenum tin sulfide (Mo_6S_8Sn or $Mo_6Sn_xS_{8-z}$),.

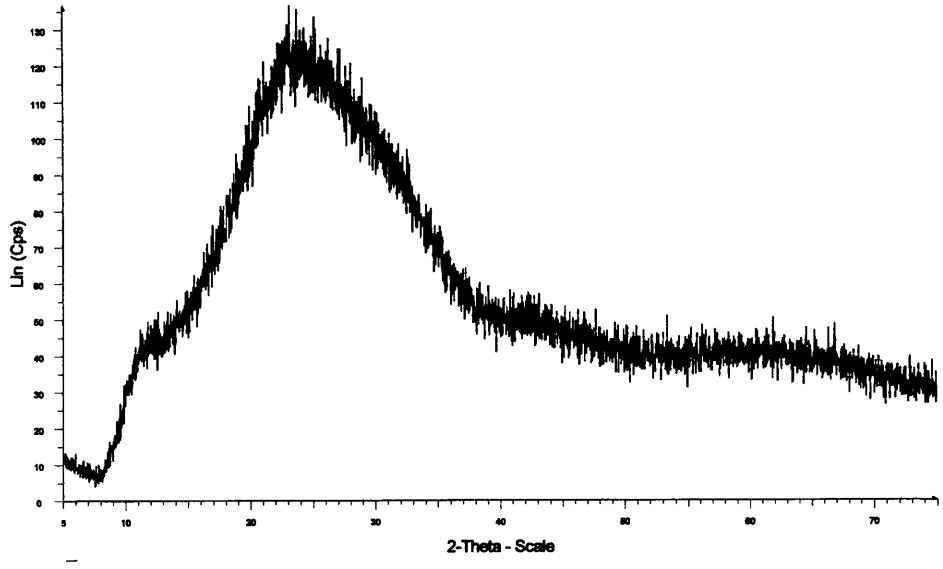

Fig. 3.29 Glancing angle X-ray diffraction pattern for film **566**

In summary, as for films **562** and **563**, both films **565** and **566** contain tin sulfur and molybdenum. However, for film **565** the qualitative EDAX analysis revealed a tin-rich film with very small amounts of molybdenum. Furthermore, SEM analysis revealed a film with very different appearance from **562**, **563** and **565**. In fact, the crystalline appearance of film **565** is very similar to that observed for SnS films in other CVD studies. [20] In addition, materials such as tin sulfide (γ-Sn_2S_3), (suggested by Glancing Angle X-ray results) and SnS (suggested by Raman spectroscopy and Glancing Angle X-ray) could be likely for film **565** (deposited at higher temperature). Peak match software also suggested that types of tin molybdenum sulfide fit the data for film **565**. However, the SnS parameters seem to fit the obtained data the best (see **Table 3.5**). Hence, since there is evidence from all SEM/film appearance, Raman Spectroscopy and Glancing Angle X-ray for the existence of SnS in film **565** it can be concluded that film **565** consists of a crystalline SnS film with some small traces of molybdenum.

Since film **566** was amorphous and no peaks were observed in the Raman spectrum the only data to identify this film with come from the EDAX and SEM analyses. These suggest that film **566** is probably the same as **562** and **563**, i.e. a

type of tin molybdenum sulfide. The following table (**Table 3.5**) summarises the experimental and theoretical X-ray diffraction data for film **565**.

Film ID	d found (Å)	2theta (°)	SnS Herzenbergite	γ-Sn_2S_3	Mo_6S_8Sn	$Mo_6Sn_xS_{8-z}$
	3.005	29.70				
	2.923	30.56	2.931(1 0 1)	2.959(0 3 1)	2.905(2 1 1)	2.910(1 1 3, 2 1 1)
	2.826	31.64	2.835(1 1 1)	2.826(2 0 1)		
565	2.801	31.92	2.797(0 4 0)			
	2.065	43.80		2.089(2 6 0)	2.058(3 1 2)	2.061(2 1 4, 3 1 2)
	2.021	44.81	2.024(1 4 1)	2.032(3 5 0)		
	1.458	63.77	1.454(2 1 2)	1.453(5 4 1)	1.458(2 2 6)	1.460(2 2 6)

Table 3.5 Summary of the X-ray reflection data for film **565** and the data for the corresponding materials from the peak match software.

3.4 Conclusions

The successful synthesis and characterisation of pentacarbonyl transition metal tin sulfides, (**14**)-(**17**), is reported. Compounds (**15**)-(**17**) were tested for their suitability as single-source CVD precursors in depositing ternary materials of the type M/Sn/S (M = Cr, Mo).

For compound (**15**) the bulk decomposition (TGA) studies suggest that decomposition should take place via the formation of CrS_2 (*ca* 250 °C) to finally leave CrS (*ca* 623 °C). However, results from CVD experiments were slightly different. The film **557** deposited at lower temperature (180 °C), contained chromium, tin and sulfur and it is therefore suggested to be a tin containing chromium sulfide, but since no quantitative EDAX analysis could be performed (film too thin) this is speculative. The same is true for the first slide of film **556** (deposited at 250 °C) probably due to a temperature gradient within the CVD reactor. Regarding the remaining slides of film **556**, the higher temperature

CVD experiments are in accordance with the TGA results. Deposition at 250 °C resulted in a brownish film containing only chromium and sulfur leading us to the conclusion that a type of chromium sulfide is formed at higher temperatures.

For compound (**17**) the bulk decomposition (TGA) studies suggest that decomposition could take place via the formation of MoSnS or $MoSnS_2$ (*ca.* 220 °C) to leave finally MoS (*ca.* 600 °C). Results from CVD experiments were in accordance with the bulk studies. The film **563** deposited at lower temperature (270 °C) contained molybdenum, tin and sulfur and from the X-ray analysis it is concluded to be a tin molybdenum sulfide. The film **562** deposited at higher temperature (300 °C) also contained molybdenum, tin and sulfur and as for film **563** X-ray analysis suggested tin molybdenum sulfide as the possible deposited material.

For precursor (**16**) the bulk decomposition (TGA) studies did not result in any useful information since decomposition took place along with evaporation of the precursor. Results from CVD experiments show that film **565** deposited at higher temperature (450 °C) was tin-rich with very small amounts of molybdenum. X-ray analysis suggests that the deposited film could be SnS. In addition, Raman spectroscopy also suggests SnS deposition. Therefore, from all the above data and the obvious difference in appearance of film **565** we conclude that it is a tin sulfide film (SnS) with some very small amounts of molybdenum present. For film **566** deposited at lower temperature (300 °C) all data suggest that it is the same type of film as **562** and **563**, *i.e.* tin molybdenum sulfide

3.5 Experimental

Starting materials were obtained commercially (e.g. Aldrich) and were used without further purification. Standard Schlenk-line techniques were employed where applicable. For further details about instrumentation see **Appendix One**.

The synthesis of tributyltin tert-butyl sulfide $^{t}BuSSnBu_3$ (12).

A round bottom flask with a condenser was charged with the sodium salt of tert-butyl thiol, (1.85 g, 16.5 mmol) and dissolved in toluene (50 ml). Tributyltin chloride (4 ml, 15 mmol) was added to the resulting solution, which was then refluxed for two hours. Sodium chloride was filtered off and the resulting oil was further purified by vacuum distillation (bp 100 °C at 0.1 mmHg). Yield 0.4 g, 70%.

Elemental Analysis:
Found (Calculated for $C_{16}H_{36}SSn$): %C 49.7 (50.7); %H 9.35(9.50).
^{1}H NMR [δ (ppm), $CDCl_3$]:
0.84 [m, 3H, CH_3 ^{n}Bu]; 1.07 [m, 2H, CH_2-Sn]; 1.29 [m, 2H, CH_2-CH_2-CH_2]; 1.36 [s, 9H, CH3 ^{t}Bu]; 1.50 [m, 2H, CH_3-CH_2].
^{13}C NMR [δ (ppm), $CDCl_3$]:
13.3 [CH_3, ^{t}Bu]; 14.0 [CH_2, CH_2-Sn]; 26.8 [CH_2, CH_2-CH_2-CH_3]; 28.4 [CH_2, CH_3-CH_2]; 36.3 [CH_3, ^{n}Bu]; 42.9 [C, ^{t}Bu].
^{119}Sn NMR [δ (ppm), $CDCl_3$]:
49.9.
IR [(cm^{-1})]:
2956, 2871, 2855, 1456, 1417, 1377, 1363, 1341, 1292, 1259, 1151, 1073, 1021, 960, 875, 814, 668, 583.
Mössbauer [mms^{-1}]:
δ=1.26, ΔE_Q=1.58.

The synthesis of trimethyltin tert-butyl sulfide $^{t}BuSSnMe_3$ (13).

(**13**) was prepared via the same method to that used for (**11**). The sodium salt of tert-butyl thiol (1.85 g, 16.5 mmol) dissolved in toluene (50 ml) and trimethyltin chloride (2.99 g, 15 mmol) were refluxed for two hours. Sodium chloride was filtered off and the resulting oil was further purified by vacuum distillation (bp 42 °C at 0.1 mmHg). Yield 1.9 g, 65%.

Elemental Analysis:

Found (Calculated for $C_7H_{18}SSn$): %C 36.0 (33.2); %H 7.19 (7.12).

^{1}H NMR [δ (ppm), $CDCl_3$]:

-0.04 [s, 3H, CH_3-Sn]; 0.96 [s, 3H, CH_3-^{t}Bu];

^{13}C NMR [δ (ppm), $CDCl_3$]:

-4.7 [CH_3, CH_3-Sn]; 35.8 [CH_3, ^{t}Bu]; 42.7 [C, ^{t}Bu].

^{119}Sn NMR [δ (ppm), $CDCl_3$]:

58.2.

IR [(cm^{-1})]:

2989, 2892, 2857, 1469, 1456, 1362, 1260, 1212, 1186, 1152, 1024, 774, 583, 528.

Mössbauer [mms^{-1}]:

δ=1.24, ΔE_Q=1.54.

The synthesis of pentacarbonyl (tributyltin tert-butyl sulfide) chromium (0) $(CO)_5CrS(^{t}Bu)SnBu_3$ (14). [8]

A Pyrex glass cylinder with three exits, containing an ultraviolet lamp protected by a quartz double wall, was charged with hexacarbonyl chromium(0) (2.6 g, 12 mmol) and dissolved in THF (50 ml). The colourless solution was stirred and irradiated for two hours. Monitoring of CO evolution showed the reaction completion; the solution became orange yellow in colour. Tributyltin tert-butyl sulfide (4.54 g, 12 mmol) was added and the system was stirred for 30 minutes.

The solution changed to a yellowish colour. Tetrahydrofuran was removed by evaporation at room temperature and reduced pressure; at the same time under these conditions, the excess hexacarbonyl chromium sublimed in approximately two hours and was collected on a cold finger. Dissolving in pentane and filtering using a cannula filter further purified the resulting orange yellow oil. Yield of purified product 2.4 g, 53%.

Elemental Analysis:

Found (Calculated for $C_{21}H_{36}O_5SSnCr$): %C 42.7 (44.2); %H 8.06 (6.31).

^{1}H NMR [δ (ppm), $CDCl_3$]:

0.83 [m, 3H, CH_3 ^{n}Bu]; 1.08 [m, 2H, CH_2-Sn]; 1.30 [m, 2H, CH_2-CH_2-CH_2]; 1.37 [s, 9H, CH3 ^{t}Bu]; 1.50 [m, 2H, CH_3-CH_2].

^{13}C NMR [δ (ppm), $CDCl_3$]:

12.6 [CH_3, ^{t}Bu]; 13.4 [CH_2, CH_2-Sn]; 26.1 [CH_2, CH_2-CH_2-CH_3]; 27.7 [CH_2, CH_3-CH_2]; 35.7 [CH_3, ^{n}Bu]; 46.9 [C, ^{t}Bu]; 214.7 [CO, *cis*]; 221.0 [CO, *trans*].

^{119}Sn NMR [δ (ppm), $CDCl_3$]:

101.7.

IR [(cm^{-1})]:

2956, 2922, 2869, 2851, 2062, 1978, 1935, 1457, 1418, 1377, 1363, 1340, 1291, 1260, 1153, 1073, 1020, 960, 874, 804, 668, 653.

The synthesis of pentacarbonyl (trimethyltin tert-butyl sulfide) chromium(0)
$(CO)_5CrS(^tBu)SnMe_3$ (15). [8]

(**15**) was prepared by the same method as for (**14**). Hexacarbonylchromium (0) (2.6 g, 12 mmol) dissolved in THF (50 ml) was irradiated for two hours. Upon reaction completion the solution became orange yellow in colour. Trimethyltin tert-butyl sulfide (3.03 g, 12 mmol) was added and the system was stirred for 30 minutes. The solution changed to a yellowish colour. The resulting product was an orange-yellow solid. Yield 1.6 g, 52%, mp 58-60 °C.

Elemental Analysis:

Found (Calculated for $C_{12}H_{18}O_5SSnCr$): %C 32.5 (32.4); %H 4.58 (4.05).

^{1}H NMR [δ (ppm), $CDCl_3$]:

0.61 [m, 3H, CH_3-Sn]; 0.68 [s, 3H, CH_3-^{t}Bu];

^{13}C NMR [δ (ppm), $CDCl_3$]:

-1.3 [CH_3, CH_3-Sn]; 34.3 [CH_3, ^{t}Bu]; 48.2 [C, ^{t}Bu]; 215.3 [CO, *cis*]; 221.5 [CO, *trans*].

^{119}Sn NMR [δ (ppm), $CDCl_3$]:

120.1.

IR [(cm^{-1}), nujol mull]:

2955, 2921, 2854, 2062, 1976, 1934, 1919, 1459, 1377, 1366, 1260, 1153, 1088, 1021, 799, 669, 653.

Mössbauer [mms^{-1}]:

δ=1.30, ΔE_Q=2.06.

Synthesis of pentacarbonyl (tributyltin tert-butyl sulfide) molybdenum (0) $(CO)_5MoS(^tBu)SnBu_3$ (16).

(**16**) was prepared by the same method as for (**14**). Hexacarbonylmolybdenum (0) (3.17 g, 12 mmol) dissolved in THF (50 ml) was stirred and irradiated for two hours. At completion; the solution became yellow in colour from colourless. Tributyltin tert-butyl sulfide (4.54 g, 12 mmol) was added and the system was stirred for 30 minutes. The solution changed to a yellow brown colour. The resulting product was brown-black oil. Yield 4.54 g, 50%.

Elemental Analysis:

Found (Calculated for $C_{21}H_{36}O_5SSnMo$): %C 46.7 (41.0); %H 8.83 (5.86).

^{1}H NMR [δ (ppm), $CDCl_3$]:

0.85 [m, 3H, CH_3 ^{n}Bu]; 1.12 [m, 2H, CH_2-Sn]; 1.30 [m, 2H, CH_2-C<u>H</u>$_2$-CH_2]; 1.38 [s, 9H, CH3 ^{t}Bu]; 1.51 [m, 2H, CH_3-C<u>H</u>$_2$].

^{13}C NMR [δ (ppm), $CDCl_3$]:

13.5 [CH_3, ^tBu]; 14.3 [CH_2, CH_2-Sn]; 27.0 [CH_2, CH_2-$\underline{C}H_2$-CH_3]; 28.6 [CH_2, CH_3-$\underline{C}H_2$]; 36.56 [CH_3, ^nBu]; 43.2 [C, ^tBu]; 204.8 [CO, *cis*], 210.6 [CO, *trans*].

^{119}Sn NMR [δ (ppm), $CDCl_3$]:

97.8

IR [(cm^{-1})]:

2958 2920, 2870, 2855, 2069, 1981, 1958, 1910, 1456, 1414, 1376, 1361, 1340, 1260, 1150, 1095, 1019, 960, 873, 805, 692, 663.

The synthesis of pentacarbonyl (trimethyltin tert-butyl sulfide) molybdenum(0)

$(CO)_5MoS(^tBu)SnMe_3$ (17).

(**17**) was prepared by the same method as for (**14**). Hexacarbonylmolybdenum (0) (3.17 g, 12 mmol) dissolved in THF (50 ml) was irradiated for two hours. The solution became yellow in colour from colourless. Trimethyltin tert-butyl sulfide (3.03 g, 12 mmol) was added and the system was stirred for 30 minutes. The solution changed to a yellow brown colour. The resulting product was a brown-black solid. Yield 1.3 g, 42%, mp 55-57 °C.

Elemental Analysis:

Found (Calculated for $C_{12}H_{18}O_5SSnMo$): %C 28.5 (29.5); %H 3.87 (3.68).

^1H NMR [δ (ppm), $CDCl_3$]:

0.61 [s, 3H, CH_3-Sn]; 1.40 [s, 3H, CH_3-^tBu];

^{13}C NMR [δ (ppm), $CDCl_3$]:

-1.3 [CH_3, CH_3-Sn]; 34.5 [CH_3, ^tBu]; 48.2 [C, ^tBu]; 204.9 [CO, *cis*]; 212.0 [CO, *trans*].

^{119}Sn NMR [δ (ppm), $CDCl_3$]:

116.0

IR [(cm^{-1}), nujol mull]:

2919, 2871, 2070, 1983, 1936, 1917, 1874, 1458, 1376, 1260, 1152, 1020, 798, 722, 510

Mössbauer [mms^{-1}]:

δ=1.31, ΔE_Q=2.04.

3.6 References

[1] G. Wilkinson, F. Gordon, E. Abel, 'Comprehensive Organometallic Chemistry', **618**, Pergamon Press: New York, 1982, ch 11.

[2] W. S. Rees, Jr., 'CVD of Nonmetals' VCH, 1996, Ch 4, 7.

[3] J. A. Costamagna, J. Granifo, M. Y. Darensbourg, P. A. Tooley, *Inorg. Syn.*, **23**, 1985, 1.

[4] J. Pickardt, H. Schumann, C.F. Campana, L.F. Dahl, *J. Organomet. Chem.*, **216**, 1981, 245.

[5] W. Erhl, H. Vahrenkamp, *Chem. Ber.*, **103**, 1970, 3563.

[6] W. Strochmeier, F. J. Muller, *Chem. Ber.*, **102**, 1969, 3608.

[7] E. W. Abel, K. G. Orrell, K. B. Qureshi, V. Sik, *Polyhedron*, **9**, 1989, 703.

[8] H. Schumman, O. Stelzer, W. Gick, *Angew. Chem. Int. Ed. Eng.*, **8**, 1969, 271.

[9] E. W. Ainscough, A. M. Brodie, A. R. Furness, *J. Chem. Soc., Dalton Trans.*, 1973, 2360.

[10] F. A. Cotton, C. S. Krainhanzel, *J. Am. Chem. Soc.*, **84**, 1962, 4432.

[11] E. W. Ainscough, E. J. Birch, A. M. Brodie, *Inorg. Chim. Acta*, **20**, 1976, 187.

[12] W. Strohmeier, *Angew. Chem. Int. Ed. Eng.*, **3**, 1964, 730.

[13] F. Mirzaeli, L. Han, M. Tanaka, *Chem. Commun.*, 2000, 657.

[14] R. C. Mehrotra, V. D. Gupta, D. Sukhani, *Ind. J. Chem*, **7**, 1969, 708.

[15] E. W. Abel, D. B. Brady, *J. Chem. Soc. (A),* 1965, 1192.

[16] M. E. Peach, *Can. J. Chem.*, **46**, 1968, 211.

[17] J.D. Kennedy, W. McFarlane, *J. Chem. Soc., Perkin II*, 1974, 146.

[18] E. V. Van den Berghe, D. F. Van de Vondel, G. P. Van der Kelen, *Inorg. Chim. Acta*, 1967, 97.

[19] R. C. Weast, M. J. Astle, 'CRC Handbook of Chemistry and Physics', 63rd Ed.

[20] L. S. Price, I. P. Parkin, A. M. E. Hardy, R. J. H. Clark, T. G. Hibbert, K. C. Molloy, *Chem. Mater.*, **11**, 1999, 1792.

CHAPTER FOUR

The Synthesis, Characterisation and CVD Properties of Transition Metal Tetracarbonyl Complexes of Chelating Organotin (IV) Aminothiols.

4.1 Introduction

In the previous chapter the synthesis of pentacarbonyl transition-metal tin thiolate complexes was examined. However, these compounds proved to be extremely difficult to handle and since one of the criteria for good CVD precursors is relative ease of handling attention was given to the synthesis of more stable complexes.

It is a well-known fact that chelation within a complex increases its stability, therefore one way to introduce extra stability to the compounds synthesised previously could be to substitute the thiolate (monodentate) ligand with a chelating (bidentate) one.

Chelated metal carbonyl complexes are still ideal as CVD precursors due to their potentially clean decomposition pathways. In addition, they still incorporate the correct M-S-Sn linkage for the deposition of mixed-metal sulfide films using single-source precursors. The following diagram summarises the desired decomposition process.

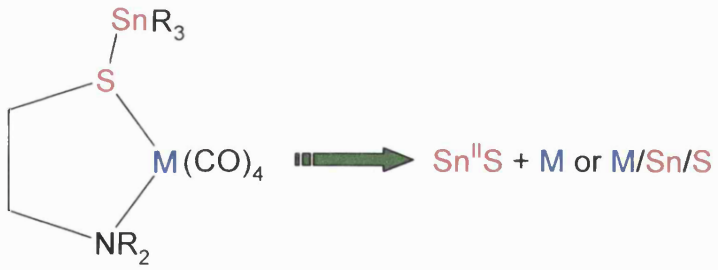

4.2 Results and Discussion

4.2.1 Synthesis and Characterisation

During this study a selected range of compounds were synthesised and tested for their suitability as CVD precursors. The hexacarbonyl complexes of the transition metals, tungsten and chromium, and the tetracarbonyl molybdenum norbornadienyl complex were utilised as starting materials. As the substitution ligand, trimethyltin(diethylaminoethanethiolate) was employed. This is a potentially bidentate ligand, which can form donor bonds from either the nitrogen and/or the sulfur atom. [1-4] The following equation (**Eq. 4.1**) summarises the ligand synthesis:

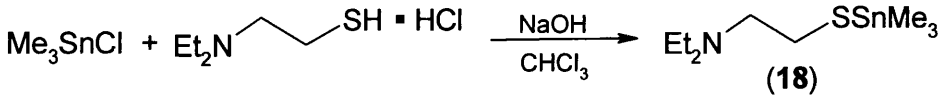

Eq. 4.1

This reaction takes place in a two-layer system where the product, trimethyltin(diethylamino ethanethiolate) (**18**), is finally dissolved in the organic layer while the by-products remain in the aqueous layer. The bidentate tin-containing ligand was obtained pure after distillation and the yield after purification was 23%.

For compound (**18**) both the ^{1}H and ^{13}C NMR spectra were as expected and coupling constants were resolved. In the ^{1}H NMR spectrum couplings were observed between the methyl protons and the ^{119}Sn isotope, ($^{2}J(^{119}Sn\text{-}^{1}H) = 55.3$ Hz). In the ^{13}C NMR spectrum couplings were observed between the methyl carbons and the ^{119}Sn and ^{117}Sn isotopes, ($^{1}J(^{119}Sn\text{-}^{13}C) = 354$, $^{1}J(^{117}Sn\text{-}^{13}C) = 338$ Hz). In the ^{119}Sn NMR spectrum a coupling was also resolved between the ^{13}C and ^{119}Sn isotopes, ($^{1}J(^{13}C\text{-}^{119}Sn) = 350$ Hz). In addition, Mössbauer parameters were measured ($\delta = 1.24$, $\Delta E_Q = 1.58$ mms^{-1}). The isomer shift corresponds to a Sn(IV) centre ($\delta < 2.70$ mms^{-1}) and the quadrupole splitting value is typical for tetrahedral tin.

In order to facilitate attachment of the ligand on to the transition metal, complexes with labile ligands were employed. The following equation (**Eq. 4.2**) illustrates the reactions that took place: [6]

$$M(CO)_6 \xrightarrow[\text{Reflux}]{\text{CNEt}} M(CO)_4(CNEt)_2$$

M = W (**19**), Cr (**20**)

Eq. 4.2

The bis(propionitrile)tetracarbonyl complexes, (**19**) and (**20**), were obtained after prolonged reflux. The reflux duration differed from metal to metal. For the tungsten complex reflux duration was around 6 hrs, while for the chromium complex around 4 hrs and 30 mins. The reactions were constantly monitored by IR until all the intermediates and starting materials were consumed ($M(CO)_6$, $M(CO)_5L$) and the desired product ($M(CO)_4L_2$) was formed. The final products were purified by recrystallisation from diethyl ether and isolated by filtration. The tungsten complex was quite air stable for short periods of time but decomposed on extended exposure to air turning green, which indicated some surface oxidation. The chromium complex was much more air-sensitive than its tungsten analogue turning green within seconds. [6] Yields after purification were moderate ranging from 36% for the chromium to 66% for the tungsten complex. [6]

For both compounds (**19**) and (**20**) the ^{13}C and ^{1}H NMR spectra were as expected. However, one important feature appeared in the ^{13}C NMR spectrum where two signals were observed in the carbonyl region. This suggests that the carbonyl ligands exist in two different environments i.e. that they are not all equivalent. This can be explained by the fact that the substituting propionitrile ligands exist in *cis* geometry to each other (**Fig. 4.1**).

Fig. 4.1 *cis*- and *trans*- isomers of the compound $M(CO)_4L_2$.

The substituted tetracarbonyl ligands were obtained by reacting the bis(propionitrile)tetracarbonyl complexes with one equivalent of ligand (**18**). The following diagrams summarise the ligand substitution reactions that took place:

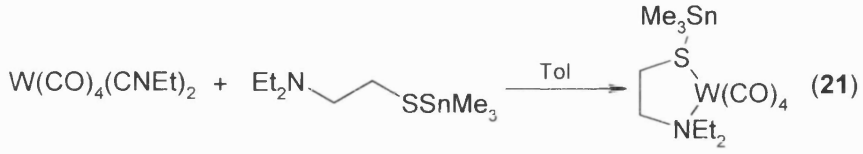

Eq. 4.3

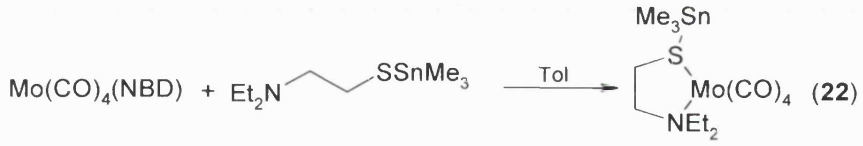

Eq. 4.4

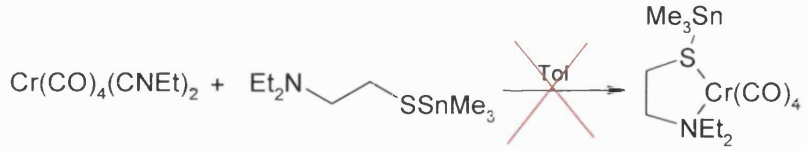

Eq. 4.5

The tetracarbonyl trimethyltin (diethylamino ethanethiolate) tungsten(0) (**21**) complex was synthesised according to **Eq. 4.3** by substitution of the two propionitrile ligands with the chelating ligand (**18**). Dissolving in toluene and precipitating from dry hexane further purified (**21**), which was a very dark brown solid. In the same manner (**Eq. 4.4**), trimethyltin (diethylamino

ethanethiolate) molybdenum(0) (**22**) was synthesised by the substitution of the norbonadiene ligand with the chelating ligand (**18**). Tetracarbonyl molybdenum norbornadienyl was employed as the starting material for the synthesis of (**22**) since norbornadiene also is a very labile ligand and the starting material can be obtained commercially at a reasonable price. [10-12] Dissolving in toluene and precipitating from dry hexane further purified (**22**), which was also a very dark brown solid. Yields were very good ranging from 66% for (**21**), to 76% for (**22**).

For compounds (**21**) and (**22**) NMR spectra were as expected. In addition, for compound (**22**) two carbonyl shifts were observed in the ^{13}C NMR spectrum. This is in accordance with the view that the two propionitrile ligands, undergoing substitution, were *cis* to each other. However, in the ^{13}C NMR spectrum of compound (**21**) these shifts were not observed probably due to the fact that the prepared NMR sample was too weak for the carbonyl carbons to be shown. Furthermore, Mössbauer parameters were measured for both compounds (**21**) ($\delta = 0.68$, $\Delta E_Q = 2.20$ mms^{-1}) and (**22**) ($\delta = 1.17$, $\Delta E_Q = 2.90$ mms^{-1}). The isomer shifts correspond to Sn(IV) centres for both complexes ($\delta < 2.70$ mms^{-1}) and the quadrupole splitting values are typical for tetrahedral tin.

For tetracarbonyl complexes four resonances are observed (C_{2v} symmetry) in the infrared spectrum. These are A_1, A_2, B_1 and B_2. These resonances are strongly dependent on both the substituents and the transition metal. However, some typical values reported in literature for $M(CO)_4L_2$, where M is either W, Cr or Mo and L is a nitrile ligand (acetonitrile, acrylonitrile) are: [7-9]

	W (cm^{-1})	Cr (cm^{-1})	Mo (cm^{-1})
A_1	2021-2024	2019-2028	2023-2027
A_2	1900-1913	1908-1910	1905-1921
B_1	1870-1898	1878-1882	1870-1881
B_2	1825-1840	1833-1839	1831-1833

Table 4.1 Literature IR resonances for compounds $M(CO)_4L_2$. [7-9]

Consequently, the observed values in the IR spectra collected for compounds (**19**)-(**22**) are summarised in the table below (**Table 4.2**).

	(19) (cm^{-1})	(20) (cm^{-1})	(21) (cm^{-1})	(22) (cm^{-1})
A_1	2015	2017	2017	2022
A_2	1933	1943	1958	1906
B_1	1895	1840	1927	1876
B_2	1836	1801	1850	1798

Table 4.2 Summary of IR data for compounds (**19**)-(**22**).

The synthesis of trimethyltin (diethylamino ethanethiolate) chromium(0) according to **Eq. 4.5** was not successful. Instead, another species (**23**) was formed and this was characterised by X-ray crystallography (**Fig. 4.2**).

Crystals of bis(chromium pentacarbonyl) diethylamino ethane thiol (**23**) were grown from a toluene/hexane solution (1:5). The crystals were colourless cubes and relatively air-stable **Table 4.3** summarises the relevant bond lengths and angles for compound (**23**).

Bonds (Å)		Angles (°)	
Cr-S	2.4799(4)	Cr-S-Cr	121.06(2)
	2.4717(4)		
S-C	1.835(1)	C-S-Cr	105.71(5)
			109.13(5)
N-C	1.507(2)	C-N-C	111.13(12)
	1.511(2)		110.51(12)
	1.511(2)		112.33(12)

Table 4.3 Summary of selected metric data for compound (**23**).

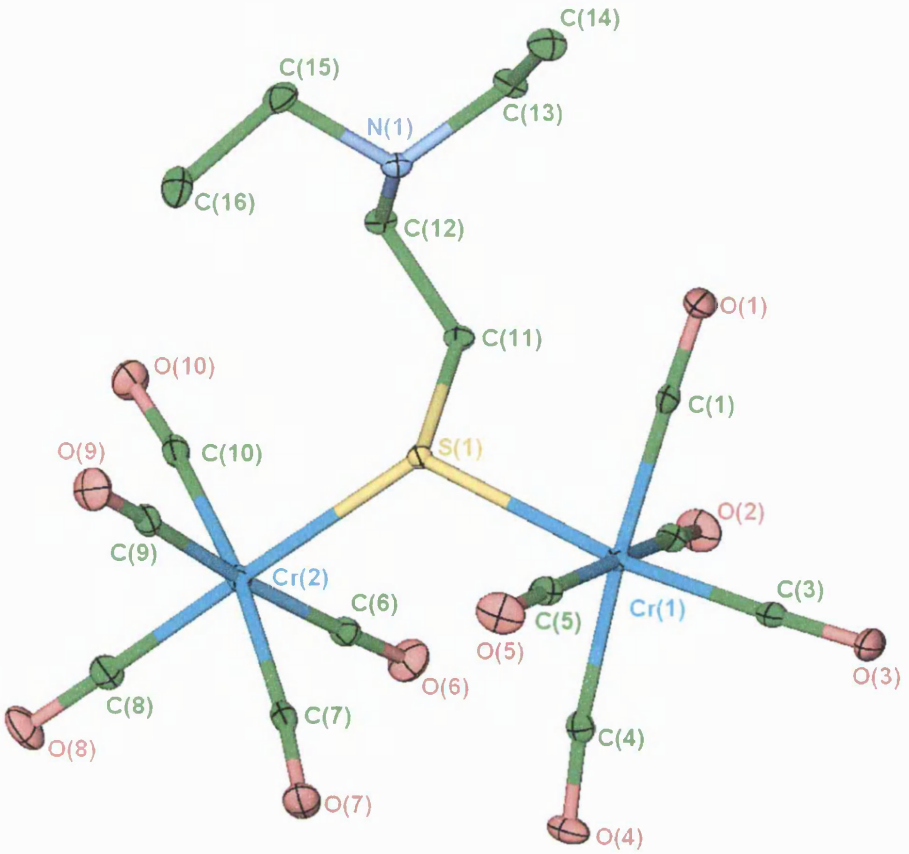

Fig. 4.2 The asymmetric unit of (**23**). Thermal ellipsoids are at 30% probability level.

Both chromium centres in compound (**23**) are Cr(0) and the complex is neutral. The bridging sulfur atom acts as a four-electron donor, contributing two electrons to each chromium centre. However, the neutral ligand is in its zwitterionic form with a hydrogen atom attached on the nitrogen ($Et_2HN^+CH_2CH_2S^-$). The chromium-sulfur bonds in compound (**23**) varied between 2.4799(4) and 2.4717(4) Å. Other analytical data of complexes relevant to this one gave similar values for the Cr-S bond. These are tabulated in **Table 4.4**. The Cr-S-Cr bond angle in compound (**23**) has a value of 121.06(2)°, which is comparable to values reported in literature for the same sulfur bridged unit. [13-15] Literature values for this bond angle are also summarised in **Table 4.4**. The two chromium pentacarbonyl units exist in a staggered conformation with respect to each other, minimising steric interactions.

Cr-S Bond Length(Å)	Cr-S-Cr Bond Angle (°)	Compound	Ref.
2.509(1)	117.11(5)	$^{t}BuS[Cr(CO)_5]_2^-$	13
2.518(1)			
2.457(6)	122.79(25)	$[PPN]^+[HSCr_2(CO)_{10}]^-$	15
2.481(7)			
2.495(9)	98.7(3)	$Cp_6Cr_8S_8(dtc)_2$	14
2.552(10)	99.2(3)		
2.581(10)			
2.505(9)			

Table 4.4 Metric data from literature for compounds containing the Cr-S-Cr linkage.

Fig. 4.3 illustrates the complete dimer of compound (**23**). The formation of hydrogen bonding between one carbonyl oxygen and the hydrogen on the amide group is evident. H(1) bonds to O(5) of the lattice neighbour generated by the transformation ½-x, ½+y, ½-z. The hydrogen bond length is 2.41 Å [O(5)···H(1)] and the O-N distance is 3.204 Å. The hydrogen bond angle <OHN is 146.6 °. Both bond length and bond angle are of the expected value for a relatively weak hydrogen bond between the donor group R_2NH and the acceptor carbonyl oxygen [H-O 1.69-2.32 Å, <OHN 169-171 °]. [19]

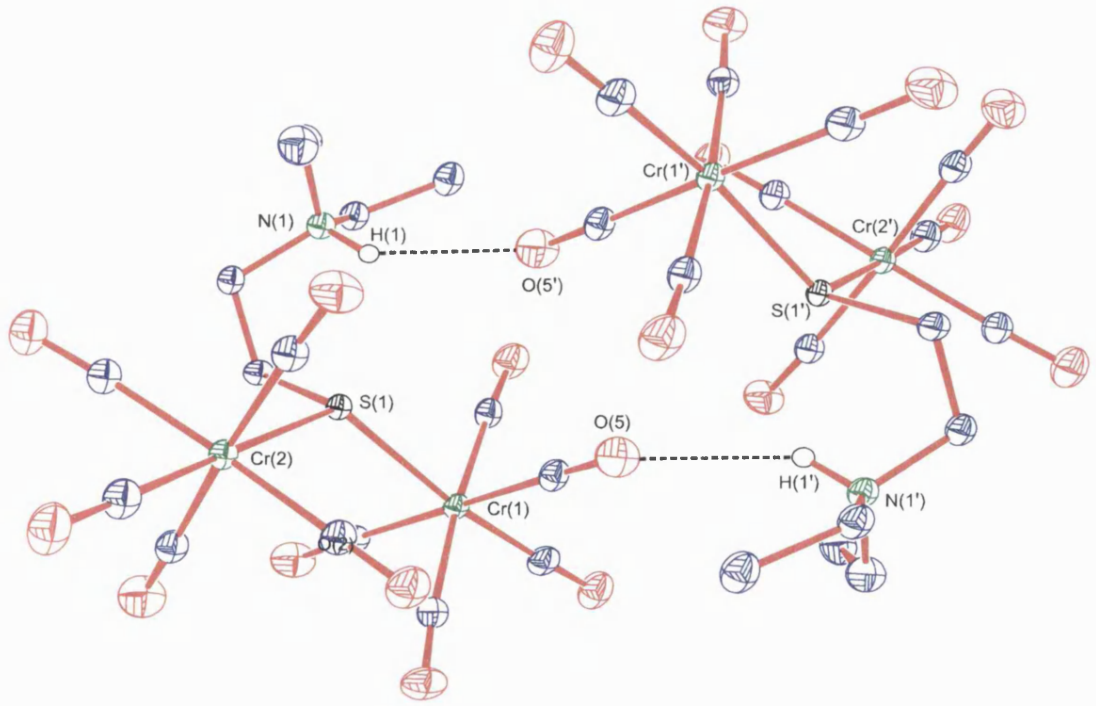

Fig. 4.3 The molecular unit of (**23**). Primed atoms are related to their unprimed counterparts in the asymmetric unit by ½-x, ½+y, ½-z. Thermal ellipsoids are at the 30% probability level.

In addition to the tetracarbonyl complexes of (**18**) attention was given to the synthesis of other transition metal complexes of (**18**) in an effort to deposit materials involving different transition metals than previously studied. Metals such as Cu(II) and Ni(II) were employed but unfortunately none of the syntheses were successful. However, for the cadmium analogue a reaction took place without solvent present and the product (**24**) was extracted into dichloromethane. It must be noted that CdI_2 used, as the starting material is completely insoluble in dichloromethane (hot or cold). **Eq. 4.6** summarises the synthesis:

$$CdI_2 + Et_2N\text{-}SSnMe_3 \xrightarrow{-Me_3SnI} [CdI(SCH_2CH_2NEt_2)]_4 \ (\mathbf{24})$$

Eq. 4.6

Even though the reaction took place at room temperature the ligand (**18**) eliminated trimethyltin iodide resulting in product (**24**), (diethylaminoethane thiolato) cadmium iodide and the reaction is almost quantitative.

Compound (**24**) is a tetramer and **Fig. 4.4** shows the molecular unit which consists of an 8-membered Cd_4S_4 ring. The iodine atoms attached on to cadmium are arranged in a *trans* configuration to minimise steric interactions and the aminothiolate ligands chelate from both S and N to each cadmium atom.

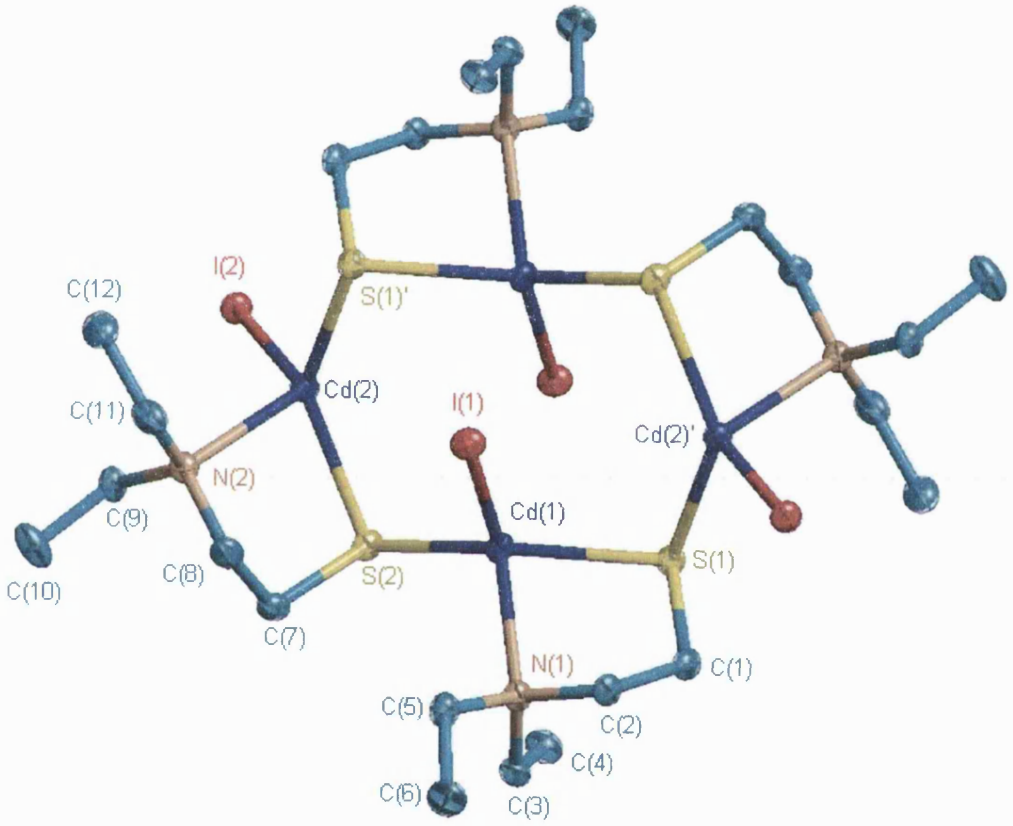

Fig. 4.4 The molecular unit of $[CdI(SCH_2CH_2NEt_2)]_4$ (**24**). Primed atoms are related to their unprimed counterparts in the asymmetric unit by -x+1, -y+1, -z+1. Thermal ellipsoids are at the 30% probability level.

Crystals of diethylaminoethane thiol cadmium iodide (**24**) were grown from dichloromethane. The crystals were colourless needles and relatively air-stable. **Table 4.5** summarises the relevant bond lengths and angles for compound (**24**). The complex is neutral and the nitrogen atom of the chelating ligand acts as a 2-

electon donor. The cadmium centre exhibits a distorted tetrahedral co-ordination with angles ranging from 82.10 to 115.02 °. The mean bond length between cadmium and sulfur is 2.603(2) Å, the S-Cd-S bond angle varies from 130.80(4) to 135.31(4)°, while the Cd-S-Cd bond angle varies from 99.09(4) to 102.48(5)°.

Bonds (Å)		**Angles (°)**	
Cd-S	2.529(1)	S-Cd-S	135.31(4)
	2.504(1)		130.80(4)
	2.512(1)		
	2.521(1)		
Cd-I	2.8023(5)	S-Cd-I	112.28(3)
	2.7487(5)		107.71(3)
			106.47(3)
			115.02(3)
Cd-N	2.392(4)	I-Cd-N	101.85(10)
	2.375(4)		108.55(10)
S-C	1.834(5)	N-Cd-S	109.98(10)
	1.840(5)		106.12(11)
			82.10(10)
			82.73(11)
		Cd-S-Cd	99.09(4)
			102.48(5)
		C-S-Cd	103.96(18)
			97.31(17)
			97.77(16)
			106.77(17)

Table 4.5 Summary of selected metric data for compound (**24**).

Furthermore, the cadmium-nitrogen bond varies from 2.375(4) to 2.392(4) Å and the value for N-Cd-S bond angle varies from 109.98(10) to 106.12(11)°. These values are in accordance with values reported in literature (**Table 4.6**).

Cd-S (Å)	Cd-N (Å)	Cd-S-Cd (°)	S-Cd-S (°)	Compound	Ref.
2.558(4)	2.36(2)	91.8(1)	172.3(2)	$(Cd[SC(CH_3)_2CH_2NH_2]_2$ $CdCl_2)_2 \cdot 2H_2O$	16
2.520(6)	2.35(2)	93.0(2)	113.2(2)		
2.506(5)					
2.563(7)	2.38(2)			$[Cd\{NH_2CH(CO_2)C$ $(Me_2)S\}]$ $\cdot H_2O$	17
2.567(7)					
2.518(3)	2.366(9)	95.2(1)	161.0(1)	$Cd_4\{S(CH_2)_2NMe_2\}_4Br_4$	18
2.501(2)	2.375(9)	93.5(1)	126.3(1)		
2.510(3)					
2.494(2)					
2.538(3)	2.371(9)	84.58(8)	116.20(9)	$[Cd\{CdL)_2\}_2](ClO_4)_2$ $\cdot H_2O$ L=2[(3aminopropyl) amino]ethanethiol	5
2.533(3)	2.338(9)	84.92(9)	99.15(9)		
2.706(3)	2.375(9)		115.11(9)		
2.695(3)	2.385(1		113.0(1)		
	0)		91.23(9)		

Table 4.6 Selected metric data from literature

Similar compounds have been previously synthesised [18] and selected metric data for comparison with (**24**) are presented in **Table 4.6**. Complexes of Zn, Cd and Hg with 2-(dimethylamino)ethanothiolate (L) ligands have been prepared. Complexes of the type $M_4L_4X_4$ (X = Cl or Br) were obtained from anhydrous MX_2, HL·HX and triethylamine in acetonitrile, as well as from the metal acetate, HL·HX and sodium hydroxide in aqueous solution. [18] All complexes have a central centrosymmetric M_4S_4 8-membered ring (**Fig. 4.5**) in an extended-chair conformation with two opposite M atoms disposed on each side of the M'_2S_4 plane, and with the aminothiolate ligands chelating from both S, N to M' atoms and S-bridging between M and M' atoms. It should be noted that even though compound (**24**) has the same molecular formula as $M_4L_4X_4$ it is structurally very different from the compound in **Fig. 4.5** and therefore is a unique complex.

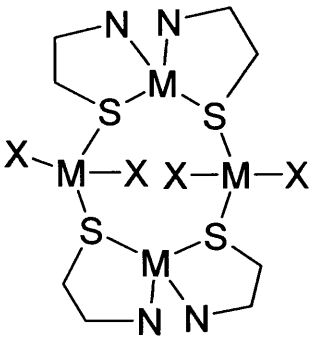

Fig. 4.5 The M_4S_4 unit in $M_4L_4X_4$ complexes. [18]

4.2.2 Thermal Analysis

Compound (**22**) was investigated using Thermal Gravimetric Analysis (TGA) in order to obtain an indication of the temperature at which decomposition maybe expected to start and also of the type of intermediate species that might be generated during the decomposition process.

The TGA of (**22**) (**Fig. 4.6**) shows the decomposition to begin at around 100 °C and complete at 650 °C. Mass loss observed at 150 °C corresponds to 44.7% weight residue and can be attributed to MoSnS (observed residual mass: 44.7, theoretical: 48.9%). Further weight loss, which takes place between 350 and 650 °C, results in a species with residual mass of 37.7%. This can be attributed to either SnS (observed residual mass: 37.7, theoretical: 29.9%) or MoS_2 (observed residual mass: 37.7, theoretical: 31.8%).

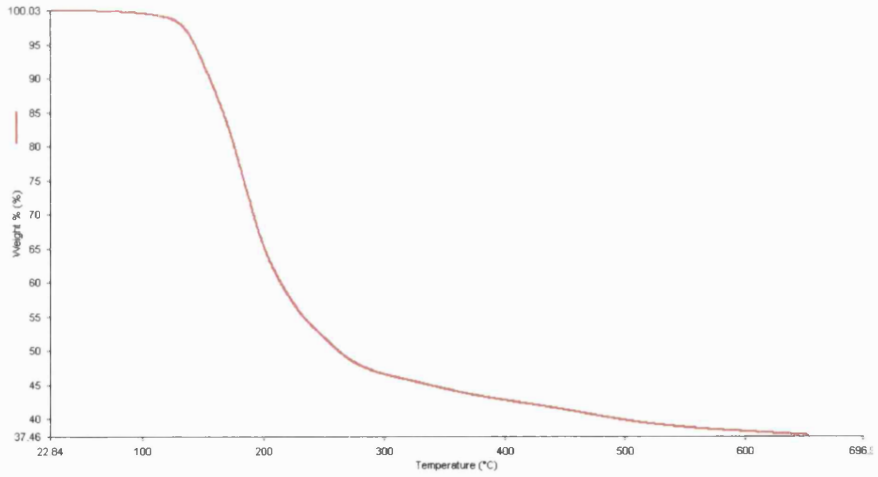

Fig. 4.6 TGA of $(CO)_4Mo(Et_2NCH_2CH_2SSnMe_3)$ (**23**).

4.3 Film Growth Results

4.3.1 Introduction

Only compound (**22**) was actually tested for its suitability as a CVD precursor. Since it was very soluble in most solvents AACVD was employed as the delivery technique.

4.3.2 Deposition Conditions

Films were deposited on standard borosilicate glass slides. The substrate was heated at temperatures ranging from 300 to 400 °C. For each growth experiment approximately 0.2 g of complex was dissolved in THF (~20 ml).

Deposition conditions for the films deposited are displayed in **Table 4.7**. Both low and high temperature runs were carried out for all the complexes in order to ascertain any differences in the films deposited.

Compound	(23)	(23)
Film ID	**567**	**568**
Reactor Temp (°C)	300	400
Carrier Gas (Ar) Flow Rate (l/min)	1.0	1.0
Run Time (min)	30	30

Table 4.7 AACVD conditions for experiments with compound (**23**).

4.3.3 Film Analysis

Films were examined using a number of techniques: Visual inspection, Glancing Angle X-Ray Diffraction, Energy Dispersive X-Ray Analysis (EDAX). Scanning Electron Microscopy (SEM) and Raman Spectroscopy.

*Visual Inspection, Scanning Electron Microscopy (SEM) and Raman Spectroscopy for films **567** and **568***

Film **567** (deposited at the lowest temperature) covered the first two slides of the eight constituting the glass substrate, while **568** (deposited at the highest temperature) covered only the first one. Both films **567** and **568** were very similar in appearance to films **562**, **563**, **565** and **566** (chapter three). All slides were dark brown with a metallic finish and very reflective. They were very well adhered to the substrate with no powdery surface layer.

Raman spectroscopy was also employed to analyse these two films. Unfortunately due to the fact that these films were very thin no valuable data could be obtained from the Raman spectra. However, for film **568** some graphitic carbon was evident as a broad band at 1500-1700 cm^{-1}.

Scanning electron microscopy was also used to analyse these films, SEM images of both films (**Fig. 4.7.** to **Fig. 4.10**) showed a uniform coverage of small spheres and crystallites of various sizes.

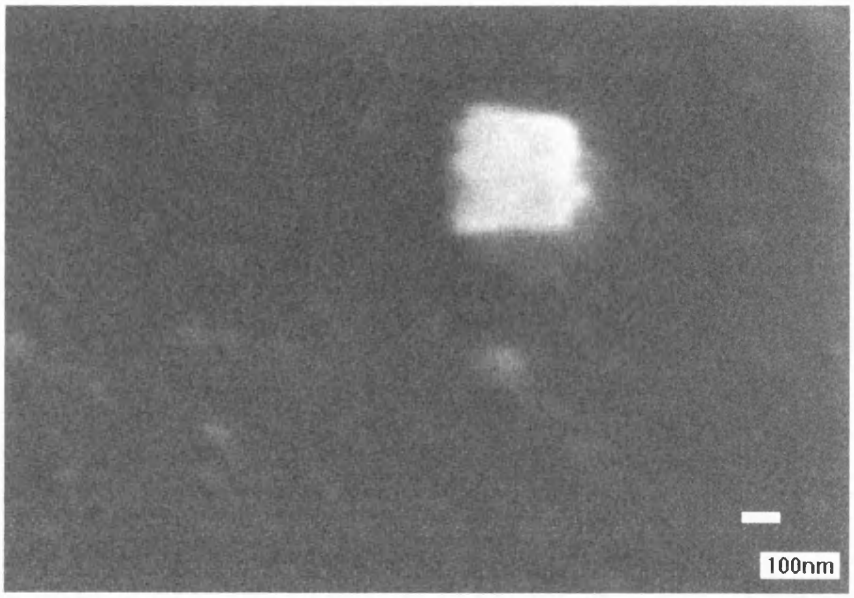

Fig. 4.7 0 ^{o} tilt SEM image of film **567** (slide 1).

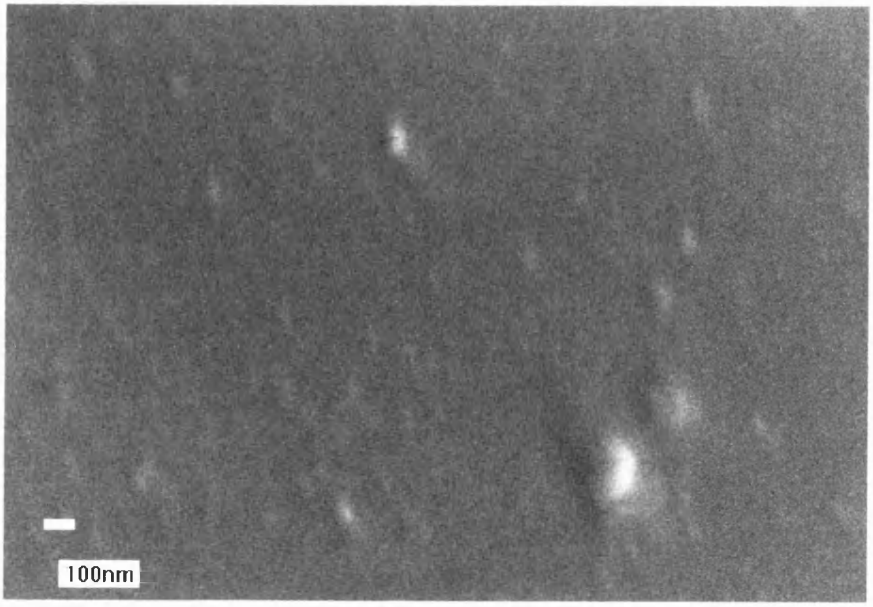

Fig. 4.8 45 ^{o} tilt SEM image of film **567** (slide 1)

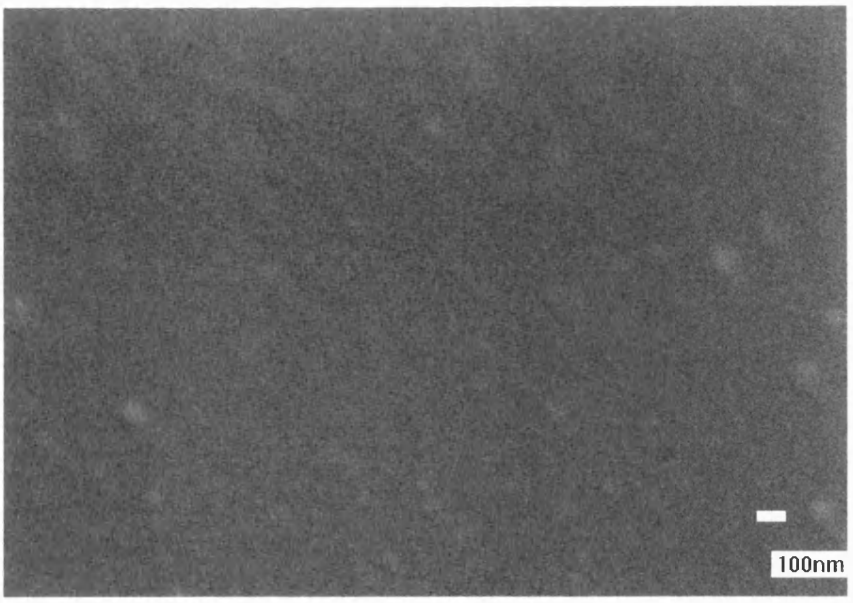

Fig. 4.9 0 ° tilt SEM image of film **567** (slide 1).

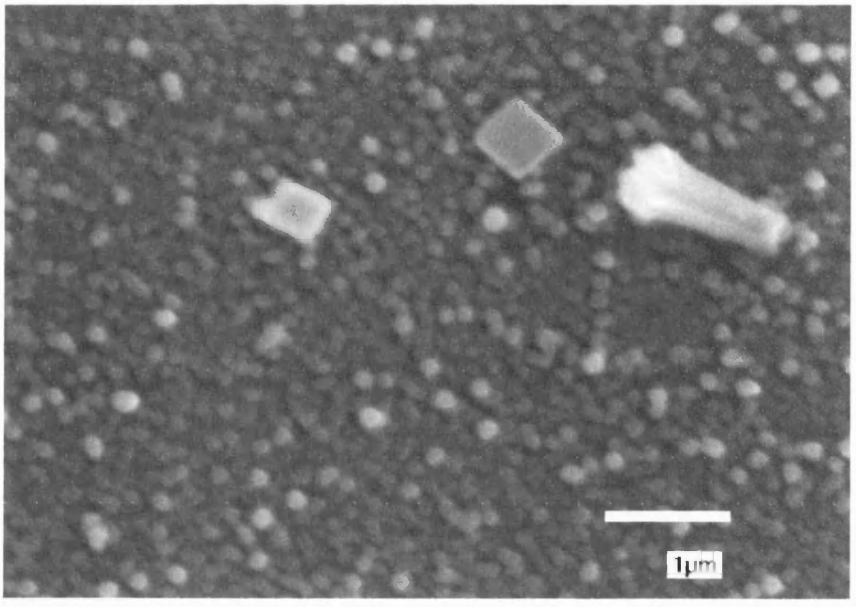

Fig. 4.10 0 ° tilt SEM image of film **568** (slide 1), featuring crystallites. EDAX analysis verified the fact that the crystallites were the same type of material as the bulk of the film.

Energy Dispersive X-Ray Analysis (EDAX) for films 567 and 568

EDAX analysis showed both films (**567** and **568**) to contain molybdenum tin and sulfur. However, qualitative EDAX analysis was only performed for film **568** (**Fig. 4.11**).

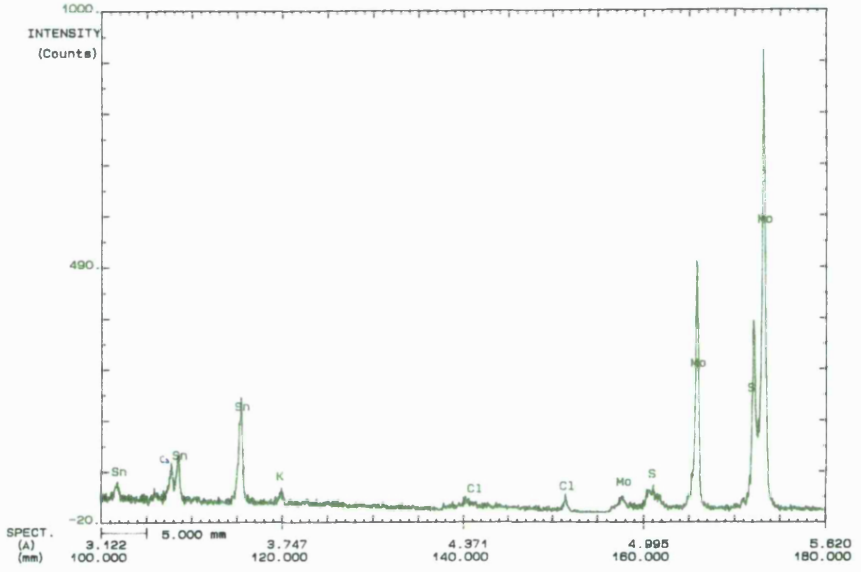

Fig. 4.11 EDAX qualitative analysis of film **568** (accelerating voltage 6.0 kV)

*Glancing Angle X-Ray Diffraction for films **567** and **568***

Glancing Angle X-Ray Diffraction studies were performed to determine whether the films were crystalline or amorphous and to get some information on the types of materials deposited. The X-ray patterns were obtained with incident angle, ϑ (theta), locked at 2.5° and over the 2ϑ range of 0° to 75°.The diffraction pattern of film **567** was amorphous while of film **568** crystalline (see **Fig. 4.12** and **Fig. 4.13**).

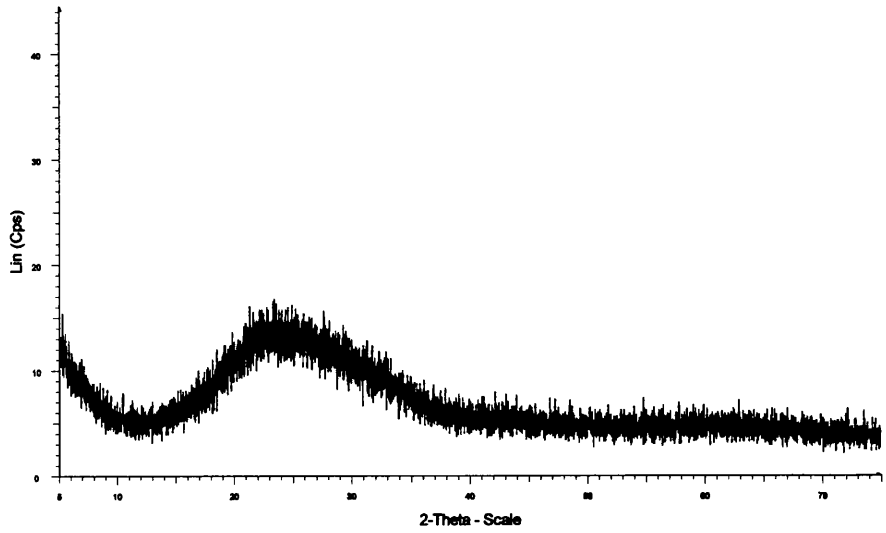

Fig. 4.12 Glancing angle X-ray pattern of film **567** precursor (**22**)

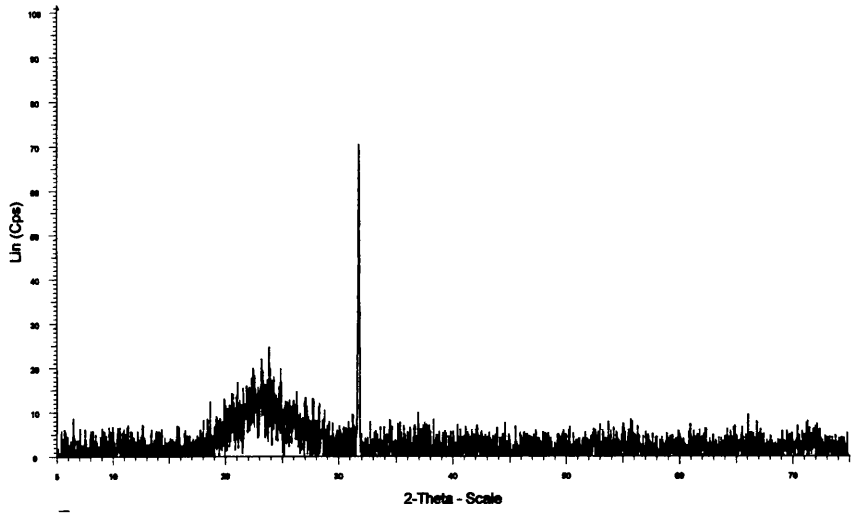

Fig. 4.13 Glancing angle X-ray pattern of film **568** precursor (**22**)

The pattern shown in **Fig. 4.13** is indicative of the kind of material present in film **568**. Peak match software suggested γ-Sn_2S_3, SnS and SnS (Herzenbergite) as the possible deposited material.

In summary, both films **567** and **568** contain tin, sulfur and molybdenum. For film **567** deposited at lower temperature TGA analysis suggests a tin molybdenum sulfide as a possible deposition product and the EDAX evidence

supports this. However, for film **568** peak match software suggests that the resulting film is a type of SnS. This could be a possibility since the film was deposited at high enough temperature for SnS to be formed, as implied by the TGA data. Regarding the peaks observed in the X-ray diffraction pattern of film **568**, possibly some amount of crystalline SnS could have formed along with amorphous tin molybdenum sulfide and hence tin sulfide could be identified in the film. However, because of the large amount of molybdenum observed in the EDAX analysis of film **568** it must consequently be a mixture of amorphous molybdenum with crystalline tin sulfide.

Film ID	d found (Å)	2theta (°)	hkl	d theoretical (Å)	Material
568	2.825	31.64	2 0 1	2.826	γ-Sn_2S_3
			1 3 0	2.823	SnS
			1 1 1	2.835	SnS Herzenbergite

Table 4.8 Summary of the X-ray reflection data for films **568** and the data for the corresponding materials from the peak match software.

4.4 Conclusions

The successful synthesis and characterisation of transition metal tetracarbonyl complexes of chelating organotin (IV) aminothiols, (**21**)-(**22**), is reported. In addition, the synthesis and characterisation of sulfur-bridged transition metal carbonyl complexes (**23**) and (**24**) is also reported.

Compound (**22**) was tested for its suitability as a single-source precursor for the deposition of ternary materials (Mo/Sn/S) by the CVD method. Both films (**567**, **568**) obtained from precursor (**22**) were proved to contain all three elements and

hence concluded to be a type of tin molybdenum sulfide for the film obtained at lower temperature (**567**) and a mixture of crystalline SnS and amorphous molybdenum for film **568** deposited at higher temperature.

Since depositions for precursor (**22**) took place at similar temperatures to depositions for precursors (**16**) and (**17**) similar results should be expected. Indeed, this is true for all depositions but one. The film deposited from precursor (**16**) at 450 °C proved to contain mostly tin and sulfur, while all other films contained all three desired elements. However, in the case of precursor (**22**) both films formed, even at high temperature (400 °C), contained molybdenum, tin and sulfur. Therefore, from this result can be concluded that the decomposition process of precursor (**22**) is not one controlled only by temperature (as seen previously) but it is the ligand chelation which creates greater stability and has the effect of retaining the Mo-S-Sn unit in the film.

4.5 Experimental

Starting materials were obtained commercially (e.g. Aldrich) and were used without further purification. Standard Schlenk line techniques were employed where applicable. For further details about instrumentation see **Appendix One**.

The synthesis of trimethyltin(diethylamino ethanethiolate) $Et_2N(CH_2)_2SSnMe_3$ (18). [4]

A conical flask was charged with an aqueous (*ca.* 30 ml) solution containing trimethyltin chloride (2.0 g, 11.78 mmol) and 2-diethylaminoethane thiol hydrochloride (2.35 g, 11.78 mmol). An equal volume of chloroform was added and the mixture was stirred vigorously to mix the two phases. An aqueous solution of sodium hydroxide was added dropwise, until the aqueous phase reached pH 10. The mixture was then stirred for another two hours and the chloroform layer was isolated using a separating funnel. This was then washed with water three times, dried with anhydrous magnesium sulfate and filtered.

The solvent was removed *in vacuo* resulting in colourless oil (0.46 g 23%), which was further purified by distillation (bp 65 °C at 23 mmHg).

Elemental Analysis:

Found (Calculated for $C_9H_{23}NSSn$): %C 37.5 (36.5); %H 7.97 (7.78); %N 5.1 (4.74).

^{1}H NMR [δ (ppm), $CDCl_3$]:

0.16 [s, 9H, CH_3-Sn]; 0.75 [t, 6H, CH_3-Et]; 2.27 [q, 4H, CH_2-Et]; 2.32 [m, 4H, CH_2].

^{13}C NMR [δ (ppm), $CDCl_3$]:

-5.8 [CH_3, CH_3-Sn]; 11.4 [CH_3, Et_2N-]; 23.8 [CH_2-S]; 46.5 [CH_2, Et_2N]; 56.8 [N-CH_2].

^{119}Sn NMR [δ (ppm), $CDCl_3$]:

88.2.

Mössbauer [mms^{-1}]:

δ=1.24, ΔE_Q=1.58

The synthesis of tetracarbonyl bis(propionitrile)tungsten (0) $W(CO)_4(NCEt)_2$ (19). [6]

A mixture of tungsten hexacarbonyl (1.0 g, 2.84 mmol) and 50 ml of propionitrile was placed in a Schlenk tube equipped with a reflux condenser. Heating to reflux under nitrogen gradually dissolved the hexacarbonyl. Once all of the latter was consumed the reflux was vigorous and the solution became yellow, deepening to brown-red. The reaction was monitored by IR and after 6 hrs the bands due to the hexacarbonyl and pentacarbonyl complexes became non-existent. The solvent volume was then reduced and on addition of diethyl ether (ca. 30 ml) a yellow-brown precipitate was formed. This was then filtered, washed with diethyl either and dried in vacuo. Yield 0.66 g 66%, mp 96 °C.

Elemental Analysis:

Found (Calculated for $C_{10}H_{10}O_4N_2W$): %C 29.7 (29.6); %H 2.58 (2.46); %N 6.83 (6.90).

^{1}H NMR [δ (ppm), $CDCl_3$]:

0.35 [t, 3H, CH_3]; 1.32 [q, 2H, CH_2];

^{13}C NMR [δ (ppm), $CDCl_3$]:

9.4 [CH_3]; 11.3 [CH_2]; 126.5 [C]; 201.9, 208.2 [4CO].

IR [(cm^{-1}), nujol mull]:

2989, 2950, 2241, 2015, 1933, 1895, 1836, 1789, 1458, 1427, 1384, 1314, 1073, 1003, 785.

The synthesis of tetracarbonyl bis(propionitrile)chromium(0) $Cr(CO)_4(NCEt)_2$ (20). [6]

(**20**) was prepared via the same method to that used for (**19**). Chromium hexacarbonyl (1.6 g, 6.82 mmol) and 50 ml of propionitrile was refluxed and the solution became yellow, deepening to brown-red. The reaction was monitored by IR and after four and a half hours the bands due to the hexacarbonyl and pentacarbonyl complexes became non-existent. The solvent was then reduced and on addition of diethyl ether (ca. 30 ml) a yellow-green precipitate was formed. Yield 0.58 g 36%.

Elemental Analysis:

Found (Calculated for $C_{10}H_{10}O_4N_2Cr$): %C 32.8 (43.8); % H 2.94 (2.65); %N 6.13 (10.22).

^{1}H NMR [δ (ppm), $CDCl_3$]:

0.32 [t, 3H, CH_3]; 1.38 [q, 2H, CH_2];

^{13}C NMR [δ (ppm), $CDCl_3$]:

9.4 [CH_3]; 11.5 [CH_2]; 127.0 [C]; 202.7, 210.3 [4CO].

IR [(cm^{-1}), nujol mull]:

2990, 2952, 2242, 2017, 1943, 1901, 1840, 1798, 1460, 1428, 1386, 1315, 1072, 1006, 787.

The synthesis of tetracarbonyl trimethyltin(diethylamino ethanethiolate) tungsten (0)
$W(CO)_4[Et_2N(CH_2)_2SSnMe_3]$ (21).

A Schlenk tube was charged with tetracarbonyl bis(propionitrile)tungsten (~0.16 g, 0.39 mmol). Toluene (*ca.* 20 ml) was added creating yellow-green dispersion. To the mixture was added trimethyltin(diethylamino ethanethiolate) (0.12 g, 0.39 mmol). The mixture was stirred at RT and within a few minutes the colour changed to dark brown-red solution. The resulting solution was left stirring for a further one hour. The solvent was then removed *in vacuo* leaving a solid residue. This was then purified by dissolving in toluene (10 ml) and adding hexane in a 1:5 ratio. The dark brown-red precipitate formed was isolated by filtration and dried *in vacuo*. Yield 0.12 g 66%.

Elemental Analysis:
Found (Calculated for $C_{10}H_{10}O_4N_2W$): %C 25.6 (26.4); %H 3.21 (3.89); %N 3.31 (2.37).
^{1}H NMR [δ (ppm), $CDCl_3$]:
0.25 [s, 9H, CH_3-Sn]; 0.92 [t, 6H, CH_3-Et]; 2.40 [q, 4H, CH_2-Et]; 2.70 [m, 4H, CH_2].
^{13}C NMR [δ (ppm), $CDCl_3$]:
-6.9 [CH_3, CH_3-Sn]; 11.1 [CH_3, Et_2N-]; 24.1 [CH_2-S]; 46.2 [CH_2, Et_2N]; 57.1 [N-CH_2].
^{119}Sn NMR [δ (ppm), $CDCl_3$]:
83.7.
IR [(cm-1), nujol mull]:
2989, 2950, 2241, 2017, 1958, 1927, 1850, 1458, 1389, 1328, 1069, 1013.
Mössbauer [mms^{-1}]:
δ=0.68, ΔE_Q=2.20

The synthesis of tetracarbonyl trimethyltin(diethylamino ethanethiolate) molybdenum (0)

$Mo(CO)_4[Et_2N(CH_2)_2SSnMe_3]$ (22).[11]

A Schlenk tube was charged with tetracarbonyl norbornadienyl molybdenum (0.5 g, 1.67 mmol). Toluene (*ca.* 50 ml) was added creating yellow-green dispersion. To the mixture was added trimethyltin(diethylamino ethanethiolate) (0.49 g, 1.67 mmol). The mixture was stirred at RT and within 10 min the colour started changing to dark brown-red solution. After one hour the colour change was complete and the solution was left stirring for a further 1hr. The solvent was then removed *in vacuo* leaving a solid residue. This was then purified by dissolving in toluene (10 ml) and adding hexane in a 1:5 ratio. The dark brown-red precipitate formed was isolated by filtration and dried *in vacuo*. Yield 0.38 g, 76%.

Elemental Analysis:

Found (Calculated for $C_{13}H_{23}MoNSSn$): %C 34.4 (31.0); %H 5.33 (4.57); %N 4.57 (2.78).

^{1}H NMR [δ (ppm), $CDCl_3$]:

0.39 [s, 9H, CH_3-Sn]; 0.97 [t, 6H, CH_3-Et]; 2.48 [q, 4H, CH_2-Et]; 2.59 [m, 4H, CH_2].

^{13}C NMR [δ (ppm), $CDCl_3$]:

11.5 [CH_3, CH_3-Sn]; 25.2 [CH_3, Et_2N-]; 46.8 [CH_2-S]; 56.9 [CH_2, Et_2N]; 67.5 [N-CH_2]; 199.8, 205.4 [4 CO].

^{119}Sn NMR [δ (ppm), $CDCl_3$]:

90.5.

IR [(cm^{-1}), nujol mull]:

2928, 2853, 2022, 1906, 1876, 1798, 1463, 1427, 1377, 1067, 722.

Mössbauer [mms^{-1}]:

δ=1.17, ΔE_Q=2.90

The synthesis of cadmium (diethylamino ethanethiolate) iodide $\{CdI[Et_2N(CH_2)_2S]\}_4$ (24).

A Schlenk tube was charged with cadmium iodide, CdI_2, (0.5 g, 1.37 mmol) and trimethyltin(diethylamino ethanethiolate) (0.40 g, 1.37 mmol). The mixture was stirred at RT overnight forming a creamy white paste. On addition of chloroform (15 ml) the mixture dissolved and slightly yellow crystals were precipitated on cooling. Subsequent filtration and drying *in vacuo* isolated the product as a crystalline white solid. Yield 0.45 g, 90%.

4.6 References

[1] G. Domazetis, R. J. Magee, B. D. James, *J. Inorg. Nucl. Chem.*, **43**, 1981, 1351.

[2] N. F. Albertson, R. O. Clinton, *J. Am. Chem. Soc.*, **67**, 1945, 1223.

[3] H. R. Snyder, J. M. Steward, J. B. Ziegler, *J. Am. Chem. Soc.*, **69**, 1947, 12673.

[4] B. S. Saraswat, J. Mason, *Polyhedron.*, **5**, 1986, 1449.

[5] M. Mikuriya, X. Jian, S. Ikemi, T. Kawahashi, H. Tsutsumi, A. Nakasone, J.W Lim, *Inorg. Chim. Acta*, **312**, 2001, 183.

[6] G. J. Kubas, L. S. Van Der Sluys, R. A. Doyle, R. J. Angelici, *Inorg. Synth.*, **28**, 1990, 29.

[7] B. L. Ross, J. G. Grasseli, W. M. Ritchey, H. D. Kaesz, *Inorg. Chem.*, **2**, 1963, 1023.

[8] I. W. Stolz, G. R. Dobson, R. K. Sheline, *Inorg. Chem.*, **2**, 1963, 323.

[9] E. W. Ainscough, E. J. Birch, A. M. Brodie, *Inorg. Chim. Acta*, **20**, 1976, 187.

[10] D. T. Dixon, J. C. Kola, J. A. S. Howell, *J. Chem. Soc., Dalton Trans.*, 1984, 1307.

[11] E. Delgado, M. A. Garcia, E. Gutierrez-Puebla, E. Hernandez, N. Mansilla, F. Zamora, *Inorg. Chem.*, **37**, 1998, 6684.

[12] S. L. Mukerjee, S. P. Nolan, C. D. Hoff, R. L. de la Vega, *Inorg. Chem.*, **27**, 1988, 81.

[13] J. Springs, C. P. Jansen, M. Y. Darensbourg, J. C. Calabrese, P. J. Krusic, J. N. Verpeaux, C. Amatore, *J. Am. Chem. Soc.*, **112**, 1990, 5797.

[14] L. Y. Goh, Z. Weng, W. K. Leong, P. H. Leung, *Angew. Chem. Int. Ed. Eng.*, **40**, 2001, 3236.

[15] R. C. Hynes, K. F. Preston, J. J. Springs, A. J. Williams, *Organometallics*, **10**, 1991, 180.

[16] T. G. Fawcett, C. C. Ou, J. A. Potenza, H. J. Schugar, *J. Am. Chem. Soc.*, 1978, 2058.

[17] S. M. Kupchan, C. K. Kim, K. Miyano, *J. Chem. Soc., Chem. Commun.*, 1976, 91.

[18] I. Casals, P. Gonzalez-Duarte, W. Clegg, C. Foces-Foces, F. H. Cano, M. Martinez-Ripoll, M. Gomez, X. Solans, *J. Chem. Soc., Dalton Trans.*, 1991, 2511.

[19] G. A. Jeffrey, 'An Introduction to Hydrogen Bonding', Oxford University Press, 1997, ch 4.

CHAPTER FIVE

The Synthesis, Characterisation and CVD Properties of (Triphenylphosphine gold) trialkyltin (IV) Sulfides.

5.1 Introduction

In this chapter the search for ideal precursors for the deposition of ternary materials is continued. The compounds examined in this chapter are non-chelating transition metal tin sulfides and the initiative behind examining this type of compounds is the fact that synthesis of a precursor with pre-existing the desired Sn-S-M linkage could potentially promote the deposition of films containing the three elements.

P. Oliver et al. [9, 10] have reported a similar synthetic strategy in order to deposit ternary materials containing a group 13 element, a second metal and a chalcogen. In their study they report the synthesis of heterobimetallic complexes, $\{R_2M[\mu\text{-}SSn(C_6H_{11})_3]\}_2$ (M = Ga, In and R = Ph, m-Xyl), formed by the reaction of bis(tricyclohexyltin) sulfide with triarylgallium and -indium.

The most characteristic feature of sulfur as a ligand in metal complexes is its tendency of three- or four-co-ordination by bridging several metal atoms. This has long been known for classical as well as organometallic co-ordination chemistry. In contrast, transition metal complexes containing divalent sulfur in monomeric M-S-M arrays are not common. Such examples constitute compounds such as $R_3M\text{-}S\text{-}MR_3$, where M is either group 12, 13 or 14 metals. [14-21]

Complexes containing the M-S-M′ unit, like the ones examined in this chapter, are even less common. Only compounds such as RZnSHgR', [11] $Et_2HgSGeMe_3$, [24] $Et_3SnSGeEt_3$ [23] and $EtZnSGePh_3$ [22] were found in literature.

5.2 Results and Discussion

5.2.1 Synthesis

During this study the approach has been to synthesise relatively simple molecules, which contain the Sn-S-M linkage. The types of compounds

considered were metal phosphine complexes of the type $(Ph_3P)_nMSSnR_3$, R = Me, Cy and M = Ag, Au. The following equation describes the syntheses.

$$(Ph_3P)_nMX + 1/2\ (R_3Sn)_2S \xrightarrow{Tol} (Ph_3P)_nMSSnR_3 + R_3SnX$$

Eq. 5.1

$(Cy_3Sn)_2S$ was found to react with $(Ph_3P)AuCl$ [4, 5, 8] with elimination of one equivalent of Cy_3SnCl to generate $(Ph_3P)AuSSnCy_3$ (**25**). [6] Compound (**25**) is only moderately air-stable and is soluble in most organic solvents.

A similar synthetic strategy has been reported by J. F. Corrigan et al. [12-13] which utilised $E(SiMe_3)_2$ (E = S, Se and Te) to form binary metal-chalcogenide nanoclusters where the formed metal-chalcogenide cores were stabilised by phosphines ligands (**Eq. 5.2**).

$$CuOAc + 3\ PPr_3 + E(SiMe_3)_2 \xrightarrow{-AcOSiMe_3} (Pr_3P)_3CuESiMe_3$$

$$(Pr_3P)_3CuESiMe_3 \xrightarrow{1/2\ Hg(OAc)_2 \cdot 2\ PPr_3} [Hg_{15}Cu_{20}E_{25}(PPr_3)_{18}] + AcOSiMe_3 + PPr_3$$

Eq. 5.2

The ^{119}Sn NMR spectrum of (**25**) shows a chemical shift at 43.3 ppm clearly distinguishable from that of the starting material [$(Cy_3Sn)_2S$ 19.4 ppm)]. In the ^{31}P NMR spectrum a singlet can be observed at 39.1 ppm very different from that of the free phosphine (-4.6 ppm). In addition, Mössbauer parameters were measured (δ=1.39, ΔE_Q=1.35 mms^{-1}). The isomer shift for (**25**) corresponds to a Sn(IV) centre (δ < 2.70 mms^{-1}) and the quadrupole splitting value is typical for four co-ordinate tin of the type R_3SnX (ΔE_Q 1.00-2.40 mms^{-1}).

However, this approach was not always successful. The analogous reaction of $(Ph_3P)AgCl$ with $(Cy_3Sn)_2S$ yielded only an insoluble black powder, which can

be assumed to be Ag_2S. The process believed to have taken place is summarised in the following equation:

$$(Ph_3P)_nAgX + (R_3Sn)_2S \Rightarrow (Ph_3P)_nAgSSnR_3 + R_3SnX$$

$$\Downarrow \begin{matrix}(Ph_3P)_nAgX \\ -R_3SnX\end{matrix}$$

$$(Ph_3P)_nAgSAg(PPh_3)_n$$

$$\Downarrow$$

$$nPPh_3 + Ag_2S$$

The process seems to rely, at least in part, on sufficient bulk in the ligands attached to either Sn and/or M in order to disfavour loss of a second equivalent of Cy_3SnCl. However, it is the stability and insolubility of Ag_2S, which seems to drive the reaction beyond $(Ph_3P)_nAgSSnCy_3$ despite the presence of the same bulky groups as in (**25**). $(Ph_3P)_2AgBr$ [7] was also reacted with $(Cy_3Sn)_2S$ giving the same results.

Compound (**25**) has been also characterised crystallographically (**Fig. 5.1**). Crystals of triphenylphosphine gold tricyclohexyltin sulfide were grown from a toluene-hexane solution (1:5). Selected metric data are summarised in **Table 5.1**.

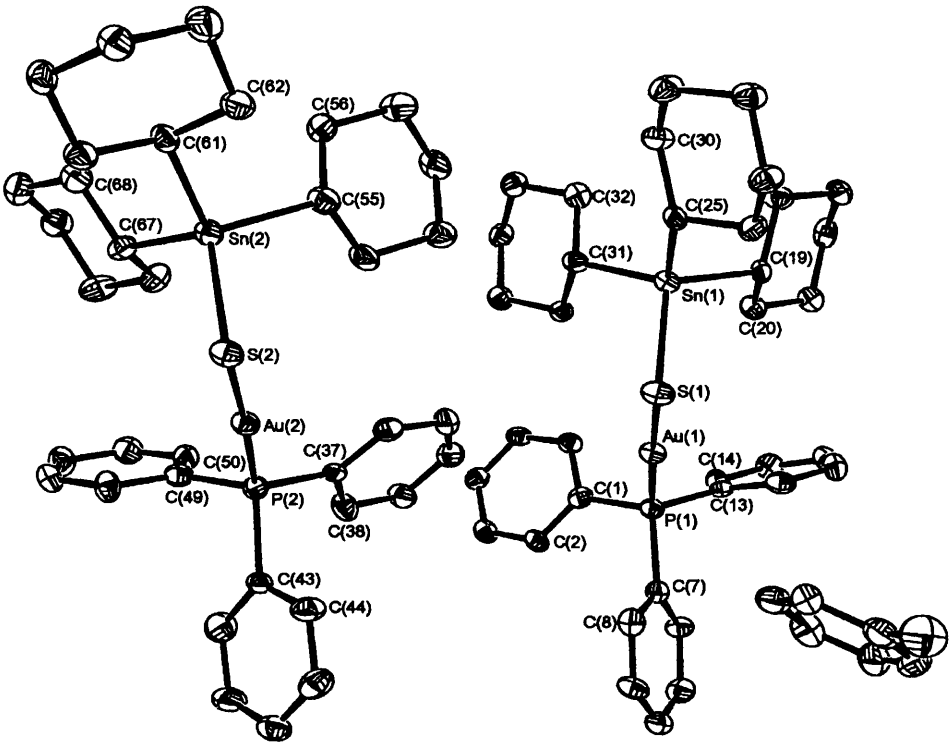

Fig. 5.1 The molecular unit of $(Ph_3P)AuSSnCy_3$ (**25**). There are two molecules in the asymmetric unit and one molecule of solvent (toluene). Thermal ellipsoids are at the 30% probability level.

There are two molecules in the asymmetric unit and a molecule of the solvent (toluene). The molecular structure of the complex $(Ph_3P)AuSSnCy_3$ consist of discrete monomeric units containing two subunits (Ph_3PAu and Cy_3Sn) connected by the sulfur atom. Therefore, the unsupported Sn-S-Au (**Fig. 5.1**) linkage is confirmed and the Sn-S-Au angle (98.2, 101.7 °) has been found to be remarkably acute given the groups attached to each metal. In the Ph_3PAu subunit a slightly distorted linear environment can be observed around the gold metal centre, (< P-Au-S 177°) comparable to that reported for complex $(PPh_3)Au\{S[(C_6H_4)Sn(Cl)(Me)_2]\}$ (< P-Au-S 176.6 °). [25] The Au-S bond lengths in compound (**25**) range from 2.280(3) Å to 2.294(3) Å and are typical of this type of bond (Au-S 2.16-2.31 Å). [2, 25] The phosphorus atom lies in an almost tetrahedral configuration and the P-C bonds (*ca.* 1.8 Å) are of the expected length (P-C 1.8-1.9 Å). [2] Finally, the Au-P bond length is 2.26 Å, very similar to values reported in literature [2] although slightly longer from that reported for the starting material Ph_3PAuCl (Au-P 2.24 Å). [3] In the Cy_3Sn subunit the tin atom is

in an almost tetrahedral environment (111.7-109.0°), with Sn-C bond lengths of 2.16 Å. The Sn-S bond length is typical for trialkyltin sulfides (Sn-S 2.4 Å). [1]

Bonds (Å) and Angles (°)	Molecule 1	Molecule 2
Au-P	2.256(3)	2.270(3)
Au-S	2.280(3)	2.294(3)
Sn-S	2.409(3)	2.408(3)
Sn-C	2.160(10)	2.151(10)
	2.169(9)	2.153(11)
	2.170(11)	2.161(10)
P-C	1.812(10)	1.812(11)
	1.815(11)	1.816(10)
	1.839(11)	1.849(10)
P-Au-S	177.024(11)	176.38(10)
Au-S-Sn	101.68(10)	98.15(10)

Table 5.1 Selected bond lengths and angles for $(Ph_3P)AuSSnCy_3$ (**25**).

An analogous compound to (**25**) $[(PPh_3)AuSSnMe_3$ (**26**)] has also been synthesised via the same route, by reaction of $(Me_3Sn)_2S$ (**33**) with PPh_3AuCl. However, (**26**) proved to be much more air-sensitive than (**25**) and crystals grown were of insufficient quality for an X-ray structure to be obtained. The ^{119}Sn NMR spectrum of (**26**) shows a chemical shift at 85.0 ppm clearly distinguishable from that of the starting material $[(Me_3Sn)_2S$ 92.1 ppm] and of the by-product Me_3SnCl (164.0 ppm). In the ^{31}P NMR spectrum a singlet can be observed at 17.0 ppm very different from that of the free phosphine (PPh_3 -4.6 ppm).

5.3 Film Growth Results

5.3.1 Introduction and Thermal Analysis

Compounds (**25**) and (**26**) were assessed for their suitability as CVD precursors. Both compounds were investigated by Thermal Gravimetric Analysis (TGA) in order to obtain an indication of their possible decomposition pathways.

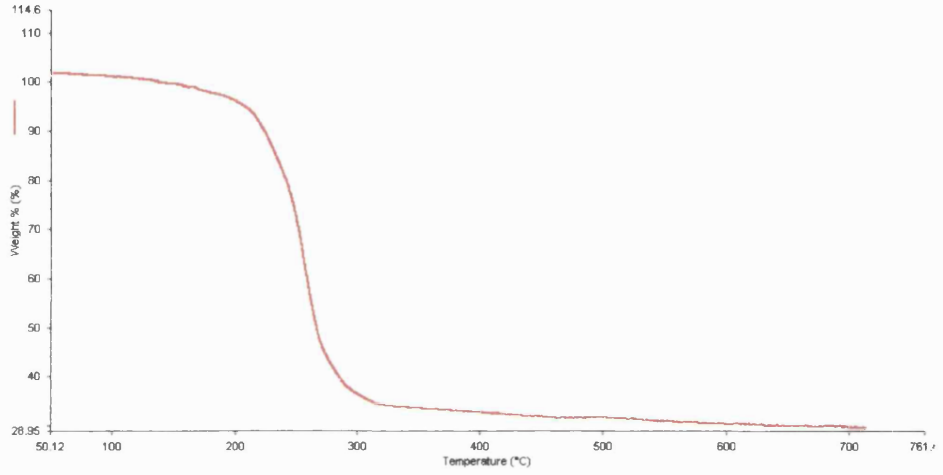

Fig. 5.2 TGA of $(PPh_3)AuSSnCy_3$ (**25**).

The TGA of (**25**) (**Fig. 5.2**) shows the decomposition to begin at around 80 °C and complete at 650 °C. The first step observed at 200 °C corresponds to a weight residue of 37% and can be attributed to $AuSnS_{1.5}$ (observed residual mass: 37.0, theoretical: 42.4%). A small further decomposition occurs until 650 °C and the remaining residue 32% can speculatively be attributed to the formation of some SnS (observed residual mass: 32.0, theoretical 17.6 %) with the possibility of some incorporated gold and carbon particles.

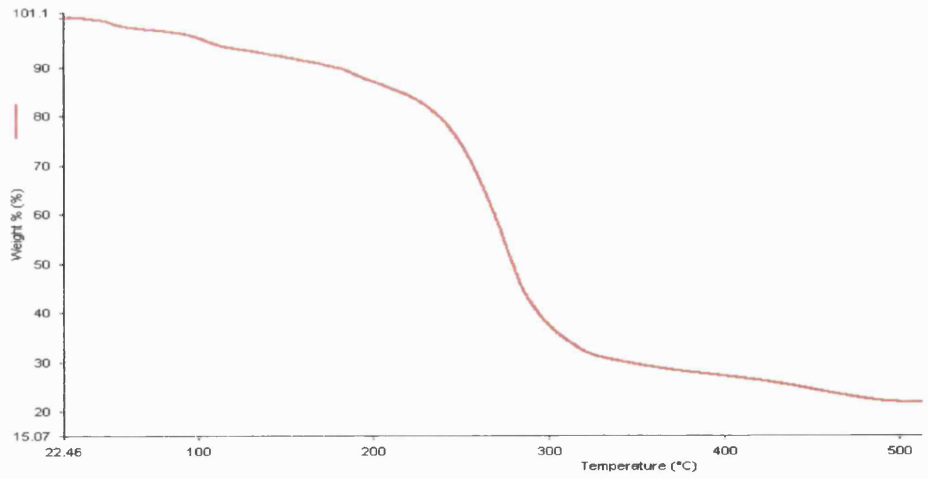

Fig. 5.3 TGA of $(PPh_3)AuSSnMe_3$ (**26**).

The TGA of (**26**) (**Fig. 5.3**) shows the decomposition to begin at room temperature (*ca* 25 °C) and complete at 500 °C. The fact that decomposition starts at such a low temperature indicates the fact that (**26**) is not as stable a compound as (**25**) and decomposes very quickly. The first step observed at 220 °C results to a weight residue of 30% which can be attributed to SnS_2 (observed residual mass: 30.0, theoretical: 27.9%). However, the residual mass could also correspond to Au (observed residual mass: 30.0, theoretical: 30.1%), but this is unlikely since (**25**) continues to decompose leaving a residue that can be attributed to SnS (observed residual mass: 23.0, theoretical: 23.1%).

5.3.2 Deposition Conditions

Because of the solubility of compounds (**25**) and (**26**), the technique employed for deposition was AACVD. Films were deposited on standard borosilicate glass slides and heated at 550 °C. For each growth experiment approximately 0.2 g of complex was dissolved in THF (~20 ml). Growth took place under a continuous flow of N_2.

Deposition conditions for the films grown in this chapter are displayed in **Table 5.2**.

Compound	(25)	(26)	(26)
Film ID	**Au1**	**Au2**	**Au3**
Reactor Temp (°C)	520	550	550
Carrier Gas (N_2)Flow Rate (l/min)	1.0	0.5	1.0
Run Time (min)	30	35	30

Table 5.2 AACVD conditions for experiments with compounds (**25**) and (**26**).

5.3.3 Film Analysis

Films were examined using a number of techniques: Visual inspection, Energy Dispersive X-Ray Analysis (EDAX), Scanning Electron Microscopy (SEM) and Raman Spectroscopy.

Film **Au1** was deposited from precursor (**25**) at 520 °C. It covered only the first slide of the eight constituting the glass substrate and it had red colour. It was well adhered to the substrate but no refrigence patterns were observed. Film **Au1** was analysed at UCL by Professor I. Parkin's group.

SEM analysis performed on this film revealed that it consisted of elongated crystals. All areas examined on this film revealed similar Raman patterns and the patterns coincide with those identified for SnS. However, a few bands in the Raman spectrum were shifted from their expected values leading to the conclusion that possibly some included gold could be present in trace amounts. Presence of gold in trace amounts could also be justified by the red colour of the film, since SnS films are usually yellow/brown and colloidal gold films are usually red or blue/violet.

Films **Au2** and **Au3** were both deposited from the same precursor (**26**) at the same temperature (550 °C) but at different flow rates. Film **Au2** was deposited at the slowest rate, while **Au3** at the fastest. Both films appeared very similar and

red in colour, were very well adhered, and covered most of the glass substrate. However, film **Au3** was visibly thicker than **Au2**. Both films were analysed by SEM and EDAX. The X-ray analysis revealed that they both contained mostly gold with **Au2** containing some chlorine impurities as well. It is obvious in the EDAX analysis of film **Au3** (**Fig 5.4**) that no tin is present. Furthermore, one cannot speculate on the existence of any sulfur since the signals corresponding to gold and sulfur overlap. SEM analyses (**Fig. 5.5** to **Fig. 5.7**) showed that both films were very uniform containing crystallites of various sizes.

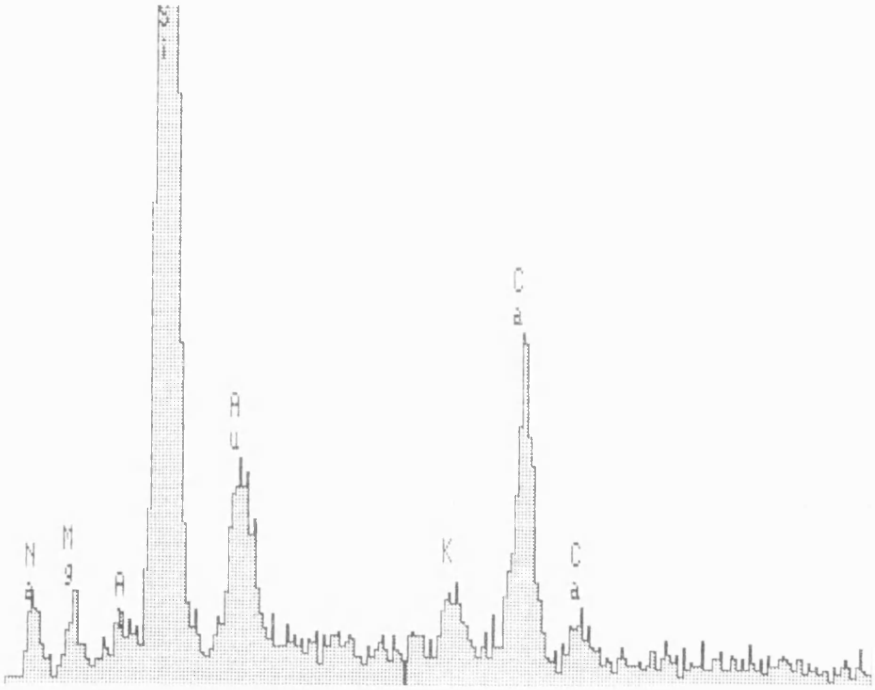

Fig. 5.4 EDAX analysis of film **Au3**.

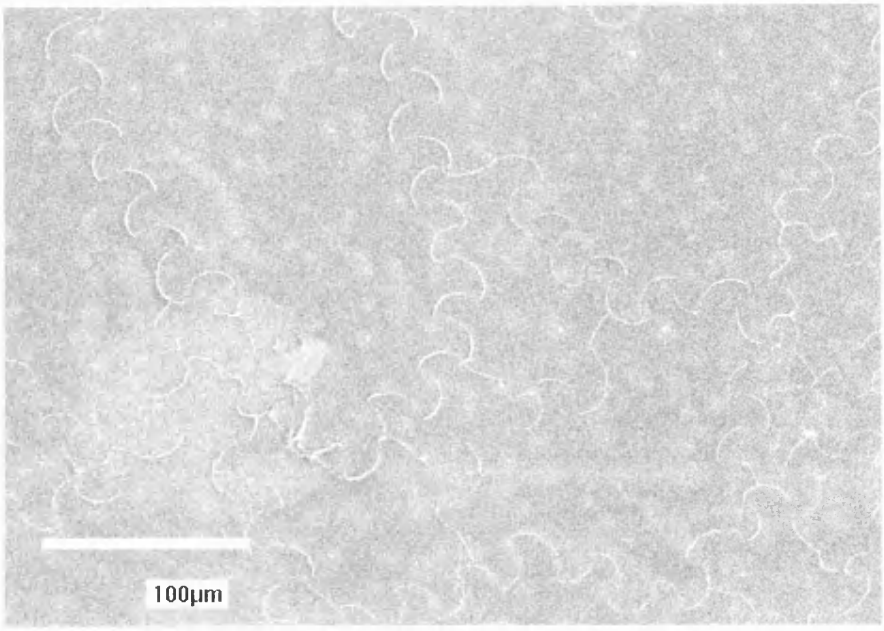

Fig. 5.5 0° tilt SEM image of film **Au2** precursor (**26**).

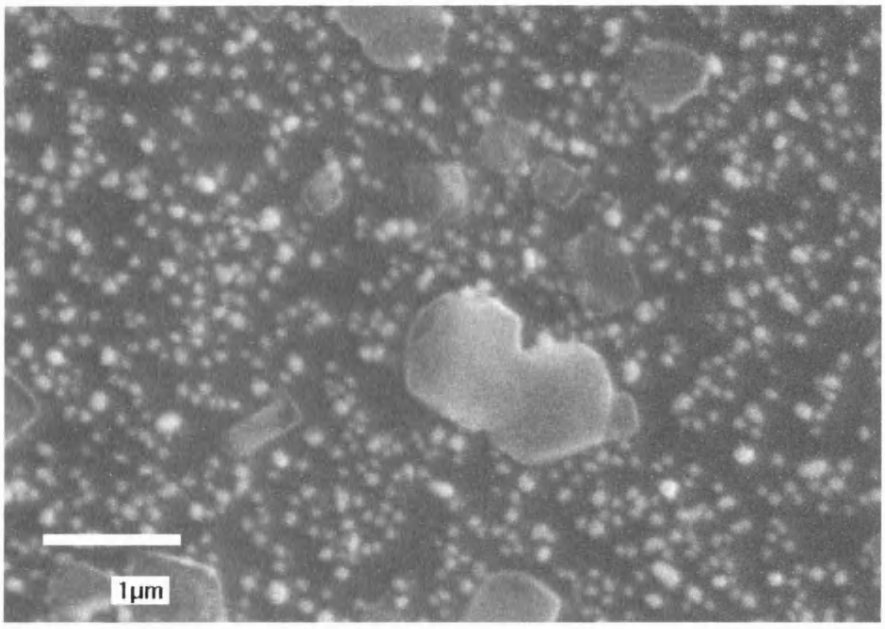

Fig. 5.6 0° tilt SEM image of film **Au2** at higher magnification, precursor (**26**).

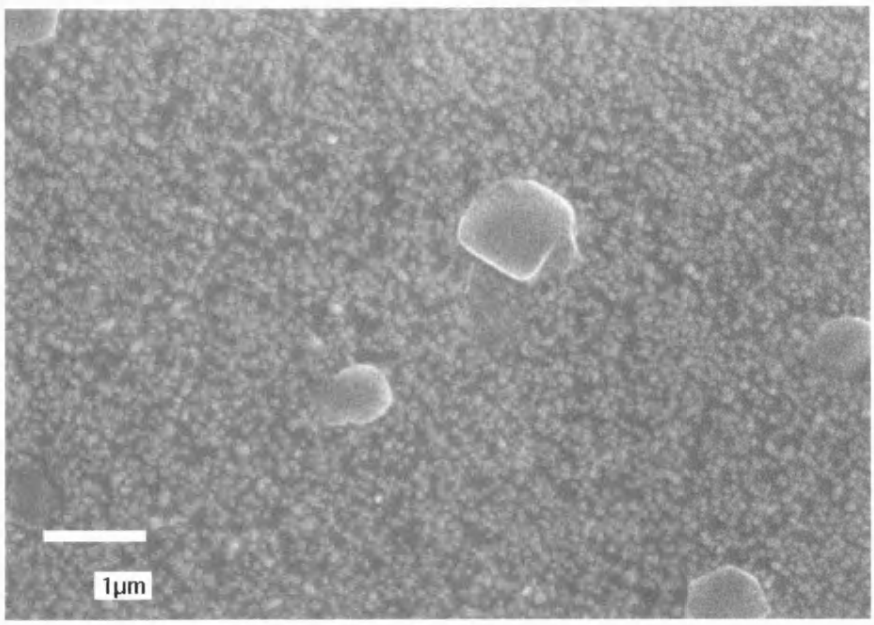

Fig. 5.7 0^{o} tilt SEM image of film **Au3**, precursor (**26**).

In summary, for both precursors the decomposition results are in conflict with those from the bulk decomposition (TGA) studies. In particular, CVD results suggest that the film **Au1** deposited from the single-source precursor $(PPh_3)AuSSnCy_3$ (**25**) is mostly SnS with possibly some traces of gold, also suggested by the red colour of the film, while TGA results are inconclusive as to what type of material could be present (quite big discrepancies between the theoretical and observed residual mass values). For films **Au2** and **Au3** deposited from precursor (**26**) TGA results suggest that the possible materials formed should be tin sulfides, while the deposited films were identified as gold. These conflicting results between the bulk decomposition and CVD studies can be attributed to the fact that precursors can behave differently in the bulk and in the vapour phase.

Films **Au1**, **Au2** and **Au3** are all very similar in the fact that they all contain colloidal gold particles resulting in the red colour observed for all films. In addition, the particle size of films **Au2** and **Au3** observed in the SEM pictures compares well with the size of colloidal particles (*ca.* 500 nm). However, in the case of film **Au1**, SnS was deposited as well as colloidal gold particles. In the

case of films **Au2** and **Au3**, since precursor (**26**) is so much more air-sensitive than (**25**), the deposition resulted in the formation of a colloidal gold film.

5.4 Conclusions

The syntheses and characterisation of two triphenylphoshine gold alkyltinsulfides have been described in this chapter. Furthermore, some studies on the precursor suitability to deposit ternary materials by CVD have also been reported. The fact that ternary materials were not so readily obtained from these precursors, (**25**)-(**26**), in comparison with the precursors in chapter four can be attributed to the fact that the former lack chelation. The added stability that chelation offers in a complex suggests that during deposition it promotes decomposition at the substrate surface. In contrast, non-chelating complexes seem to undergo some kind of vapour phase decomposition before reaching the substrate and therefore resulting in films that do not always contain the desired elements.

5.5 Experimental

Starting materials were obtained commercially (e.g. Aldrich) and were used without further purification. Standard Schlenk line techniques were employed where applicable. For further details about instrumentation see **Appendix 1**.

The synthesis of triphenylphosphine gold chloride PPh_3AuCl. [5]

PPh_3AuCl was prepared by a known route. A solution of triphenylphosphine (0.77 g, 2.94 mmol) in ether (*ca.* 10 ml) was added dropwise to a solution of hydrogen tetrachloroaurate(III) trihydrate (0.58 g, 1.47 mmol) in ether (*ca.* 30 ml) at 0 °C. On addition a yellow precipitate appeared and the mixture was left stirring. After one hour the precipitate became white and the mixture was left stirring for two more hours at RT. The crude product was obtained by filtration

and further purified by recrystallisation from warm ethanol. Yield 0.29g, 50%. PPh_3AuCl exhibited spectroscopic properties identical to those reported.

The synthesis of bis(trimethyltin) sulfide $(Me_3Sn)_2S$ (27).

A conical flask was charged with sodium sulfide nonahydrate (3 g, 12 mmol) dissolved in distilled water (20 ml). A solution of trimethyltin chloride (2.41 g, 12 mmol), dissolved in ether (15 ml), was added dropwise; the system was stirred at room temperature for 3 hours. The organic layer was then separated using a separation funnel and dried with magnesium sulfate. Filtration and *in vacuo* removal of the solvent resulted in a yellow viscous oil. Yield 1.74 g, 72%.

Elemental Analysis:
Found (Calculated for $C_6H_{18}SSn_2$): %C 21.95 (20.03); %H 5.22 (5.01).

^{1}H NMR [δ (ppm), $CDCl_3$]:
0.35 [s, 9H, CH_3].
^{13}C NMR [δ (ppm), $CDCl_3$]:
-2.1 [CH_3].
^{119}Sn NMR [δ (ppm), $CDCl_3$]:
92.1.
Mössbauer [mms^{-1}]:
δ=1.26, ΔE_Q=1.62

The synthesis of triphenylphosphine gold tricyclohexyltin sulfide $PPh_3AuSSnCy_3$ (25). [6]

Bis(tricyclohexyltin)sulfide (0.64 g, 0.83 mmol) was added to a solution of triphenylphosphine gold chloride (0.38 g 0.83 mmol) in toluene (*ca.* 60 ml).

After a few minutes of stirring the reactants dissolved and a clear solution was obtained. In addition of hexane (10 ml) a white precipitate deposited from the solution. This was then washed twice with hexane and dried under vacuum. A crystalline solid was precipitated from a toluene/hexane solution, 1:5 ratio. Yield 0.39 g 56%.

Elemental Analysis:

Found (Calculated for $C_{36}H_{48}SPSnAu$): %C 46.9 (50.31); %H 5.30 (5.59).

^{1}H NMR [δ (ppm), $CDCl_3$]:

1.38 [m, 6H, CH_2]; 1.80 [m, 12H, CH_2]; 1.99 [m, 12H, CH_2]; 2.30 [m, 3H, CH-Sn]; 7.07 [m, 3H, p-CH]; 7.50 [m, 2H, o-CH].

^{13}C NMR [δ (ppm), $CDCl_3$]:

27.9 [CH_2]; 30.2 [CH_2]; 31.2 [Sn-CH]; 39.0 [CH_2]; 129.4, 129.6 [m, p-CH]; 131.5 [o-CH]; 134.8 [d, P-C ($^{1}J^{13}C$-^{31}P = 13.2 Hz)].

^{119}Sn NMR [δ (ppm), $CDCl_3$]:

43.3.

^{31}P NMR [δ (ppm), C_6D_6]:

39.1

Mössbauer [mms^{-1}]:

δ=1.39, ΔE_Q=1.35

The synthesis of triphenylphosphine gold trimethyltin sulfide $PPh_3AuSSnMe_3$ (26).

This compound was synthesised in the same way as for compound (**31**). Bis(trimethyltin)sulfide (0.36 g, 1.01 mmol) was added to a solution of triphenylphosphine gold chloride (0.5 g 1.01 mmol) in toluene (*ca.* 60 ml). After a few minutes of stirring and on addition of hexane (10 ml) a white precipitate deposited from the solution. This was then washed twice with hexane and dried under vacuum. Yield 0.31 g, 47%.

Elemental Analysis:

Found (Calculated for $C_{21}H_{24}SPSnAu$): %C 39.4 (37.5); %H 3.16 (6.24).

^{1}H NMR [δ (ppm), $CDCl_3$]:

0.6 [s, 9H, CH_3; 7.03 [m, 2H, p-CH]; 7.13 [m, 1H, m-CH]; 7.36 [m, 2H, o-CH].

^{13}C NMR [δ (ppm), $CDCl_3$]:

1.2 [Sn-CH_3]; 129.0, 129.1 [m, p-CH]; 130.4 [o-CH]; 134.0 [d, P-C ($^{1}J^{13}C$-^{31}P = 16 Hz].

^{119}Sn NMR [δ (ppm), $CDCl_3$]:

85.0.

^{31}P NMR [δ (ppm), C_6D_6]:

17.0

5.6 References

[1] G. Wilkinson, F. Gordon, A. Stone, E. Abel, 'Comprehensive Organometallic Chemistry', **618**, Pergamon Press, 1982, ch 11.

[2] W. Bos, J. J. Bour, P. P. Schlebos, P. Hageman, W. P. Bosman, J. M. M. Smits, J. A. C. van Wietmarschen, P. T. Beurskens, *Inorg. Chim. Acta*, **119**, 1986, 141.

[3] N. C. Baenzinger, W. E. Bennet, D. M. Soboroff, *Acta Cryst.*, **B32**, 1976, 962.

[4] D. M. L. Goodgame, C. A. O'Mahoney, S. D. Plank, D. J. Williams, *Polyhedron*, **12**, 1993, 2705.

[5] M. I. Bruce, B. K. Nicholson, O. Bin Shawkataly, J. R. Shapley, T. Henly, *Inorg. Synth.*, **32**, 324.

[6] E. Delgado, E. Hernandez, *Polyhedron*, **11**, 1992, 3135.

[7] R. G. Goel, P. Pilon, *Inorg. Chem.*, **17**, 1978, 286.

[8] H. Schmidmaur, J. Adkofer, K. Schwirten, *Chem. Ber.* **105**, 1972, 3382.

[9] S. U. Ghazi, M. J. Heeg, J. P. Oliver, *Inorg. Chem.*, **33**, 1994, 4517.

[10] B. Yearwood, S. U. Ghazi, M. J. Heeg, N. Richardson, J. P. Oliver, *Organometallics*, **19**, 2000, 865.

[11] M. Rombach, H.Vahrenkamp, *Eur. J. Inorg. Chem.*, 2002, 2022.

[12] D. T. T. Tran, L. M. C. Beltran, C. M. Kowalchuk, N. R. Trefiak, N. R. Taylor, J. F. Corrigan, *Inorg. Chem.*, **41**, 2002, 5693.

[13] D. T. T. Tran, J. F. Corrigan, *Organometallics*, **19**, 2000, 5202.

[14] L.C. Willemsens, G. J. M. Van der Kerk, J. *Organomet. Chem.*, **15**, 1968, 117.

[15] Von K. H. Flegler, A. Haas, *Z. Anorg. Allg. Chem.*, **426**, 1976, 288..

[16] J. E. Drake, B. M. Glavincevski, R. T. Hemmings, *J. Inorg. Nucl. Chem.*, **41**, 1979, 457.

[17] E. W. Abel, D. A. Armitage, D. B. Brady, *Trans. Faraday Soc.*, **62**, 1966, 3459.

[18] T. Harada, *J. Inorg. Nucl. Chem.*, **37**, 1975, 288.

[19] M. Dadic, D. Grdenic, *Croat. Chem. Acta*, **32**, 1960, 39.

[20] M. Boleslawski, S. Pasynkiewicz, A. Kunicki, J. Smola, J. *Organomet. Chem.*, **65**, 1974, 161.

[21] E. J. Kupchik, C. T. Theisen, J. *Organomet. Chem.*, **11**, 1968, 627.

[22] R. F. Galiullina, Y. N. Krasnov, T. R. Shnol, *J. Gen. Chem, USSR (Engl. Transl.)*, **47**, 1977, 1528.

[23] A. N. Egorochkin, N. S. Vyazankin, G. A. Razuvaev, O. A. Kruglaya, M. N. Bochkarev, *Dokl. Chem. (Engl. Transl.)*, **170**, 1966, 333.

[24] E. N. Gladyshev, V. S. Andreevichev, A. A. Klimov, N. S. Vyazankin, G. A. Razuvaev, *J. Gen. Chem, USSR (Engl. Transl.)*, **42**, 1972, 1077.

[25] E. J. Fernandez, M. B. Hursthouse, M. Laguna, R. Terroba, *Organometallics*, **16**, 1997, 5637.

CHAPTER SIX

Conclusions and Future Work

6. Conclusions and Future Work

One of the aims of this study was to prepare precursors for the deposition of metal sulfides. In the past, all studies had led in the deposition of tin sulfides by temperature control and sometimes by the addition of H_2S. However, in this thesis (chapter two) we report the synthesis of precursors [$(dtc)_4Sn$ and $(dtc)_2(RS)_2Sn$], which decompose directly to SnS_2 and SnS respectively, by virtue of their specific decomposition pathways. In addition these tin sulfide films can be grown at relatively low temperatures (*ca.* 350 °C). Furthermore, it has been shown that tin sulfide films can be grown under low pressure conditions from precursors $(dtc)_2(CyS)_2Sn$ and $[(dtc)_2SnS]_2$.

In this aspect, further work should concentrate in developing new tin compounds with an all sulfur co-ordination sphere around tin in order to obtain an optimum proportion of sulfur relative to tin for tin sulfide film deposition. One way to achieve this could be by investigating further the reactions involving the cyclic dimers (**5a**) and (**5b**). Rather than substituting the labile amide groups with simple thiolates one could use the bidentate ligand (**18**) which already has a tin atom attached on to sulfur. This could possibly eliminate the formation of polymeric materials and give instead soluble compounds that will be useful for CVD studies.

In chapters three and four the synthesis of pentacarbonyl and tetracarbonyl transition-metal tin sulfides were examined, the latter containing chelating tin sulfides. In both cases, films with the desired elements were obtained but this was particularly true for the complexes stabilised by chelation. In this aspect, further work could concentrate in creating more stable complexes, i.e. less air sensitive compounds. One way to achieve this could be to utilise a different chelating tin sulfide. For example, by substituting the amide group for a phosphide group, the chelation of the sulfide should improve due to the better ability of phosphorus to back bond. Therefore, better chelation could be interpreted as better ability for the desired elements to hold together in the

M-S-Sn unit under decomposition conditions and hence result in better quality films.

In the final chapter the syntheses and decompositions of two triphenylphosphine gold alkyltinsulfides were examined. The fact that no ternary materials were obtained from these precursors could be attributed to the fact that they lack the stability chelation offers. Furthermore, since the precursors were so sensitive with respect to decomposition (very air sensitive), high temperature CVD experiments would only promote this and make deposition processes difficult to predict. However, the studies on these precursors could be extended by employing lower decomposition temperatures (i.e. low temperature AACVD), or even different decomposition techniques (e.g. LPCVD) rather than high temperature AACVD that was used previously.

APPENDICES

Appendix One

Reagents

Starting materials were obtained commercially and used without further purification unless otherwise stated. All reactions took place under an inert nitrogen or argon atmosphere and dry solvents were used throughout unless otherwise stated. Dry solvents were obtained from distillation under an inert atmosphere from the following drying agents: sodium-benzophenone (toluene, ether, THF), calcium hydride (DCM), sodium (hexane).

Instrumentation

Infra-Red Spectroscopy

Infra-red spectra were recorded as nujol (liquid paraffin) mulls or liquid films between NaCl plates. Measurements were taken using a Nicolet 510P FT-IR spectrometer within the range 4000 – 600 cm^{-1} with a medium slit width and a peak resolution of 4.0 cm^{-1}.

Microanalysis

Carbon, hydrogen and nitrogen elemental analyses were performed using a Carlo-Erba Strumentazione E. A. mod 1106 microanalyser operating at 500 °C. Results were calibrated against an acetanilide [$PhNHC(O)CH_3$] standard.

Nuclear Magnetic Resonance Spectroscopy

^{1}H and ^{13}C NMR spectra were recorded using either Jeol JNM-GX270FT (270 MHz) or JNM-EX400 (400 MHz) Fourier Transform spectrometers using $SiMe_4$ as an internal reference, while ^{119}Sn NMR spectra were recorded on a Jeol JNM-EX400 FT spectrometer using either saturated $CDCl_3$ or C_6D_6 solutions.

Scanning Electron Microscopy (SEM)

SEM images were collected on a JEOL-6310 scanning electron microscope, operating at an accelerating voltage of 15 kV.

Energy Dispersive X-Ray Analysis (EDAX)

EDAX analyses were performed using an Oxford Instruments AN-10,000 Energy Dispersive X-Ray Analyser, operating at an accelerating voltage of 15 kV. Qualitative EDAX analyses were performed on a JEOL JXA-8600 Electron Probe Microanalyser (EPMA) Wavelength Dispersive X-Ray Analyser, operating at an accelerating voltage of 6 kV.

X-Ray Diffraction (XRD)

Data were collected on a Nonius KappaCCD diffractometer. Full matrix anisotropic refinement was implemented in the final least-squares cycles throughout. All data were corrected for Lorentz and polarisation and some for extinction. Structure determination and refinement was achieved using the SHELX suite of programs and drawings were produced using ORTEX.

Appendix Two

The CVD Reactor

The CVD apparatus used in this study has been assembled as a general screening rig for the use in this and other related projects. The system consists of a horizontal cold wall reactor with associated gas lines and electrical heater controls. The reactor contains two separate systems, a heated bubbler assembly (APCVD) and an ultrasonic nebuliser system (AACVD). For the purposes of this study only the ultrasonic nebuliser system (AACVD) was employed and hence will be discussed in detail. A schematic of the reactor system is shown in **Fig. A2.1**.

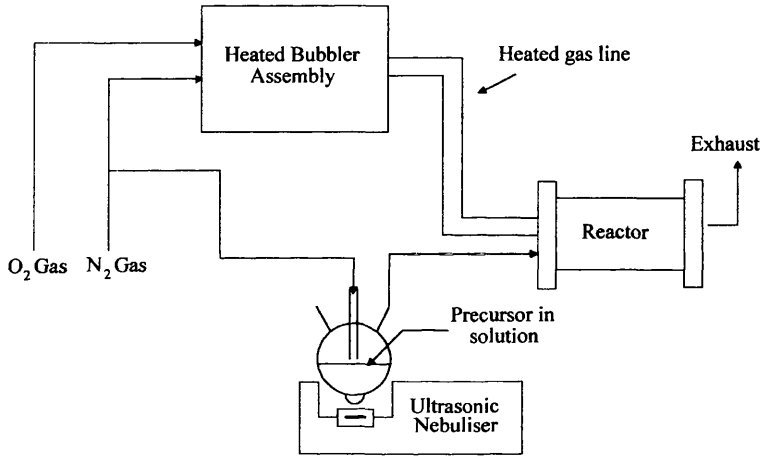

Fig. A2.1 The CVD apparatus.

The nebuliser system used for AACVD is an ultrasonic humidifier from Pifco Health (model No 1077) bought in Argos (**Fig. A2.2**). The piezoelectric transducer, situated in the reservoir containing water, transmits ultrasound through the water and the glass flask into the solution containing the precursor. The distance between the piezoelectric transducer and the flask is approximately 3-4 cm. The water in the reservoir is replaced every 30 minutes in order to cool the transducer.

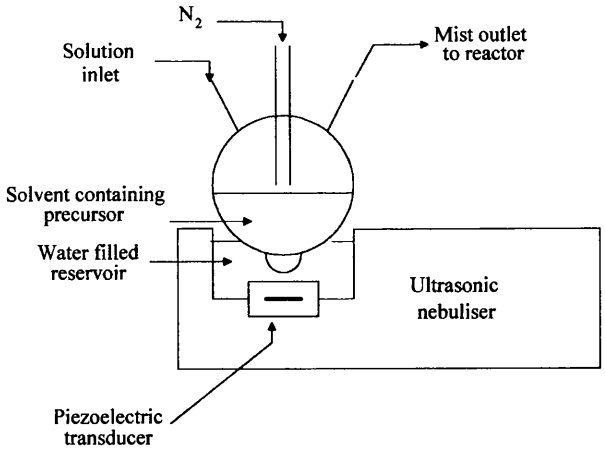

Fig. A2.2 The ultrasonic nebuliser system.

The precursor solution is injected into the flask, which is under an inert atmosphere and placed on the nebuliser. The aerosol of fine droplets created (droplet size: 0.2-5 μm) can be controlled via two controls, the mist output (MO) and the humidity level (HL). For a THF solution the efficiency of the nebuliser is 1.2 cm^3min^{-1} when the MO button is in position 1/2 or 3/4 of its full power and the HL button in position 3/4. The resulting aerosol is then swept out of the flask by a flow of argon and transported to the CVD reactor through a baffle to promote laminar flow.

The CVD reactor chamber where decomposition takes place is 8 mm high, 40 mm wide and 300 mm long. The ceiling tile and walls consist of quartz plates. The glass substrate is positioned on a large graphite susceptor, which is heated by three Watlow firerod cartridge heaters. The temperature of the graphite block is maintained by a Watlow series 965 controller, which monitors the temperature by means of thermocouples positioned inside the block. The graphite susceptor is held inside a large quartz tube (330 mm long, 100 mm diameter) suspended between stainless steel flanges upon which many of the electrical and gas line fittings are fixed. Air -tight seals are provided by 'Viton' O-rings. A schematic of the CVD reactor chamber is shown in **Fig. A2.3**.

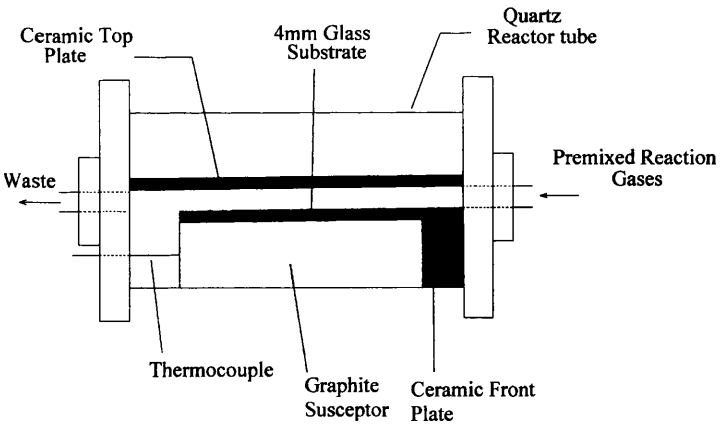

Fig. A2.3 The CVD reactor chamber.

For the LPCVD experiments a different reactor was employed and a schematic of the apparatus is shown in **Fig. A2.4**. The precursor sample to be decomposed is placed at the bottom end of the quartz tube reactor and the tube is then inserted in to the cylindrical heater, which heats the precursor. The quartz tube reactor also contains the glass substrate the graphite susceptor and a thermocouple. The glass substrate is positioned outside of the cylindrical heater and held at an angle on top of the graphite block, which is heated conductively by a ceramic heater placed underneath. The temperature is monitored and controlled via a thermocouple and the whole reactor is connected to a Schlenk line to allow for the application of vacuum and backfill of nitrogen.

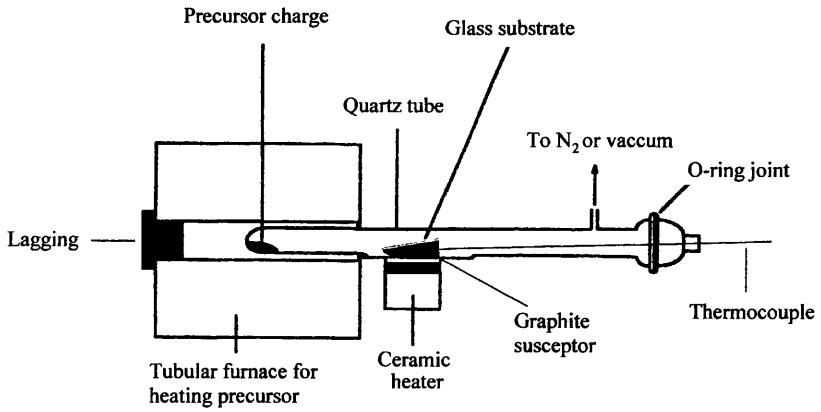

Fig. A2.4. The low pressure CVD reactor.

Substrate Preparation Procedure

All glass substrates were cleaned in an identical manner prior to use. The cleaning routine was as follows:

(i) The glass was washed thoroughly with water and detergent.

(ii) Then washed thoroughly with copious amounts of distilled water.

(iii) The substrate was finally washed with isopropyl alcohol (IPA) and allowed to dry.

The glass substrate was always prepared prior to a deposition experiment and on completion of screening each precursor the nebuliser (AACVD), reactor tube (LPCVD) and any associated pipework were thoroughly cleaned in an Acid/Base bath followed by acetone to prevent unwanted contamination in films deposited from subsequent precursors.

Appendix Three

Numerical Index of Compounds in This Thesis

(1) $(Et_2NCS_2)_4Sn$

(2) $[(Et_2NCS_2)_2SnS]_2$

(3) $(Et_2NCS_2)_2(CyS)_2Sn$

(4) $(Et_2NCS_2)_2(PhS)_2Sn$

(5a) $[Sn[N(SiMe_3)_2](\mu\text{-}S_2)]_2$

(5b) $[Sn(N(SiMe_3)_2)_2]_2(\mu\text{-}S)(\mu\text{-}S_2)]$

(6) $[(PhS)_2Sn(\mu\text{-}S)]_2$

(7) $[(dmPhS)_2Sn(\mu\text{-}S)]_2$

(7a) $(dmPhS)_4Sn$

(8) $[(^tBuS)_2Sn(\mu\text{-}S)]_2$

(9) $[(SCH_2CH_2S)Sn(\mu\text{-}S)]_2$

(10) $(Et_2NCS_2)_2Sn$

(11) $[Et_2NC(S)SS(S)CNEt_2]$ or $(Et_2NCS_2)_2$

(12) $^nBu_3SnS^tBu$

(13) Me_3SnS^tBu

(14) $(CO)_5CrS(^tBu)(^nBu_3Sn)$

(15) $(CO)_5CrS(^tBu)(Me_3Sn)$

(16) $(CO)_5MoS(^tBu)(^nBu_3Sn)$

(17) $(CO)_5MoS(^tBu)(Me_3Sn)$

(18) $Et_2NCH_2CH_2SSnMe_3$

(19) $W(CO)_4(CNEt)_2$

(20) $Cr(CO)_4CCNEt)_2$

(21) $W(CO)_4(Et_2NCH_2CH_2SSnMe_3)$

(22) $Mo(CO)_4(Et_2NCH_2CH_2SSnMe_3)$

(23) $[Cr(CO)_5]_2(Et_2NSH_2CH_2SH)$

(24) $[CdI(SCH_2CH_2NEt_2)]_4$

(25) $(Ph_3P)AuSSnCy_3$

(26) $(Ph_3P)AuSSnMe_3$


TDK
CD-R74
CD-RECORDABLE
REFLEX ULTRA X
COMPACT
disc
Recordable
650MB
Appendix Four.